UNIVERSITY OF OKLAHOMA
GRADUATE COLLEGE

AEROSOL MONITORING IN RURAL OKLAHOMA FOR APPLICATION IN UNDERSAMPLED REGIONS

A THESIS SUBMITTED TO THE GRADUATE FACULTY
in partial fulfillment of the requirements for the
Degree of
MASTER OF SCIENCE

By
Emily West
Norman, Oklahoma
2026

Downloaded from SHAREOK. Persistent Handle URL: https://hdl.handle.net/11244/342682

AEROSOL MONITORING IN RURAL OKLAHOMA FOR APPLICATION IN UNDERSAMPLED REGIONS

A THESIS APPROVED FOR
THE SCHOOL OF METEOROLOGY

BY THE COMMITTEE CONSISTING OF

Dr. Jens Redemann, Chair

Dr. Connor Flynn

Dr. Marcela Loría-Salazar

© Copyright by Emily West 2026
All Rights Reserved.

Acknowledgments

This project has taken a lot of support, and I want to take a moment to thank everyone who helped me pursue this work.

To Jens, Connor, and Marcela, thank you for sticking with me over the last three years through the ups and down of fieldwork and research hiccups. Your patience, guidance, and willingness to help shape and reshape this project into something I am truly passionate about, were more than I could ever ask for in an advising team.

Thank you to my friends and family for supporting me through the stresses of research, often outside of your own busy lives, and for celebrating the wins with me, both small and large.

I would not have made it this far without The Branch School and Paul Revaz. The Branch School nurtured my scientific curiosity, encouraged me to ask questions and seek help, and laid the foundation for this journey. Paul Revaz put a drill in my hand and gave me the confidence and skills to work effectively with tools and instrumentation of all kinds.

I could not have done this without all of you, and I am so grateful.

This research was supported by the Atmospheric Radiation Measurement (ARM) User Facility, a U.S. Department of Energy (DOE) Office of Science user facility managed by the Biological and Environmental Research Program.

Table of Contents

Acknowledgments ..... **iv**
List of Tables ..... **vii**
List of Figures ..... **viii**
Abstract ..... **xiv**
1 Background **1**
Atmospheric Composition 1
Particulate Matter Health Impacts 2
Global Monitoring 6
Public Sector Monitoring 6
Strategy 7
2 Introduction **9**
2.1 Oklahoma 9
2.1.1 Air Quality Contributors 9
2.1.2 Sampling 13
2.1.3 Populations Disproportionately Affected 14
2.2 SPICE Campaign and Dataset 15
2.3 Project Goals and Implications 17
2.4 Primary Science Questions 17
3 Data and Methods **19**
3.1 In-Situ Instrumentation 19
3.1.1 ARM Nephelometer 19
3.1.2 IMPROVE Network 21
3.1.3 SPARTAN 22
3.1.4 Beta Attenuation Monitor 1022 (BAM) 23
3.1.5 PurpleAir 24
3.2 Analysis Methodology for Filter Samples 26
3.2.1 Gravimetric 26
3.2.2 X-ray Fluorescence (XRF) Spectrometry 26
3.2.3 Hybrid Integrating Plate/Sphere (HIPS) Analysis 27
3.2.4 Fourier Transform Infrared (FT-IR) Spectroscopy and Thermal Optical Reflectance (TOR) 27
3.2.5 Ion Chromatography (IC) 28
3.3 Revised SPARTAN Sampling for SPICE 29

3.3.1 Data Collocation..... 33
3.4 Retrieved Variables..... 34
3.5 EPA and WHO PM2.5 Exceedances..... 35
3.6 Data Processing Choices..... 36
3.6.1 OLS vs ODR..... 36
3.6.2 Fine-Mode Dataset..... 38
3.6.3 Nephelometer Calibration..... 40
3.6.4 Blue and Green Derived “Nephelometer-Derived Mass” Comparison..... 42
4 Results..... 47
4.1 In-Situ Instrument Comparison..... 47
4.2 Calibration Tests using Observed Data..... 50
4.2.1 Calibration (Nephelometer-Derived Mass Concentration) and IMPROVE..... 51
4.2.2 Calibration (Nephelometer-Derived Mass Concentration) and SPARTAN..... 57
4.2.3 Calibration (Nephelometer-Derived Mass Concentration) and PurpleAir..... 61
4.3 Calibration Behavior when Extended to Fine Time Scale..... 65
4.4 Application of Calibration to SPICE Dates..... 70
4.5 Application of Calibration to Interpolated Speciation..... 72
5 Discussion..... 76
5.1 Speciation Application Partial Seasonality..... 76
5.2 Implications at the ARM SGP Site..... 80
5.3 Broad Implications..... 81
6 Conclusion..... 84
Bibliography..... 87
Supplementary Material:..... 95

List of Tables

Table 1: Comparison of total DALYs and deaths in the United States and Oklahoma during 2019. (Institute for Health Metrics and Evaluation, n.d)..... 3

Table 2: Comparison of DALYs attributed to ambient particulate matter pollution in the United States and Oklahoma during 2019. The color coding refers to whether the cause is classified as communicable, maternal, neonatal, and nutritional diseases (orange) or non-communicable diseases (blue). (Institute for Health Metrics and Evaluation, n.d)..... 4

Table 3: Comparison of deaths (rather than DALYs as in Table 2). The color coding is identical to that in Table 2. (Institute for Health Metrics and Evaluation, n.d)..... 5

Table 4: List of instruments utilized in this study, as well as their datastream access point and date range of availability.....16

Table 5: Counts of WHO and EPA PM2.5 Exceedance Events: Hourly BAM vs. Consecutive-Duration Nephelometer Criteria..... 72

List of Figures

Figure 1: “Size Comparisons for PM Particles” (US EPA 2016)..... 2

Figure 2: Map of Oklahoma air pollution sources (“Oklahoma Profile, 2023”)..... 10

Figure 3: “Trends in EPA-measured PM2.5. Each point represents an EPA PM2.5 monitor active over the study period (2002-2017), and is color-coded according to the quartiles of the overall trend distribution, where black points represent trends within the interquartile range, blue points represent trends above the third quartile (less decrease than average), and green points represent trends below the first quartile (greater decrease than average).” (Burns et al. 2023)..... 12

Figure 4: Distribution map of Interagency Monitoring of Protected Visual Environments (IMPROVE) Network and the Chemical Speciation Network (CSN) across the United States. Red dots refer to CSN sites and blue dots refer to IMPROVE sites (Dillner, 2016)..... 13

Figure 5: Map of Tribal Jurisdictions in Oklahoma (Kaw Nation & Fox Nation, n.d.)..... 14

Figure 6: Vast majority income map for Oklahoma by county (“Income Map for Oklahoma Counties”, n.d.)..... 15

Figure 7: (A) “TSI model 3563 integrating nephelometer. ARM image” (Uin 2024) and (B) “Nephelometer functional diagram” (Anderson et al. 1996)..... 20

Figure 8: ARM Nephelometer impactor state status time series for February 13, 2025, from the sgpaoppsap1flynn1mE13 datastream..... 21

Figure 9: IMPROVE Sampling Enclosure Diagram (IMPROVE Program, n.d.)..... 22

Figure 10: SPARTAN Network regular 54 day sampling method (A) “Filter arrangement within each cartridge” and (B) “Example of sampling during the 9-day period of each PM2.5 filter” (SPARTAN 2018)..... 23

Figure 11: BAM 1022 and Measurement System (Met One Instruments Inc. 2019)..... 24

Figure 12: PurpleAir Sensor (Sensor Owner’s Guide 2024) and Plantower Laser Counter (PMS5003) (black and white) (Yong 2016)..... 25

Figure 13: 2023 Time series of SOGP1 IMPROVE Station PM2.5 Mass Concentration..... 30

Figure 14: (A) SPARTAN 24-hour sampling method (in use March 17 - October 8, 2025) and (B) SPARTAN 144-hour sampling method (in use October 9 - December 12, 2025) (2025-AQRC-Calendar). The dates with blue backgrounds indicate IMPROVE 24-hour midnight to midnight sample durations. Those with pink lines indicate SPARTAN sample durations..... 32

Figure 15: ARM SGP Central Facility Instrument Locations (“SGP-Central-Facility-Instrument,” n.d.)..... 33

Figure 16: Comparison of ARM nephelometer (1μm) blue total scattering and BAM (2.5μm) PM2.5 Mass Concentration measurements during the SPICE campaign (all points). Points represent concurrent hourly measurements from both instruments. The red line shows the orthogonal distance regression (ODR) fit, and the blue line shows the ordinary least squares (OLS) fit. (A) ARM nephelometer blue total scattering (x-axis) vs. BAM PM2.5 mass concentration (y-axis). (B) BAM PM2.5 mass concentration (x-axis) vs. ARM nephelometer blue total scattering (y-axis)..... 37

Figure 17: ARM nephelometer (1μm) blue total scattering and BAM (2.5μm) PM2.5 Mass Concentration measurements during the SPICE campaign. Points represent concurrent hourly measurements. The red line shows the orthogonal distance regression (ODR) fit; blue dots indicate measurements excluded, and orange dots indicate measurements included due to fine-mode fraction (FMF) filtering. (A) Fine-Mode Fraction (FMF) ≥ 0.80, (B) FMF ≥ 0.85, (C) FMF ≥ 0.90, and (D) FMF ≥ 0.95.....39

Figure 18: Orthogonal distance regression (ODR) for SPICE duration when fine-mode fraction FMF ≥ 0.85 using hourly nephelometer data. Points represent concurrent hourly measurements. The red line shows the ODR fit; grey dots indicate measurements excluded due to FMF filtering. (A) ARM nephelometer blue total scattering (1μm) vs. BAM PM2.5 Mass Concentration (2.5μm), with blue dots indicating included points. (B) ARM nephelometer green total scattering (1μm) vs. BAM PM2.5 Mass Concentration (2.5μm), with green dots indicating included points.. 41

Figure 19: Time series of BAM, green nephelometer-derived, and blue nephelometer-derived PM2.5 mass concentrations using hourly 1μm nephelometer data. (A) All available BAM and Neph data points for the SPICE duration (not filtered for fine-mode fraction, FMF). (B) All available BAM and Neph data points for May 2025 (not filtered for FMF). (C) Concurrent BAM and Neph data points for May 2025 when FMF ≥ 0.85.....42

Figure 20: Time series of BAM and nephelometer-derived PM2.5 mass concentrations using hourly 1μm and 10μm nephelometer data for March 2025. (A) Green nephelometer-derived PM2.5 Mass Concentrations and (B) Blue nephelometer-derived PM2.5 Mass Concentrations.. 44

Figure 21: Time series of BAM and blue nephelometer-derived PM2.5 mass concentrations. (A) All available BAM and hourly 1μm nephelometer data points for the SPICE duration (not filtered for fine-mode fraction, FMF). (B) Concurrent BAM and hourly 1μm nephelometer data points for the SPICE duration when FMF ≥ 0.85..... 46

Figure 22: Concurrent daily PM2.5 mass comparison (all concurrent observations). Daily averages were calculated from BAM and nephelometer hourly measurements. (A) Comparison among SPARTAN (lime green), BAM (black), and IMPROVE (green). (B) Comparison among SPARTAN (lime green), BAM (black), IMPROVE (green), and PurpleAir (purple)..... 49

Figure 23: Orthogonal distance regression (ODR) comparisons of concurrent daily PM2.5 mass concentrations. Daily averages were calculated from BAM and nephelometer hourly measurements. (A) BAM vs SPARTAN (after outlier rejection), (B) BAM vs IMPROVE (all points), (C) IMPROVE vs SPARTAN (after outlier rejection). Blue-grey points in (A) and (C) indicate observations excluded as outliers due to large discrepancies between SPARTAN and the comparison instruments, as shown in Figure 22.....50

Figure 24: Concurrent daily PM2.5 mass concentration comparison for August-October 2025. Daily averages were calculated from BAM and nephelometer hourly measurements. Bars represent 1μm nephelometer-derived mass concentration (blue), BAM (black), and IMPROVE (green). This data was not filtered according to fine-mode fraction (FMF).....51

Figure 25: Time series of PM2.5 Mass Concentrations measured by BAM, 1μm nephelometer-derived mass concentration, 10μm nephelometer-derived mass concentration, and IMPROVE. Nephelometer-derived values use hourly measurements. Blue shading indicates the IMPROVE sampling duration. This data was not filtered according to fine-mode fraction (FMF). (A) SPICE campaign duration. (B) March 2025..... 53

Figure 26: Orthogonal distance regression (ODR) between 1μm nephelometer-derived and IMPROVE measured PM2.5 mass concentrations for January-October 22, 2025. Daily averages were calculated from the nephelometer hourly measurements. Points represent concurrent daily averages; the red line shows the ODR fit, and the blue shading indicates the 1σ confidence interval of the fit. (A) All data points when fine-mode fraction (FMF) ≥0.85. (B) Data not filtered for FMF, with May data unavailable. (C) Same as (B), with additional masking of days when the absolute difference between IMPROVE-observed and nephelometer-derived PM2.5 is ≥ 30 μg m-3.....54

Figure 27: Daily PM2.5 exceedances for collocated instruments from January to October 2025. Bars show the number of days that the daily average PM2.5 mass exceeded 15 μgm-3 (left) or 35 μgm-3 (right) for 1μm and 10μm nephelometer-derived mass concentration, BAM, and IMPROVE. Daily averages were calculated from hourly nephelometer and BAM measurements. This data was not filtered according to fine-mode fraction (FMF). This data is limited to the concurrent days shown in Figure S2.....57

Figure 28: Concurrent daily PM2.5 mass comparison (all concurrent observations). Daily averages were calculated from BAM and nephelometer hourly measurements by averaging over the SPARTAN sampling period for as many days as exist. Bars represent 1μm nephelometer-derived mass concentration (blue), BAM (black), and SPARTAN (lime green). This data was not filtered according to fine-mode fraction (FMF)..... 58

Figure 29: Time series of PM2.5 Mass Concentrations measured by BAM, 1μm nephelometer-derived mass concentration, 10μm nephelometer-derived mass concentration, and SPARTAN. Nephelometer-derived values use hourly measurements. Blue shading indicates the SPARTAN sampling duration. This data was not filtered according to fine-mode fraction (FMF). (A) Available SPARTAN duration (March-November 2025). (B) April-May 2025..... 59

Figure 30: Orthogonal distance regression (ODR) between 1μm nephelometer-derived and SPARTAN measured PM2.5 mass concentrations (all concurrent observations). Daily averages were calculated from the nephelometer hourly measurements. Points represent concurrent daily averages; the red line shows the ODR fit, and the blue shading indicates the 1σ confidence interval of the fit. Orange and grey dots indicate days when the SPARTAN was operating on the 144-hour and 24-hour sampling schedules, respectively. This data was not filtered according to fine-mode fraction (FMF)..... 60

Figure 31: Concurrent daily PM2.5 mass comparison for August-September 2025. Daily averages were calculated from BAM and nephelometer hourly measurements. Bars represent 1μm nephelometer-derived mass concentration (blue), BAM (black), and PurpleAir (purple). This data was not filtered according to fine-mode fraction (FMF)..... 61

Figure 32: Time series of PM2.5 Mass Concentrations measured by BAM, 1μm nephelometer-derived mass, 10μm nephelometer-derived mass, and PurpleAir. Nephelometer-derived values use hourly measurements. This data was not filtered according to fine-mode fraction (FMF). (A) Available PurpleAir duration (August 15, 2025 - February 2, 2026). (B) December 2025..... 62

Figure 33: Orthogonal distance regression (ODR) between 1μm nephelometer-derived and PurpleAir measured PM2.5 mass concentrations for August 15, 2025-February 2, 2025. Daily averages were calculated from the nephelometer hourly measurements. Points represent concurrent daily averages; the red line shows the ODR fit, and the blue shading indicates the 1σ confidence interval of the fit. This data was not filtered according to fine-mode fraction (FMF).... 63

Figure 34: Daily PM2.5 exceedances for collocated instruments from August 15, 2025, to February 2, 2025. Bars show the number of days that the daily average PM2.5 mass exceeded 15 μgm-3 (left) or 35 μgm-3 (right) for 1μm and 10μm nephelometer-derived mass concentration, BAM, and PurpleAir. Daily averages were calculated from hourly nephelometer and BAM measurements. This data was not filtered according to fine mode fraction (FMF)..... 65

Figure 35: Time series of hourly 1μm nephelometer-derived mass concentration (royal-blue), hourly 10μm nephelometer-derived mass concentration (lavender), minutely 1μm nephelometer-derived mass concentration (cyan), and minutely 10μm nephelometer-derived mass concentration (faded cyan). This data was not filtered according to fine-mode fraction (FMF). (A) April 2025. (B) April 16, 2025..... 66

Figure 36: Time series of hourly BAM (grey), minutely 1μm nephelometer-derived mass concentration (cyan), and minutely 10μm nephelometer-derived mass concentration (faded cyan). This data was not filtered according to fine-mode fraction (FMF). (A) SPICE Campaign Duration. (B) April 16, 2025..... 68

Figure 37: Time series of PM2.5 Mass Concentrations measured by PurpleAir (purple), 1μm nephelometer-derived mass (cyan), and 10μm nephelometer-derived mass (faded cyan) for October 2025. Nephelometer-derived values and PurpleAir use minutely measurements. This data was not filtered according to fine-mode fraction (FMF).....69

Figure 38: All available daily PM2.5 exceedances for collocated instruments from January to October 2025. Bars show the number of days that the daily average PM2.5 mass exceeded 15 μgm-3 (left) or 35 μgm-3 (right) for 1μm and 10μm nephelometer-derived mass concentration (hourly and minutely datasets), BAM, and PurpleAir. Daily averages were calculated from hourly nephelometer and BAM measurements except in the case of the minutely nephelometer-derived mass concentrations. SPARTAN's exceedance is due to a coarse-mode-dominant day measured with PM10 filter conditions. This data was not filtered according to fine-mode fraction (FMF)..... 70

Figure 39: Time series of speciated PM2.5 mass concentration depicting only compounds that have a mean mass fraction ≥ 10% of the total mass for the duration of IMPROVE speciated data availability (January - May 1, 2025). This data was not filtered according to fine-mode fraction (FMF). (A) IMPROVE Network PM2.5 Dataset (sampled every third day). (B) Average estimated mass concentration using both PM10 and PM2.5 mode data from the minutely dataset. (C) Estimated speciated mass concentration using the hourly nephelometer dataset and IMPROVE mass fractions to interpolate missing days. (D) Estimated speciated mass concentration using the minutely nephelometer dataset and IMPROVE mass fractions to interpolate missing days. In plots (C) and (D), dotted lines show values associated with PM10 observations, while solid lines are PM2.5. Plots (B), (C), and (D) use mass fraction to interpolate the mass of and identity of contributing compounds when there are ≤ 2 days between IMPROVE measurements.....75

Figure 40: SOGP1's seasonal aerosol composition (January-April 2025)with partial seasonally averaged daily $PM_{2.5}$ mass concentrations (μg/m^3). The left column represents IMPROVE observed data, while the right column of pie charts represents the data from the interpolated estimation.....77

Figure 41: Five-year (2020-January 1, 2025) monthly average PM2.5 mass concentration for SOGP1 (top) and five-year monthly speciated average PM2.5 mass concentration for SOGP1 (bottom).....78

Figure 42: January - April 2025 Monthly average PM2.5 mass concentration for SOGP1 (top) and January - April 2025 Monthly average speciated PM2.5 mass concentration for SOGP1 (bottom).....79

Figure 43: Five-year average (2020-January 1, 2025) of SOGP1's Seasonal Aerosol Composition with Seasonally Averaged Daily PM2.5 Mass Concentrations (μg/m3). Spring (MAM) and Winter (DJF) are boxed for easier comparison with Figure 40..... 80

Figure S1: ARM nephelometer (1μm) blue total scattering and BAM (2.5μm) PM2.5 Mass Concentration measurements during a portion of 2025 with uncertainty. Points represent concurrent hourly measurements. The red line shows the orthogonal distance regression (ODR) fit; blue dots indicate measurements excluded, and orange dots indicate measurements included due to fine-mode fraction (FMF) filtering. (A) Fine-Mode Fraction (FMF) ≥ 0.80, (B) FMF ≥ 0.85, (C) FMF ≥ 0.90, and (D) FMF ≥ 0.95..... 95

Figure S2: Concurrent daily PM2.5 mass concentration comparison for August-October 2025. Daily averages were calculated from BAM and nephelometer hourly measurements. Bars represent 1μm nephelometer-derived mass concentration (blue), BAM (black), and IMPROVE (green). This data was not filtered according to fine-mode fraction (FMF). (A) January-April 2025. (B) May-August 2025. May data is unavailable. (C) September-October 2025..... 96

Figure S3: Concurrent daily PM2.5 mass comparison for August-September 2025. Daily averages were calculated from BAM and nephelometer hourly measurements. Bars represent 1μm nephelometer-derived mass concentration (blue), BAM (black), and PurpleAir (purple). This data was not filtered according to fine-mode fraction (FMF). (A) August-September 2025. (B) October-November 2025. (C) December 2025 - February 2026.....98

Figure S4: PM2.5 measuring site locations in Oklahoma with one site per county and U.S. population by County (“B0103: Total–Estimate”, 2021). (A) PM2.5 mass concentration measuring sites, including Teledyne T640 real-time PM Monitor, Thermo Scientific Model 2025 Sequential Air Sampler, and Met One Environmental Federal Reference Method Sampler (E-FRM). (B) PM2.5 speciated mass concentration measuring sites, including the CSN and IMPROVE network..... 99

Abstract

Aerosols are suspended solid or liquid particles in the atmosphere and, when inhaled, can affect human cardiorespiratory health and contribute to reduced quality of life. In the United States, two nationwide monitoring networks measure total aerosol mass concentrations and identify aerosol chemical composition: the Interagency Monitoring of Protected Visual Environments (IMPROVE) network and the Chemical Speciation Network (CSN). IMPROVE was established to maintain visual accessibility to natural environments and is present in more rural regions, particularly in national parks. The CSN was developed to help monitor aerosols with respect to human health implications and is therefore located in more urban communities. These networks provide valuable information to nearby communities, but station density in the central plains is sparse, leaving few stations near rural areas. The goal of this study was to expand access to total aerosol mass and speciated aerosol data by developing proxy measurements derived from nephelometer observations.

While IMPROVE and CSN rely on filter-based sampling that requires laboratory analysis and may take weeks to months before data become available, nephelometers produce measurements in near real time. Similarly, EPA-certified instruments such as the Beta Attenuation Monitor (BAM) provide more rapidly accessible data, with averaging intervals that can be set to 1, 5, 10, 15, and 30 minutes. However, the standard operating procedure reports hourly averages. Unlike the BAM, nephelometers measure aerosol scattering rather than mass concentration. In this study, observations from a BAM were used as the reference aerosol mass concentration to calibrate nephelometer measurements and develop a nephelometer-derived $PM_{2.5}$ mass concentration estimate. This calibration uses the optical measurements of blue-wavelength total scattering (Bs_B, Bs_B_1um, and Bs_B_10um) to estimate $PM_{2.5}$ mass

concentration. The resulting nephelometer-derived mass concentrations were compared with observations from a collocated IMPROVE station, PurpleAir sensor, and a SPARTAN site, as well as a five-year climatological site average derived from pre-campaign IMPROVE data, to evaluate the nephelometer-derived mass concentration performance.

While shorter averaging periods (minutely, hourly, and daily) exhibit greater apparent discrepancies, longer-term averages (monthly, seasonal, and annual) demonstrate strong agreement. This consistency at longer timescales highlights the robustness of the nephelometer-derived approach for characterizing overall $PM_{2.5}$ trends, despite variability at shorter temporal resolutions. The short-term measurement differences (maximum of only ± ~ 6 $\mu g/m^3$) likely arise from either the averaging of instantaneous peaks by existing measurement systems or the underestimation of $PM_{2.5}$ mass concentration in nephelometer-derived estimates under coarse-mode-dominated conditions. Despite these differences, short-term measurements from the BAM and the nephelometer proxy remain particularly valuable for identifying episodic pollution events and short-duration exposure peaks that may have important implications for human health.

To further expand the available dataset, speciated $PM_{2.5}$ mass concentrations were interpolated to fill gaps in the IMPROVE observational record. This approach used existing IMPROVE measurements to determine speciated mass fractions, which were then scaled by the nephelometer-derived total mass estimates to produce speciated $PM_{2.5}$ mass concentration estimates. When compared with five-year averages, the interpolated speciation results for the available months in 2025 were generally consistent with the longer-term record.

This work demonstrates that nephelometer-derived measurements can improve the temporal availability of aerosol mass and speciated aerosol data relative to existing monitoring

approaches. Higher-temporal resolution information on aerosol composition has potential applications in public health, environmental monitoring, and industry. Moreover, the nephelometer-derived total mass relationship developed here may be broadly applicable to other locations that have access to nephelometer measurements, such as sites supported by the Atmospheric Radiation Measurement (ARM) Program's mobile facilities.

Chapter 1

Background

Atmospheric Composition

The atmosphere is composed of gases and small airborne solid or liquid particles called aerosols. The atmospheric layer that humans inhabit is called the troposphere, and while it is, for the most part, consistently habitable, it is sensitive to physical and chemical atmospheric processes, and continually changing. Naturally occurring pressure changes and weather events can alter the boundary layer, as can human activities. Notable pollutant-caused events in the troposphere are acid rain and smog. These examples rely on chemical reactions involving the standard atmospheric composition, water vapor, and additional gases (e.g., SO2 and O3, respectively) released by human activities (e.g., production, transport, and domestic practices). However, gases are not the only byproducts of life that can influence air quality in the troposphere. Aerosols are produced naturally (e.g., volcanoes, wildfire, pollen, dust, or ocean spray) and with human assistance (e.g., combustion and fabrication processes).

Aerosols can be anywhere from a few nanometers in diameter to several micrometers and are often classified by their size; in this case, they are commonly referred to as particulate matter (PM), as shown in Figure 1. Like any pollutant, particulate matter can have adverse environmental impacts such as decreased visibility, obnoxious smells, or cause breathing difficulties. In 2023, ambient air pollution, which is exclusively outdoor air pollution, was responsible for 3.5 million premature deaths globally (WHO, 2023).

Particulate Matter Health Impacts

$PM_{2.5}$ is any particulate matter with a diameter of 2.5 micrometers or less (New York State Department of Health, 2024). $PM_{2.5}$ is detrimental to human health (Figure 1) because it is small enough to bypass the body's natural defenses (eyelashes, nose hairs, mucus, etc.) and embed in the lungs. Several notable health conditions that affect the cardiovascular system, respiratory system, and neonatal development are summarized in Table 1. Numerous studies have shown that exposure to $PM_{2.5}$ can contribute to health problems across all age groups ("Inhalable Particulate Matter," n.d.). Exposure is classified as acute or chronic. Chronic exposure to poor air quality can be described as prolonged exposure to low/moderate levels of pollution; it affects the body slowly, but continuous inhalation of the air can result in health problems later (delayed response of years-decades). Acute exposure is more instantaneous and can occur with short (minutes to days) exposure durations; exposure to high levels of air pollution can cause distress in minutes to weeks after exposure.

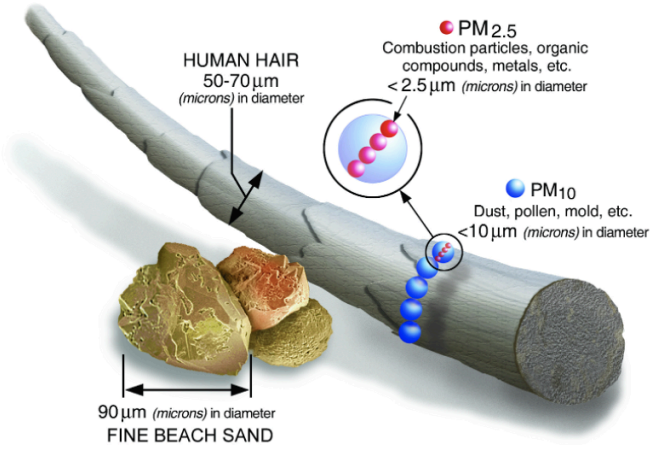

Figure 1: "Size Comparisons for PM Particles" (US EPA 2016)

Acute exposures do not necessarily mean that the $PM_{2.5}$ levels are high; rather, relatively small doses of toxic compounds can also be an acute exposure. For example, the U.S. Environmental Protection Agency (EPA) recommends that 24-hour averaged $PM_{2.5}$ not exceed 35 $\mu m/m^3$, however, according to the National Institude of Occupational Safety and Health

(NIOSH), exposure to airborne arsenic, a known carcinogen, should be limited to below 2 μm/m^3 at all times ("*2012_aqi_factsheet*", 2016; "*Hazardous Substance Fact Sheet*", 2008).

Disability-Adjusted Life Years (DALYs) are a measure used to assess the global burden of disease (Tulchinsky & Varavikova, 2014). One DALY is statistically equivalent to the loss of one year of healthy life (WHO, n.d.; WHO 2024). In 2019, Oklahoma had ~0.3% more DALYs attributed to ambient particulate matter pollution than the United States as a whole. This result is striking because, given the state's extensive rural areas, Oklahoma is not generally considered a pollution hotspot. While DALYs are a useful measure of reduced quality of life, they do not fully capture the magnitude of the problem. Table 1 shows the total DALYs and deaths attributed to all causes for both the United States and Oklahoma in 2019.

Table 1: Comparison of total DALYs and deaths in the United States and Oklahoma during 2019. (Institute for Health Metrics and Evaluation, n.d)

	United States	**Oklahoma**
DALYs (years of healthy life lost)	113,380,751.09	1,571,121,4
Deaths (number of deaths)	2,856,704.42	40,666.41

Table 2: Comparison of DALYs attributed to ambient particulate matter pollution in the United States and Oklahoma during 2019. The color coding refers to whether the cause is classified as communicable, maternal, neonatal, and nutritional diseases (orange) or non-communicable diseases (blue). (Institute for Health Metrics and Evaluation, n.d)

Disease	United States (% of total DALYs attributed to ambient particulate matter pollution)	Oklahoma (% of total DALYs attributed to ambient particulate matter pollution)	Difference (Oklahoma - United States)
Ischemic Heart Disease (IHC)	0.35	0.50	+ 0.15
Stroke	0.15	0.18	+ 0.03
Lung Cancer	0.15	0.19	+ 0.04
Diabetes	0.22	0.25	+ 0.03
Chronic Obstructive Pulmonary Disease (COPD)	0.16	0.21	+ 0.05
Neonatal Disorders	4.09×10^{-2}	4.42×10^{-2}	+ 3.3×10^{-3}
Lower Respiratory Infections (LRI)	2.91×10^{-2}	3.34×10^{-2}	+ 4.3×10^{-3}

The deadly consequences of ambient particulate matter pollution are shown in Table 3. Ambient particulate matter pollution is attributed to ~1.6% of all deaths in the United States and ~2.0% in Oklahoma in 2019 (Table 3). For reference, road injury fatalities were responsible for 1.4% and 1.75% in the United States and Oklahoma, respectively, in 2019, and 640 lives were lost due to road injuries in Oklahoma alone (Institute for Health Metrics and Evaluation, n.d; Martin Jean & Jackson, n.d.).

Table 3: Comparison of deaths (rather than DALYs as in Table 2). The color coding is identical to that in Table 2. (Institute for Health Metrics and Evaluation, n.d)

Disease	United States (% of total deaths attributed to ambient particulate matter pollution)	Oklahoma (% of total deaths attributed to ambient particulate matter pollution)
Ischemic Heart Disease (IHC)	0.65	0.86
Stroke	0.22	0.26
Lung Cancer	0.28	0.33
Diabetes	0.15	0.17
Chronic Obstructive Pulmonary Disease (COPD)	0.24	0.32
Neonatal Disorders	1.71×10^{-2}	1.84×10^{-2}
Lower Respiratory Infections (LRI)	7.20×10^{-2}	7.37×10^{-2}

Environmental equity is "the equitable distribution of environmental protection benefits" so that no group of people or community is disproportionately affected by environmental problems (US EPA, 1992). The personal danger of $PM_{2.5}$ can be assessed using an equation that accounts for the pollution level, frequency of exposure, and duration of exposure. Populations that are especially susceptible to harmful $PM_{2.5}$ exposure can be categorized into two groups: those who spend more time than average outdoors (landscapers, farmers, homeless populations) and individuals with more fragile physiological systems (children, older adults, immunocompromised individuals). While the exposure of landscapers and farmers may be classified as an occupational risk, environmental equity needs to be considered if these careers are made up of a disproportionate number of people from minority backgrounds or who are living below the poverty line. It must also be considered for homeless populations and individuals with more fragile body systems.

Global Monitoring

Public Sector Monitoring

Beyond the human health impacts, air quality and aerosol pollution are increasingly studied fields due to their importance in a variety of disciplines (Vilcassim et al., 2023). As of 2021, 51% of countries do not have air quality data access (Bishop 2025). Globally collaborative ground observation networks are notably less common, causing researchers to turn to satellite data that, while informative, is less resolved than in-situ measurements, especially in the lower atmosphere (Xin et al. 2015; Nguyen et al. 2019). Globally extensive aerosol monitoring efforts, such as the AErosol RObotic NETwork (AERONET) and NOAA's Global Monitoring Laboratory's Aerosol Network, are used to characterize aerosols and their contributing factors to improve health and climate modeling (GML Web Team, n.d.; Smirnov et al. 2002). Both of these networks have regulated instruments and are increasingly used to validate satellite remote sensing data for aerosol studies; their major difference comes down to AERONET being a standardized network of sun/sky radiometers for optical property observations, while the Aerosol Network is a variety of instruments including a nephelometer, an absorption photometer, and a condensation nuclei counter (GML Web Team, n.d.; Smirnov et al. 2002; GML Web Team 1996).

Strategy

According to a 2021 United Nations Environment Programme (UNEP) report, approximately one-third of countries lack legally mandated ambient air quality standards (Rukikaire 2021). While monitoring and regulation practices are improving, and more countries are committing to implementing air quality standards and creating monitoring networks, there is still work to be done (WHO Media Team, n.d.; Beagley, n.d.). The World Health Organization (WHO) sets air quality guidelines to help countries achieve healthy air quality standards and improve global air

quality conditions (Bishop 2025). These standards are expressed as mass concentration ($\mu g/m^3$) and are recommended for a 24-hour period.

In the United States, EPA Air Quality Index (AQI) alerts rely on mass concentration ($\mu g/m^3$) measurements to assess the risk that PM in the air poses to exposed populations. While this method is widely used, research increasingly suggests that it may not be the most accurate for assessing the health risks associated with air pollution (El Haddad et al., 2023). Given the substantial number of deaths attributable to ambient particulate matter, experts advocate for incorporating specific PM components as more precise indicators in health risk assessments (El Haddad et al., 2023).

More detailed requirements would move systems, such as AQI alerts, away from reliance on mass concentrations. Instead of every aerosol being weighed as equally dangerous with respect to its mass, the most damaging compounds would be considered more significantly, even in low doses. One such component is aerosol oxidative potential, which is the potential of an aerosol to "generate reactive, oxygen-based chemicals that can lead to a variety of health problems in the cells of lung tissue" (Yoksoulian, 2022). While the "relationship between $PM_{2.5}$ mass and toxicity is [still] unclear," a group at the University of Illinois Urbana-Champaign has shown that, despite the "misconception that air pollution is more toxic in urban areas than in rural areas," the oxidative potential for aerosols in rural areas are roughly equal to those of urban areas and are therefore just as dangerous (Yoksoulian, 2022). Studies that use oxidative potential to assess pollutants' danger to human health, such as Yoksoulian's, are quite expensive. However, chemically speciated aerosol data can provide similarly informative guidance and limit additional costs. Monitoring the chemical composition of the aerosols, rather than the mass alone, can help mitigate risks to human health.

Chapter 2

Introduction

2.1 Oklahoma

2.1.1 Air Quality Contributors

Air quality is not a new concern in Oklahoma. Oklahoma is home to several active superfund sites, including Tar Creek. Efforts to clean up the Tar Creek site have been ongoing since 2000, but the danger, mining waste referred to as 'chat', is still present ("Tar Creek Superfund Site," n.d.). The piles of chat have been a danger to respiratory health since the beginning, as the dust-like substance can be blown into neighboring communities by the wind (US EPA 2024). While these sites may have relatively small radii of influence, Oklahoma's semi-arid climate, erodible soils, and strong winds contribute to elevated dust levels, exposing populations to a disproportionate amount of aerosolized matter (Salazar et al., 2025).

According to the United States Geological Survey (USGS), Northeast Oklahoma is in the 90th-100th percentile for cadmium, arsenic, and lead geochemistry in the top 0-5 cm of the soil (Smith et al, n.d). Although this is a result of Tar Creek's waste, a study by Oklahoma State University found that Oklahoma has a higher background arsenic concentration than the EPA's Residential Screening Levels (SLs) due to the state's natural geology. These studies are important for preventing unnecessary environmental rehabilitation and for monitoring soil dispersion associated with inhaled particulates (Zhang 2017).

The prevalence of rural land in Oklahoma is important when assessing the contribution of agricultural activities to $PM_{2.5}$ production. Emissions from diesel-powered farm vehicles can react with other atmospheric components to form $PM_{2.5}$. Additionally, the vehicles can stir up

dust and fine particulates that can travel in plumes and degrade air quality. Prescribed burns and smaller agricultural burns, which are common in Oklahoma, create smoke $PM_{2.5}$ that is harmful to the human body and can be transported by wind. Moreover, extensive road networks for transporting goods across the state and Oklahoma's lack of annual vehicle inspections facilitate the statewide distribution of $PM_{2.5}$ emitted by vehicles. Likewise, combustion-fueled (biomass, coal, natural gas, and petroleum) power plants, along with petroleum refineries across the state, are additional sources of potentially harmful $PM_{2.5}$ (Figure 2).

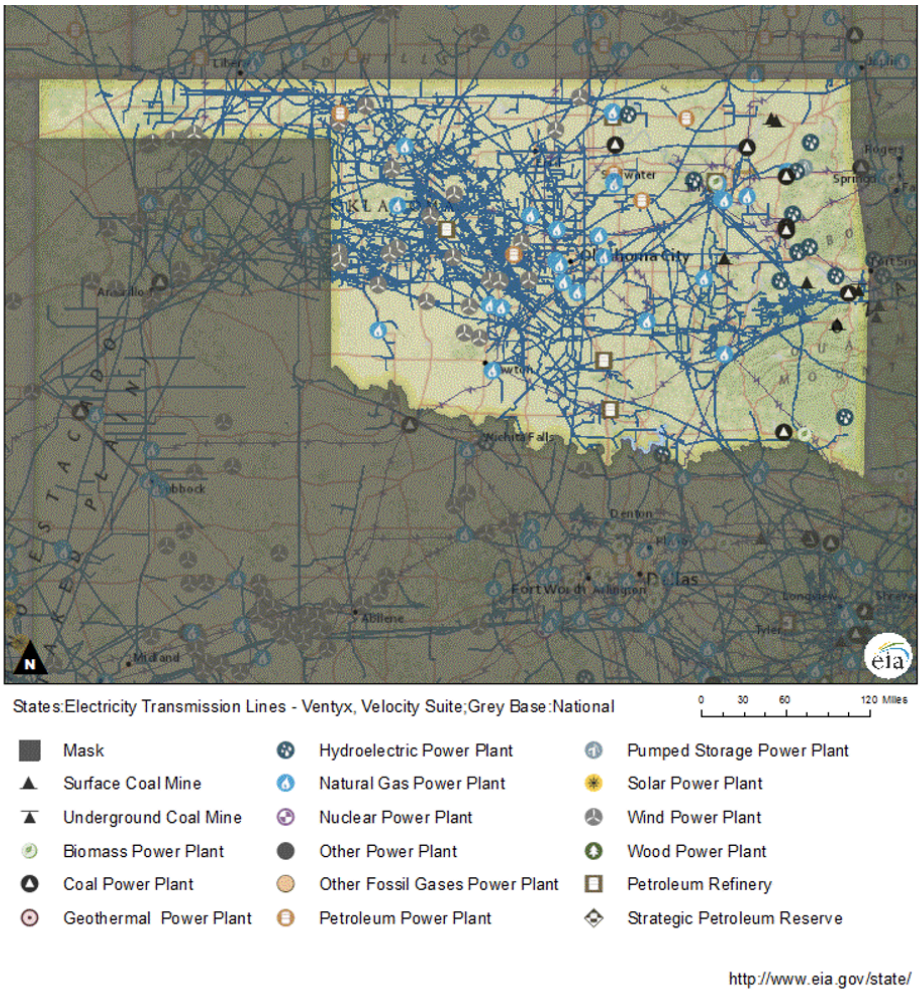

Figure 2: Map of Oklahoma air pollution sources ("Oklahoma Profile, 2023")

In rural communities, a particular concern is organic dust, which is present in agricultural environments and can be generated during agricultural processes. Organic dust can carry molds, bacteria, pesticides, chemicals, and animal particles, including droppings (“Youth in Agriculture," n.d.). Each of these can cause health problems via inhalation of organic dust. Histoplasmosis is an example of one such illness and is caused by the inhalation of organic dust containing a fungus, which can be in the droppings of chickens or other birds (“Histoplasma Capsulatum," n.d.). This is an especially important disease because it is often misdiagnosed, and delays in treatment can cause increased problems or death (CDC, 2023).

Furthermore, biosolid (sewage sludge) fertilizer, a byproduct of sewage treatment, was used as an affordable and recyclable option in Oklahoma, where approximately 80% of the produced sludge was repurposed and applied to farms (Zhang 2017). While its supply was regenerative, Katz et al. found MCCPs (medium chain chlorinated paraffins), which are toxic, in the air at the Department of Energy’s Atmospheric Radiation Measurement (DOE ARM) Site in Billings, Oklahoma (Katz et al. 2025b). MCCPs break down slowly, like ‘forever chemicals’ (PFAS). The Oklahoma State Senate passed a bill in 2025 that prohibits the land use of biosolid fertilizer after July 1, 2027, due to the prevalence of these MCCPs in the soil, but it died in the Oklahoma State House (Green 2025; Oklahoma State Legislature, n.d.). Towns, however, have independently voted to ban the fertilizer as early as 2020 (Felder 2024). Katz et al.’s study was the first detection of airborne MCCPs in the western hemisphere (Katz et al. 2025a).

In a related context, Burns et al.’s study investigated ammonia emissions from large-scale farming operations (CAFOs) in the Midwest U.S. (Burns et al. 2023). Using satellite data, they found ammonia emission hot spots in areas where CAFOs used anaerobic lagoons to break down animal waste. While not every livestock operation uses this method, every livestock operation

produces ammonia, which is a precursor to $PM_{2.5}$ formation, and is not regulated by National Ambient Air Quality Standards (NAAQS). Burns et al. concluded that existing air quality networks do not conclusively monitor agricultural air pollution ($PM_{2.5}$) and have shown that sites in the central United States, including Oklahoma, have $PM_{2.5}$ trends that are decreasing more slowly than average.

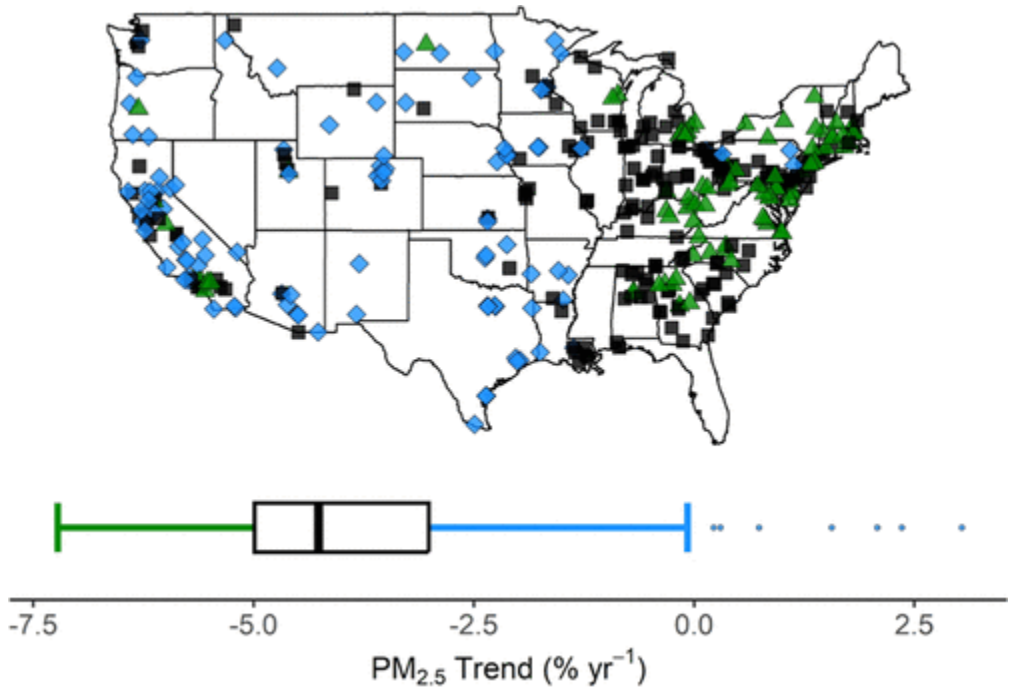

Figure 3: "Trends in EPA-measured $PM_{2.5}$. Each point represents an EPA $PM_{2.5}$ monitor active over the study period (2002-2017), and is color-coded according to the quartiles of the overall trend distribution, where black points represent trends within the interquartile range, blue points represent trends above the third quartile (less decrease than average), and green points represent trends below the first quartile (greater decrease than average)." (Burns et al. 2023)

2.1.2 Sampling

There are 27 air quality stations in Oklahoma. 12 of the Oklahoma stations measure $PM_{2.5,}$ and only 2 have chemical speciation capabilities that provide a more accurate understanding of aerosol composition ("Current Air Quality & Forecasts," n.d.). There are two extensive nationwide chemical speciation networks for aerosol monitoring in the United States (Figure 4): the first is the Interagency Monitoring of Protected Visual Environments (IMPROVE) Network, and the second is the Chemical Speciation Network (CSN). The IMPROVE Network (1985) was established and expanded in response to the Clean Air Act (1963) and the Regional Haze Rule (1999), both of which aim to preserve clean air and visibility in protected environments, e.g., national parks (IMPROVE Program, n.d.; US EPA 2015). The CSN was established after the NAAQS review (1997) to monitor aerosol composition (speciation) for health purposes (US EPA 2017). Both networks' chemical speciation components are important for improving the environmental equity of breathable air. However, while these networks are quite extensive, their representativeness is not equal. The distribution of sites within the eastern and western U.S. is more dense than in the

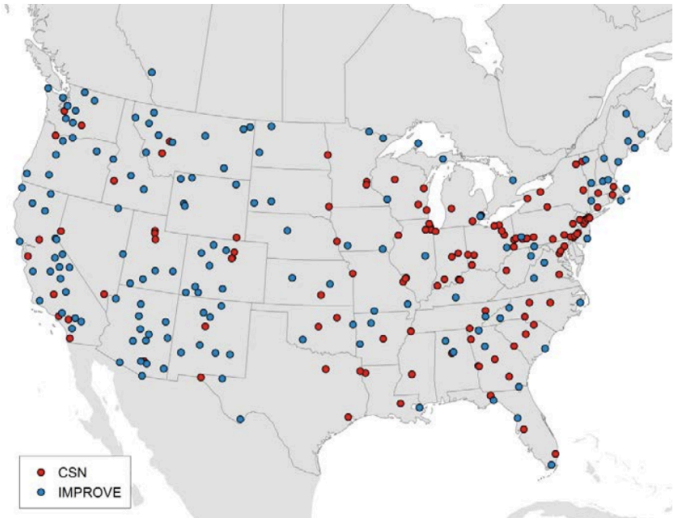

Figure 4: Distribution map of Interagency Monitoring of Protected Visual Environments (IMPROVE) Network and the Chemical Speciation Network (CSN) across the United States. Red dots refer to CSN sites and blue dots refer to IMPROVE sites (Dillner, 2016)

central United States, leaving numerous communities without access to applicable exposure information. The distribution of sensors, both speciating and mass concentration only, is shown in Supplementary Figure S4 with respect to county populations.

2.1.3 Populations Disproportionately Affected

Oklahoma is unique in that, with 37 federally recognized tribes, it has the largest relative population of indigenous people in the contiguous 48 United States ("Native American Population by State 2024", n.d.). When comparing the pollution source map (Figure 2) with the tribal jurisdictions (Figure 5) and the vast majority income (Figure 6), it becomes apparent that communities, especially those in eastern Oklahoma with increased tribal jurisdictions and the lowest income, could be disproportionately affected by air quality issues attributed to ambient particulate matter. This is especially important regarding environmental equity in Oklahoma.

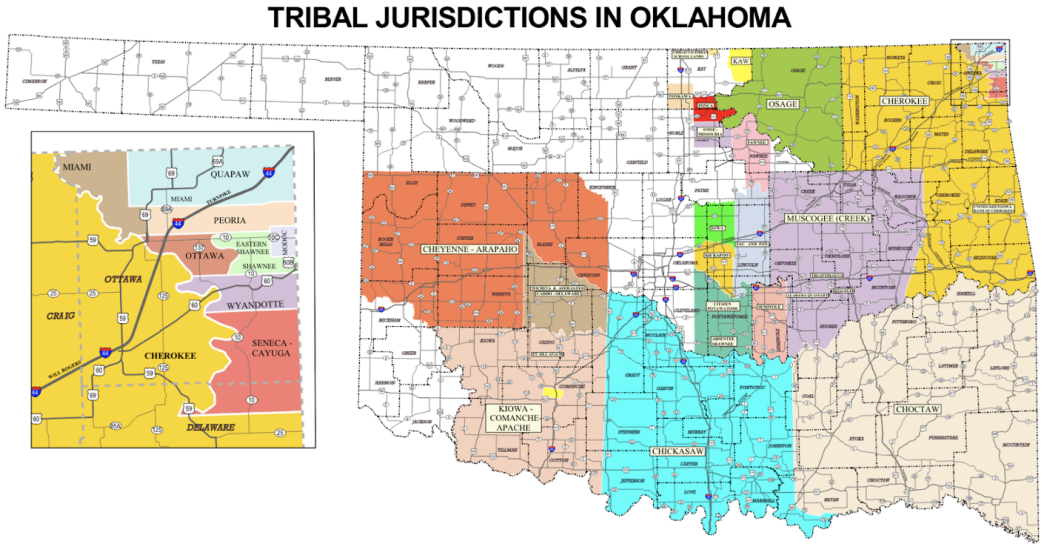

Figure 5: Map of Tribal Jurisdictions in Oklahoma (Kaw Nation & Fox Nation, n.d.)

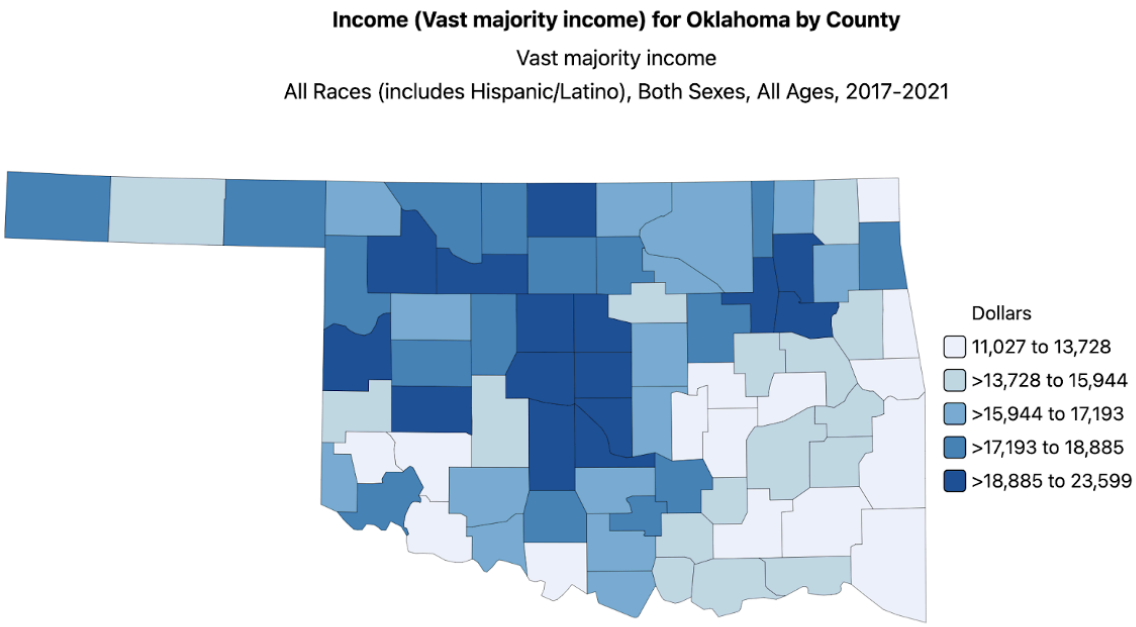

Figure 6: Vast majority income map for Oklahoma by county ("Income Map for Oklahoma Counties", n.d.)

2.2 SPICE Campaign and Dataset

The **SP**ARTAN **I**MPROVE **C**omparison **E**xperiment (SPICE) Campaign was a year-long proof-of-concept study to demonstrate that an 'aerosol pod' performs comparably to IMPROVE filter measurements and can be deployed in undersampled regions to reduce aerosol data sparsity. The installation operated for one year (January 1, 2025 - February 2, 2026) at the Department of Energy's (DOE) Atmospheric Radiation Measurement (ARM) Southern Great Plains (SGP) Site in Billings, OK. The 'aerosol pod', comprised of one Surface Particulate Matter Network (SPARTAN) sampling station and an AirPhoton IN102 nephelometer, and one Beta Attenuation Monitor (BAM), was compared to a collocated Interagency Monitoring of Protected Visual Environments (IMPROVE) station. A PurpleAir sensor was added in August of 2025.

During the campaign, an issue was identified with the SPARTAN nephelometer. To address this, the collocated ARM nephelometer was used in place of the SPARTAN nephelometer. This study uses all available data from January 2025 to February 2, 2026. Due to the labor-intensive nature of filter analysis, coverage varies between published and preliminary data. For this study, the following datasets were used:

Table 4: List of instruments utilized in this study, as well as their datastream access point and date range of availability

	Start Date	End Date
IMPROVE (Official) Accessed Through: AQS Datamart - IMPROVE Site SOGP1 (Site ID: 244)	January 1, 2025	May 1, 2025
IMPROVE (Preliminary) Accessed Through: AQS Datamart - IMPROVE Site SOGP1 (Site ID: 244)	May 1, 2025	November 1, 2025
SPARTAN (Preliminary): Gravimetric Mass Only **(24 hr)** Accessed Through: Personal Communications	March 17, 2025	October 8, 2025
SPARTAN (Preliminary): Gravimetric Mass Only **(144 hr)** Accessed Through: Personal Communications	October 9, 2025	December 12, 2025
ARM Nephelometer (Minutely) Accessed Through: ARM Data Discovery AOP - sgpaoppsap1flynn1mE13	January 1, 2025	February 2, 2026
ARM Nephelometer (Hourly) Accessed Through: ARM Data Discovery AOP - sgpaoppsap1flynn1hE13	January 1, 2025	February 2, 2026
Met One Beta Attenuation Monitor (BAM) Accessed Through: Manual Collection	January 1, 2025	February 2, 2026
PurpleAir (Minutely) Accessed Through: PurpleAir Download Tool - pm2.5_alt|3.4	August 15, 2025	February 2, 2026

2.3 Project Goals and Implications

The goal of this study is to leverage existing monitoring infrastructure to expand access to and improve the availability of aerosol monitoring by creating proxy measurements from a

nephelometer. Current infrastructure includes filter-based instruments (IMPROVE, CSN, and SPARTAN), which provide speciated data but require significant time for analysis and publication; instruments that provide faster measurements but lack speciation (BAM and PurpleAir); and near-real-time instruments that are limited in both speciation and deployment (ACSM).

The nephelometer provides near-real-time measurements reported as both minutely and hourly averages. In this study, the hourly nephelometer and BAM datasets from January 2025 to February 2026 were used to establish a relationship between total scatter coefficient at 450 nm. (1 μm aerodynamic diameter size cut) and $PM_{2.5}$ mass concentration. After establishing this relationship, daily-averaged nephelometer total scatter (1um and 10um aerodynamic diameter size cuts, derived from minutely observations) were used to interpolate speciated measurements between IMPROVE sampling days, providing more comprehensive data for exposure assessments.

Access to these enhanced datasets has the potential to improve public health by enabling more accurate exposure assessments and supporting real-time alert systems to mitigate risks during periods of elevated $PM_{2.5}$ concentrations.

2.4 Primary Science Questions

To achieve the goal of expanding $PM_{2.5}$ air quality data production and enhancing public accessibility, we will answer the following questions:

1. How well do co-incident mass concentrations align (BAM, IMPROVE, PurpleAir, SPARTAN)?

2. To what extent is nephelometer-derived mass concentration (1 μm) representative of observed mass concentrations from other instruments (BAM, IMPROVE, PurpleAir, SPARTAN)?
3. Under what conditions could risk days now be apparent that were not previously using filter-based datasets?

Chapter 3

Data and Methods

3.1 In-Situ Instrumentation

This study uses a collection of 5 ground-based, in-situ instruments.

3.1.1 ARM Nephelometer

The TSI Nephelometer is a TSI model 3563 integrating nephelometer that takes measurements using three wavelengths: 450, 550, and 700 nm (blue, green, and red). As shown in Figure 7B, air is pulled into the instrument's measurement volume, where the different wavelengths of light can illuminate the volume, and scattering (total or backscattering only) can be measured against the light trap with minimal interference from the internal mechanisms due to a light-absorbing coating (Uin 2024).

The instrument produces both minutely data and hourly data, and is continuously averaged. The hourly dataset provides data for 1 and 10 μm every hour, while the minutely dataset iterates between 1 and 10 μm impactors so that for any one minute, there is a measurement of one or the other, but never both. An excerpt of the pattern is shown below, as is a figure from the ARM DQ-Zoom Plotter depicting the impactor state over the course of one day in 2025 (Figure 8).

Impactor state 10 on for 7 minutes
Impactor state 0 on for 1 minute
Impactor state 1 on for 7 minutes
Impactor state 10 on for 46 minutes
Impactor state 1 on for 7 minutes
Impactor state 0 on for 1 minute
Impactor state 10 on for 7 minutes
Impactor state 1 on for 52 minutes

The angular truncation error for particles between 1 and 10 μm is 30-50%. This is due to the instrument's limited angular integration range of 7 to 170° instead of the full angular range of 0 to 180°.

Before 2024, TSI Nephelometers, the ones in use at the ARM SGP site, were deployed in pairs so that one could measure in ambient conditions, while the other measured in changing humidity. SPICE took place from January 2025 to February 2, 2026, and therefore relied on the measurements from only one of these nephelometers.

A



B

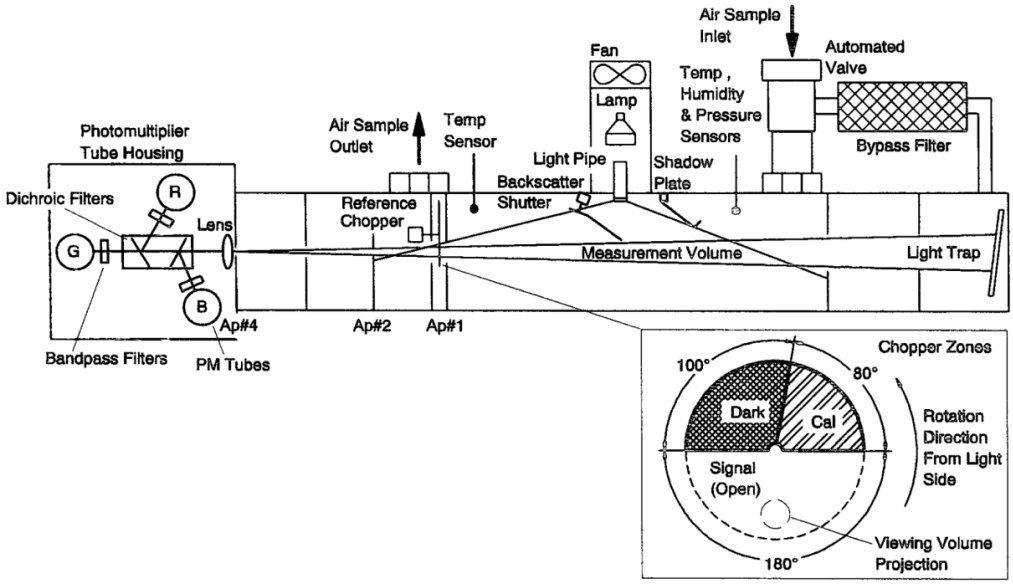

Figure 7: (A) "TSI model 3563 integrating nephelometer. ARM image" (Uin 2024) and (B) "Nephelometer functional diagram" (Anderson et al. 1996)

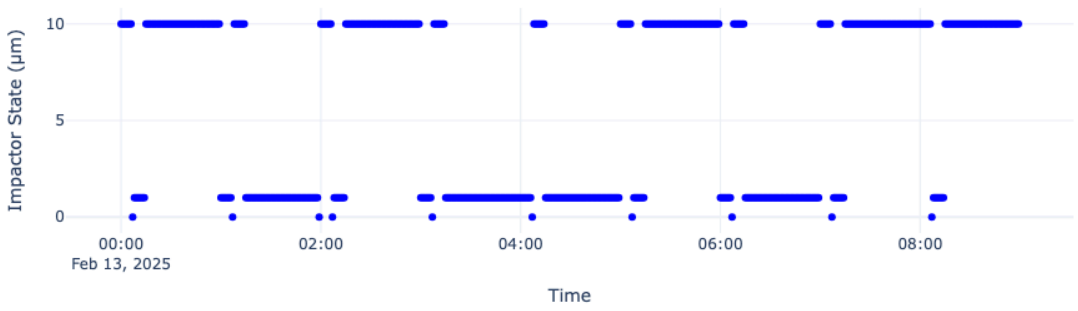

Figure 8: ARM Nephelometer impactor state status time series for February 13, 2025, from the sgpaoppsap1flynn1mE13 datastream

3.1.2 IMPROVE Network

The Environmental Protection Agency (EPA) established the IMPROVE Network to preserve the visual beauty of landscapes in the United States National Parks. The IMPROVE Network was established to enhance environmental equity in visual access, ensuring that everyone, including future generations, can see with the same clarity in national parks.

One IMPROVE station is composed of four separate sampling enclosures, modules A-D, shown in Figure 9. Modules A-C collect particles up to $PM_{2.5}$-sized particles with a flow rate of 22.8 lpm, while Module D collects up to PM_{10}-sized particles with a flow rate of 16.9 lpm. IMPROVE stations sample for 24 hours every 3 days, and the samples from each module undergo different analyses. Module A uses a Teflon® filter to analyze gravimetric fine mass, elemental concentration, and light absorption. Module B uses a Nylasorb (nylon) filter to identify sulfate, nitrate, nitrite, and chloride anions through ion chromatography. Module C uses a quartz fiber filter to identify organic and elemental carbon via thermal-optical reflectance. Module D uses a Teflon filter to determine PM_{10} aerosol mass concentration through gravimetric analysis (IMPROVE Program, n.d.).

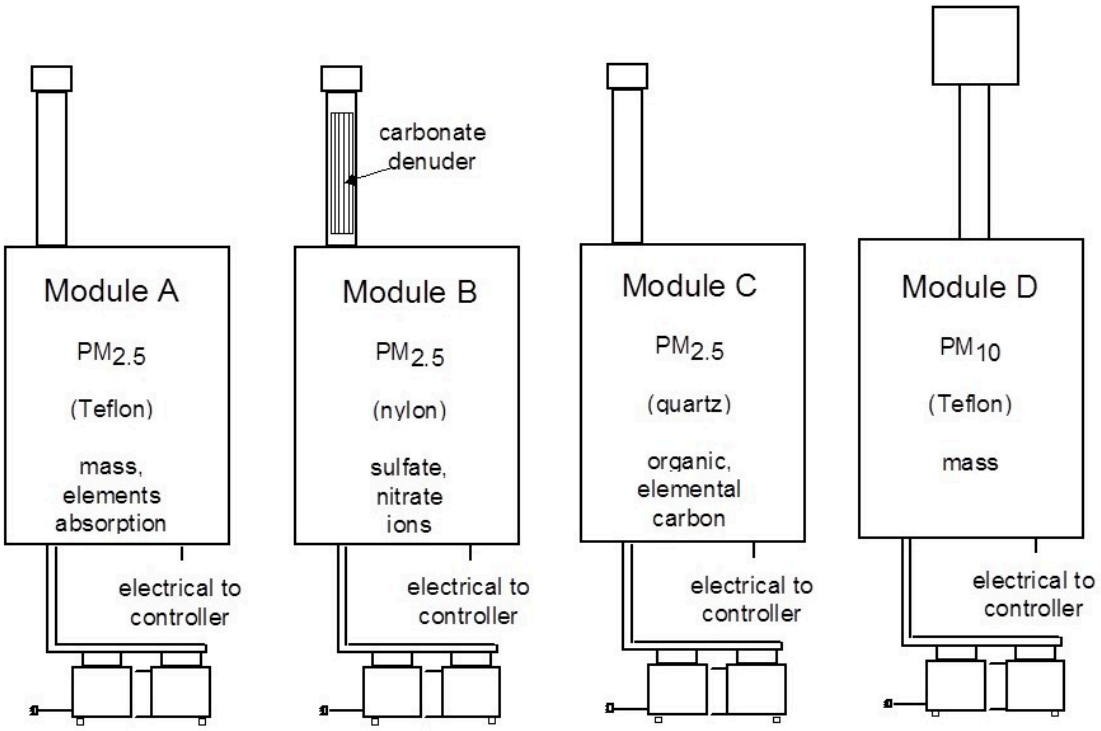

Figure 9: IMPROVE Sampling Enclosure Diagram (IMPROVE Program, n.d.)

3.1.3 SPARTAN

The Surface Particulate Matter Network (SPARTAN) is a growing global network of stations that use both sampling filters and optical measurements, including at 440 nm (a blue), a common satellite wavelength. Their goal is to develop a relationship between filter measurements and optical properties that can be used to retrieve chemical speciation from satellite measurements.

One SPARTAN station, by AirPhoton LLC, is comprised of a filter station and a nephelometer and is collocated with an AERONET station. Air is drawn in through the inlet at 5 lpm and deposited onto one of the 8 filters in a cartridge. Filters 1-6 collect $PM_{2.5}$ samples, filter 7 is a field blank, and filter 8 collects PM_{10} samples with a flow rate of 1.5 lpm. Each $PM_{2.5}$ filter collects 24 hours of sample over a period of 9 days, while the PM_{10} filter collects 4 hours of

sample per $PM_{2.5}$ filter, for a total of 24 sampled hours. Overall, the cartridge samples a total of 54 days. The hourly sampling schedule can be seen in Figure 10.

The filters undergo multiple analyses to characterize the collected samples. Many of the analyses overlap with IMPROVE; however, SPARTAN uses Fourier transform infrared (FT-IR) spectroscopy rather than Thermal Optical Reflectance (TOR) to classify organic carbon from elemental carbon. Details on analysis techniques can be found in the Analysis Methodology for Filter Samples Section.

A

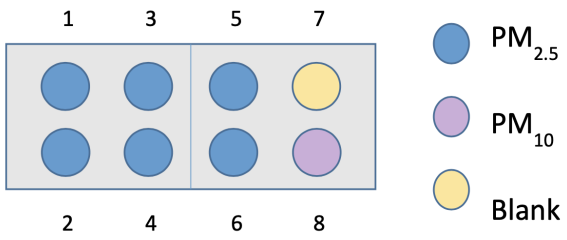

B

Day	$PM_{2.5}$	PM_{10}
1	9:00-12:00	12:00-12:30
2	12:00-15:00	15:00-15:30
3	15:00-18:00	18:00-18:30
4	18:00-21:00	21:00-21:30
5	21:00-0:00	
6		0:00-0:30
7	0:00-3:00	3:00-3:30
8	3:00-6:00	6:00-6:30
9	6:00-9:00	9:00-9:30

Figure 10: SPARTAN Network regular 54 day sampling method (A) "Filter arrangement within each cartridge" and (B) "Example of sampling during the 9-day period of each $PM_{2.5}$ filter" (SPARTAN 2018).

3.1.4 Beta Attenuation Monitor 1022 (BAM)

The BAM produces real-time mass concentration data using beta particles from a decaying carbon-14 (^{14}C) source. At the top of a sampling hour, the BAM performs a beta count test to count the beta particles through the clean filter tape. The sampler pulls in air at 16.7 lpm and deposits aerosols on the filter tape for 42 minutes. Then, the beta count test is repeated using the accumulation filter tape to find the mass concentration.

There is a heater set to maintain a relative humidity (RH) below 50%. Specifically, our unit is measuring $PM_{2.5}$, though there are PM_{10} options, and must be set to 35% RH in the United States (Met One Instruments Inc. 2019). We configured the BAM to measure $PM_{2.5}$ by installing the $PM_{2.5}$ very sharp cyclone below the PM_{10} inlet head. Ultimately, data is logged hourly.

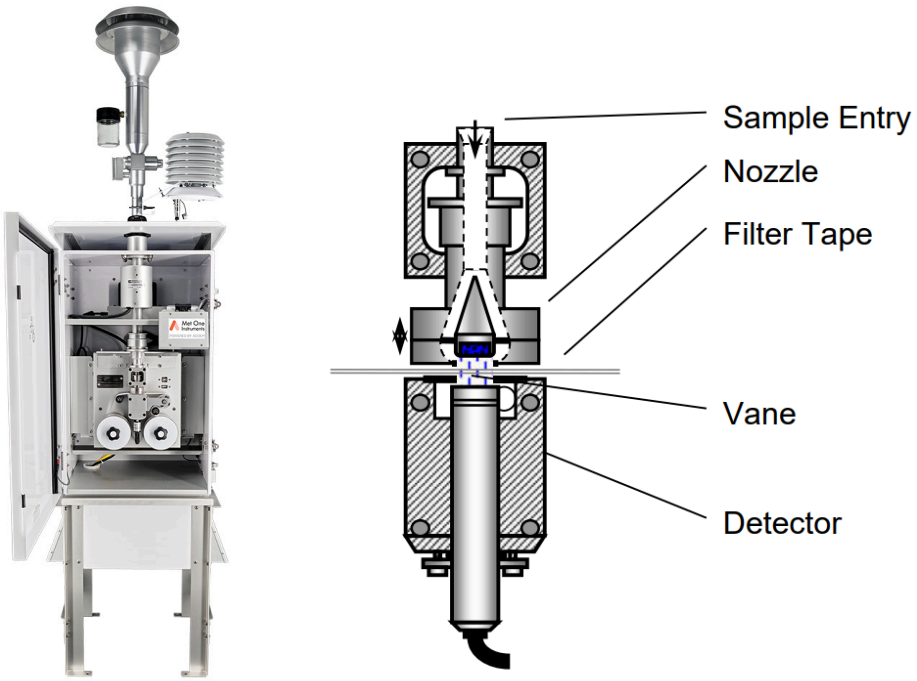

Figure 11: BAM 1022 and Measurement System (Met One Instruments Inc. 2019)

3.1.5 PurpleAir

PurpleAir is a low-cost, globally available, commercial product created to enhance the availability and accessibility of air quality data. The sensors measure atmospheric properties, including temperature, pressure, and Relative Humidity (RH), as well as properties for human health and pollution monitoring. PurpleAir uses Plantower laser counters (PMS5003) to measure particles with diameters between 0.3 μm and 10 μm (PM_{10}). PurpleAir's PM_1 and $PM_{2.5}$ mass concentration measurements have been very precise; however, they tend to significantly

underestimate PM_{10} values (PurpleAir 2023b). Along with particulate mass concentrations, PurpleAir uses the Bosch BME68X to measure volatile organic compounds (VOCs) in their gaseous form; this is an experimental product that takes on the larger issue of accurately measuring VOCs, as they are often lost in filter measurements. Though neither of these measurements can identify specific compounds, PurpleAir provides important information for health and climate resources. A subset of their sensors also measure ozone, which can be helpful for air quality alerts; however, this is not a prevalent feature.



Figure 12: PurpleAir Sensor (Sensor Owner's Guide 2024) and Plantower Laser Counter (PMS5003) (black and white) (Yong 2016)

3.2 Analysis Methodology for Filter Samples

3.2.1 Gravimetric

The IMPROVE Network and SPARTAN both use gravimetric analysis to measure the **total sample mass** collected on the filter during sampling. This mass value is necessary for the mass reconstruction process. The IMPROVE Network uses UC Davis labs, while SPARTAN uses Washington University in St. Louis. SPARTAN sends a subset of its filters to UC Davis labs to assist in contamination tests. The SPARTAN filters approved for sampling are pre-weighed after a 24-hour equilibration period. The equilibration process takes place in the Measurement Technology Laboratories (MTL) AH500E in a controlled environment (temperature and humidity-controlled room). The pre- and post-weighs must have an RH of 35 ± 1%. The filters are weighed 3 times pre- and post-deployment. The standard deviation must be < 2 μg for pre- and < 5 μg for post-deployment filters, or the filter must be reweighed. The sample mass is found by subtracting the pre-deployment mass from the post-deployment mass (Bissonnette et al. 2020). Mass concentration is later calculated using the calculated mass and the recorded flow rates. IMPROVE follows this same methodology after equilibrating their filters at 20-23℃ and 30-40% RH (“Filter Conditioning”, n.d.).

3.2.2 X-ray Fluorescence (XRF) Spectrometry

Both the IMPROVE Network and SPARTAN use X-ray Fluorescence spectrometry to classify **elements**. This non-destructive analysis directs polarized X-ray photons at a sample, which results in the removal of the inner shell of electrons and expulsion of unique signature X-rays as the outer shell’s electrons replace the inner shell vacancies. These signature X-rays identify the source elements in the sample. IMPROVE’s XRF spectrometry takes place in the Air Quality

Research Center (AQRC) at UC Davis, which uses the Epsilon 5 (E5) XRF analyzer from PANalytical (Kline 2022a). The E5 XRF analyzer is capable of identifying 24 elements. SPARTAN performs its XRF spectrometry at Washington University in St. Louis using the Epsilon 4 (E4) benchtop energy dispersive X-ray fluorescence (EDXRF) analyzer from Malvern PANalytical. The E4 EDXRF in the SPARTAN lab is capable of identifying 26 elements (McNeill & Liu 2022).

3.2.3 Hybrid Integrating Plate/Sphere (HIPS) Analysis

Following XRF analysis, both the IMPROVE Network and SPARTAN samples undergo analysis using the HIPS system at UC Davis (Kline 2020). This system analyzes light absorption to identify **black carbon** and is a non-destructive analysis technique. This analysis produces a calculated light absorption coefficient for the particles on the filters (an inferred atmospheric absorption coefficient (fAbs)) by finding the reflectance value (R) and the transmittance value (T). A HeNe laser illuminates the back of the sample filter, and the reflected light is measured by an integrating sphere to provide the *r* value. The light that penetrates the filter undergoes absorption and scattering; the remaining transmitted light is diffused by an opal glass plate and collected by the integrating plate, which detects and provides the T value (Kline 2022b).

3.2.4 Fourier Transform Infrared (FT-IR) Spectroscopy and Thermal Optical Reflectance (TOR)

SPARTAN uses FT-IR to identify **organic carbon**, while the IMPROVE Network uses TOR. This variance in technique makes organic carbon the least comparable sample component between the networks and leads to their varied mass reconstruction equations.

FT-IR uses various combinations of wavelengths of light to find the absorption of the sample at multiple wavelengths. After the FT-IR analysis, SPARTAN uses a Smoke Stain Reflectometer (SSR) to estimate the equivalent black carbon (EBC) content, which is a proxy for BC content. The reflectance (R) is measured three times. The average value is plugged into equation 1 to produce EBC in units of μg. Once the flow rates from the gravimetric measurements are taken into consideration, the final mass concentration is determined.In future iterations of this study, calculated thermal/optical transmittance (TOT) values will be excluded in favor of the thermal/optical reflectance (TOR) values. This decision applies to the carbon measurements, as there were two methods of calculating the initial organic carbon (OC), elemental carbon (EC), and charred OC (OP or POC). TOR values tend to agree in a wider range of temperatures than the TOT values (Chow et al., 2004).

Equation 1: SPARTAN Elemental Black Carbon (Weagle 2019)

$$[EBC] = \frac{-A}{qv} ln(\frac{R}{R_0})$$

"where A is the filter surface area (3.1 cm^2), v is the volume of air sampled (m^3), R is the mean measured reflectance after sampling, R_0 is the reflectance prior to sampling, and q is the product of the reflectivity path (0.5) and the mass-specific absorption cross section (σ_{SSR}, $cm^2 \mu g^{-1}$). The σ_{SSR} used is 0.1 cm^2 μg^{-1} " (Weagle 2019).

3.2.5 Ion Chromatography (IC)

SPARTAN uses labs at Washington University in St. Louis for their Ion Chromatography, while IMPROVE uses UC Davis labs. The SPARTAN samples are analyzed for chloride (Cl^-), nitrite (NO_2^-), bromide (Br-), nitrate (NO_3^-), sulfate (SO_4^{2-}), hydroxymethanesulfonate ($CH_3O_4S^-$) **(anions)**, and sodium (Na^+), ammonium ($NH4^+$), potassium (K^+), magnesium (Mg^{2+}), and calcium (Ca^{2+}) **(cations)** (Weagle et al. 2019). IMPROVE only measures **anions**, chloride (Cl^-), nitrite (NO_2^-), nitrate (NO_3^-), and sulfate (SO_4^{2-}) (Determination of Anions, n.d.).

SPARTAN uses Milli-Q water and HPLC-grade methanol to extract the sample from the filters, while IMPROVE uses deionized water. Then, both the SPARTAN and IMPROVE extracted samples are sonicated for 30 minutes, and 2 mL of the SPARTAN sample is frozen. The remaining SPARTAN sample and the sonicated IMPROVE sample are refrigerated before undergoing Ion Chromatography (IC). As indicated, this method requires extraction and is therefore done after the non-destructive analyses have finished. Following extraction, the IC procedure for both IMPROVE and SPARTAN is identical (Weagle et al 2019).

3.3 Revised SPARTAN Sampling for SPICE

Though SPARTAN's regular sampling schedule is described above, we collaborated with the SPARTAN team at Washington University in St. Louis to develop a revised methodology and schedule suitable for directly comparing SPARTAN's products to those of IMPROVE. Such an adjustment was not made in the original comparison with IMPROVE stations, where "the method of sampling a filter for 24 h spread over 9 days introduces a relative uncertainty of 13% compared with sampling over an entire 9-day interval" (Snider et al. 2015).

To account for IMPROVE's higher flow rate (22.8 L/min), we considered having the SPARTAN (5 L/min) sample for 72 consecutive hours. This modification to the standard SPARTAN sampling methodology would target a mass loading of 100 μg per filter, comparable to IMPROVE's accumulation at this site. However, this approach relies on relatively stable day-to-day atmospheric $PM_{2.5}$ concentrations, which were not observed in historical data (Figure 13).

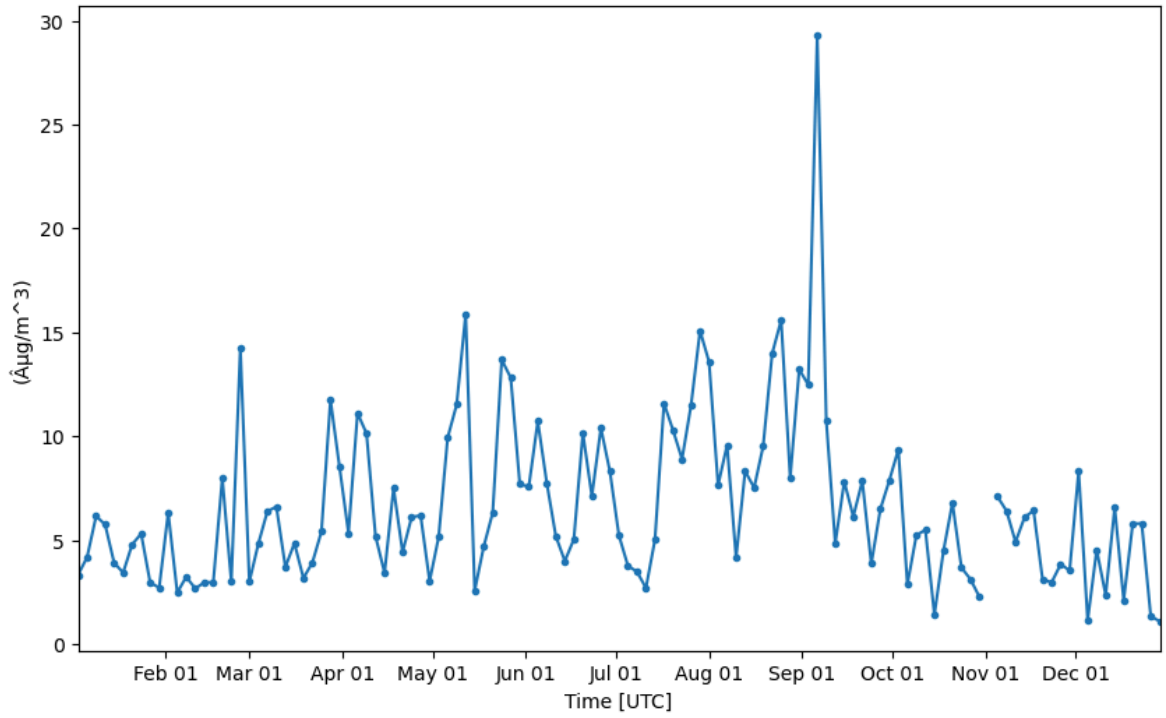

Figure 13: 2023 Time series of SOGP1 IMPROVE Station $PM_{2.5}$ Mass Concentration

To ensure that all instruments sampled the same air, the standard SPARTAN sampling procedure was modified to sample the same 24-hour period as IMPROVE. This approach carried the risk of insufficient mass loading, which is critical for accurate measurements and speciation analysis.

Initially, a goal of SPICE was to evaluate SPARTAN's ability to collect volatile organic compounds (VOCs), and the sampling method was designed with this in mind (Figure 14). One SPARTAN filter was sampled for every other IMPROVE filter for filters 1, 2, 3, and 8. The remaining filters, 4, 5, and 6, corresponded with three sequential IMPROVE filters and were removed immediately upon sample completion. This sampling pattern enabled comparison between samples that remained in the SPARTAN cartridge after sampling and those that were immediately collected and refrigerated (to prevent VOC loss), thereby assessing SPARTAN's potential volatile aerosol loss (Figure 14A).

However, insufficient mass loading became an issue with the 24-hour schedule, as many filters did not meet the minimum measurement threshold for speciated chemical analysis (~100 μg). To address this, the sampling strategy was revised to prioritize mass accumulation over day-to-day mass consistency. Each SPARTAN filter was sampled continuously for 144 hours, as shown in Figure 14B. This revised protocol successfully provided sufficient mass on each filter for subsequent analysis.

A

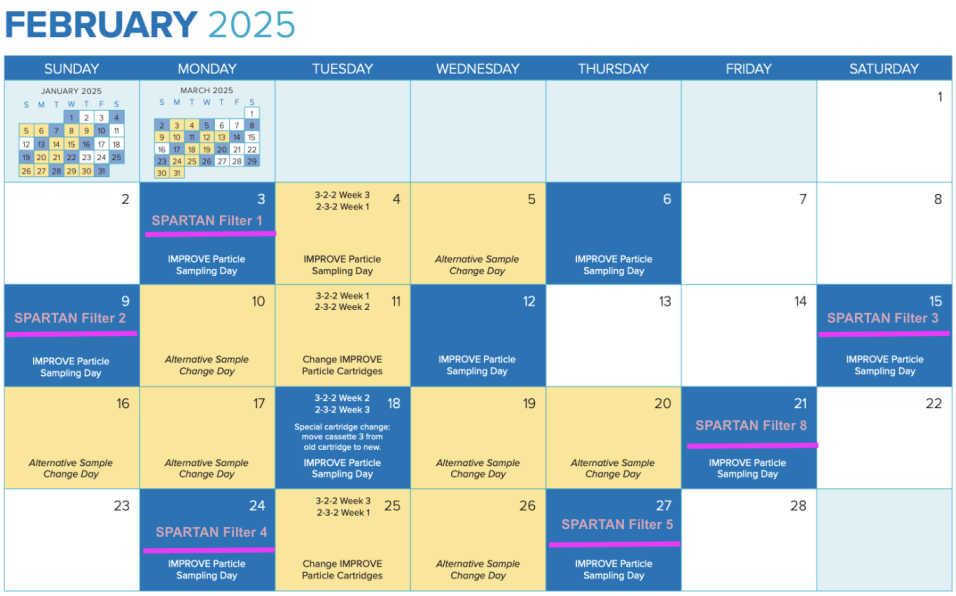

B

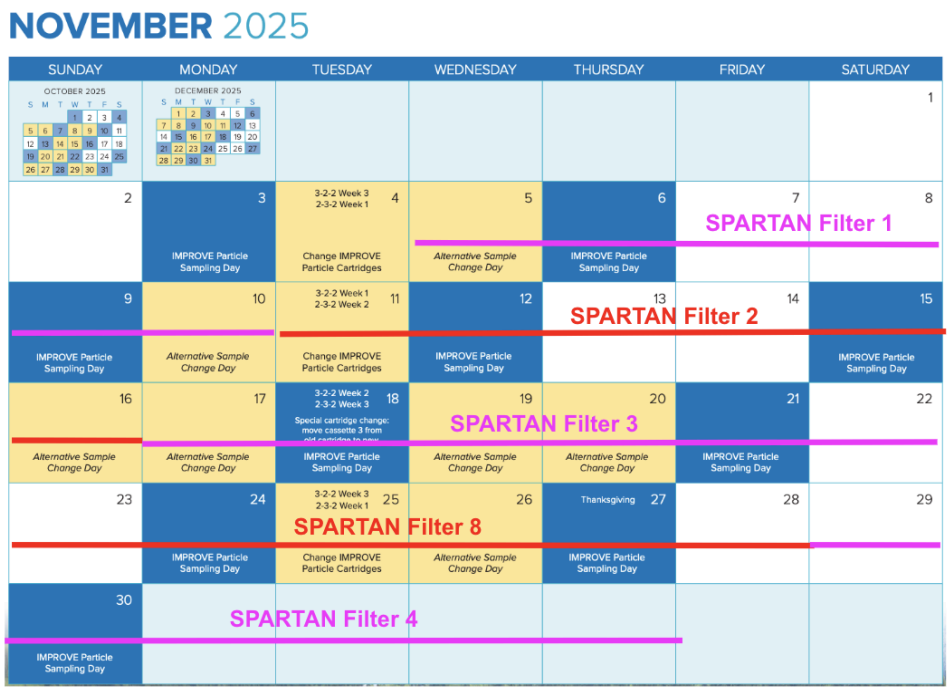

Figure 14: (A) SPARTAN 24-hour sampling method (in use March 17 - October 8, 2025) and (B) SPARTAN 144-hour sampling method (in use October 9 - December 12, 2025) (2025-AQRC-Calendar). The dates with blue backgrounds indicate IMPROVE 24-hour midnight to midnight sample durations. Those with pink lines indicate SPARTAN sample durations.

3.3.1 Data Collocation

Spatial

All instruments used in this study were located at the ARM SGP Central Facility. The IMPROVE station, SPARTAN station, BAM, and PurpleAir were collocated on the same platform above the Guest AOS, while the nephelometer sampled air from inside the SGP AOS07. All instruments were located within 50 feet of each other (Figure 15).

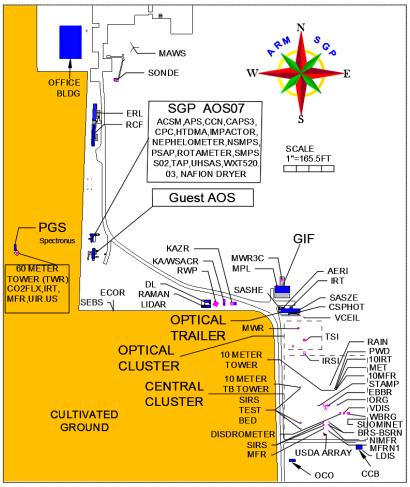

Figure 15: ARM SGP Central Facility Instrument Locations ("SGP-Central-Facility-Instrument," n.d.).

Time

To ensure that all instruments sampled the same air masses, the standard SPARTAN sampling procedure was modified to overlap with the IMPROVE 24-hour schedule, as discussed above. Details of both sampling variations are shown in Figure 14, where SPARTAN sampled from midnight to midnight in accordance with the IMPROVE Network process.

To collocate timestamps across datasets, the IMPROVE and ARM Nephelometer data were converted from UTC to local Central Time (America/Chicago). The BAM dataset was initially set to Central Standard Time without accounting for daylight savings, resulting in a one-hour offset during the summer; this was corrected so that all datasets are in true Central Time (America/Chicago). SPARTAN, its nephelometer, and PurpleAir data were already recorded in true Central Time. The nephelometer hourly dataset is reported every hour on the half-hour. To align with the BAM time indexing, timestamps were adjusted by subtracting 30 minutes so that each observation corresponds to the top of the hour.

3.4 Retrieved Variables

PurpleAir is an optical particle counter that uses a Plantower laser counter to derive particle size and count measurements based on light scattering (Yong & Haoxin 2016). In this study, $PM_{2.5}$ concentrations from PurpleAir are calculated using Lance Wallace's ALT: $PM_{2.5}$ equation, which applies a constant correction factor of 3.4 (Equation 2), as currently recommended (Wallace 2022). SPARTAN reports aerosol data in terms of filter mass; however, this study uses mass concentration, as the majority of instruments used in this study report in this form. Because the SPARTAN data is preliminary, mass concentration was calculated using Equation 3, where $mass_{\mu g}$ is the gravimetric mass of the SPARTAN filter samples, and $Volume_{m3}$ is the total volume of sample air pulled through the filter in the duration of the sampling period.. The IMPROVE dataset used in this study includes both published and preliminary data. The preliminary data only have gravimetric mass, while the published data also have reconstructed mass (see Table 4). For continuity, IMPROVE's gravimetric mass is the primary $PM_{2.5}$ mass concentration value for all analyses, excluding the speciation work found in Section 4.5. Reconstructed mass is used only in the speciation analysis (Section 4.5), where the analysis is already limited to the published IMPROVE dataset. Calculations involving mass fractions for interpolating species concentrations, therefore, use reconstructed mass.

Equation 2: PurpleAir PM2.5 Mass Concentration (Wallace 2022)

$$PM_{2.5}\,ALT = 3.4((0.00030418 \times N_1) + (0.0018512 \times N_2) + (0.02069706 \times N_3)$$

where N_1, N_2, and N_3 are bins such that N_1 = 0.3 µm - 0.5 µm, N_2 = 0.5 µm - 1.0 µm, and N_3 = 1.0 µm - 2.5 µm

Equation 3: SPARTAN Mass Concentration

$$mass_{ug} \div Volume_{m3} = \text{mass concentration}$$

From Section 3.6 onward, nephelometer total scattering was calibrated with respect to particulate mass concentration using observations from a BAM. This analysis focuses on total scattering rather than aerosol optical depth (AOD), which has been used in previous studies (e.g., Paredes-Miranda et al. 2009; Loría-Salazer et al. 2017). While AOD is a useful parameter for satellite-based aerosol studies, it represents a column-integrated optical property of the atmosphere. This work focuses on near-surface aerosol conditions that directly affect human health, and satellite retrievals often have limited sensitivity to aerosol properties within the lowest portion of the atmosphere, particularly at the nose level.

The Aerosol Observing System (AOS; Figure 15) contains several aerosol instruments that sample air from the top of a 10-meter stack. Nephelometers, like the one present in the AOS, are more commonly available than instruments designed for extinction measurements (extinctiometers). For this reason, total scattering measurements were selected as the primary optical parameter for calibration rather than AOD or extinction.

3.5 EPA and WHO $PM_{2.5}$ Exceedances

The EPA recommends that the 24-hour averaged $PM_{2.5}$ not exceed 35 μm/m^3. This guideline specifies that the 24-hour average of three years of data should not exceed 35 μm/m^3 ("*2012_aqi_factsheet*", 2016). Likewise, the WHO recommends that 24-hour averaged $PM_{2.5}$ not exceed 15 μm/m^3, allowing no more than 3-4 days per year with 24-hour $PM_{2.5}$ averages greater than or equal to 15 μm/m^3 ("*WHO global air quality guidelines*," 2021). In this study, the objective is to improve the timeliness and accessibility of public air quality data. Therefore, for the purpose of this study, an EPA exceedance is defined as any day with a 24-hour $PM_{2.5}$ average greater than or equal to 35 μm/m^3, and a WHO exceedance is any day with a 24-hour $PM_{2.5}$ average greater than or equal to 15 μm/m^3.

3.6 Data Processing Choices

3.6.1 OLS vs ODR

The nephelometer produces measurements in near-real time, while IMPROVE and CSN rely on filter-based measurements that can involve substantial analysis delays. To establish a relationship between optical scattering and aerosol mass concentration, hourly Beta Attenuation Monitor (BAM) observations were used as the observed $PM_{2.5}$ mass concentration for calibration of the nephelometer. Because no instrument in this comparison proved an absolute "truth" value, the appropriate regression approach required careful consideration. Figure 16 illustrates the regression sensitivity to axis assignment and compares the resulting Ordinary Least Squares (OLS) and Orthogonal Distance Regression (ODR) fits. ODR was selected as the preferred method for this study because both variables contain measurement uncertainty, whereas OLS assumes that the independent variable (x-axis) is measured without error. Consequently, all regressions presented in this work use ODR rather than OLS.

A

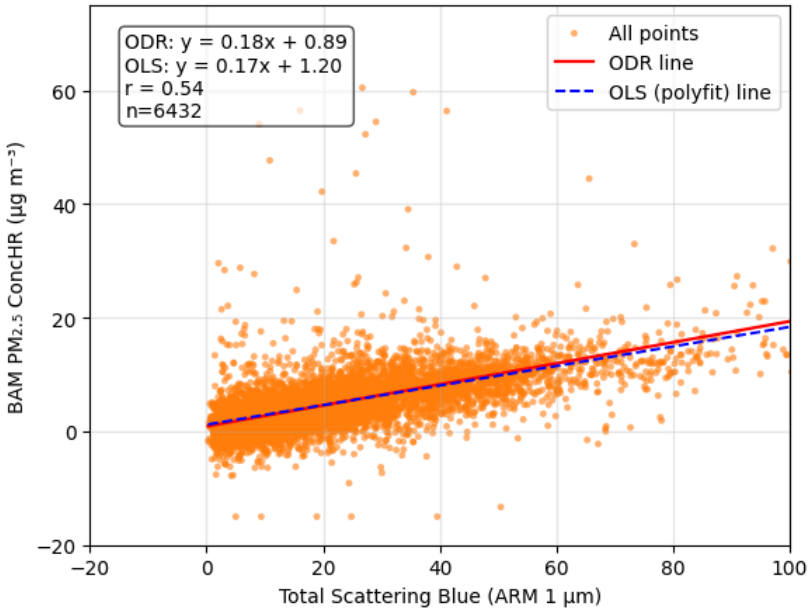

B

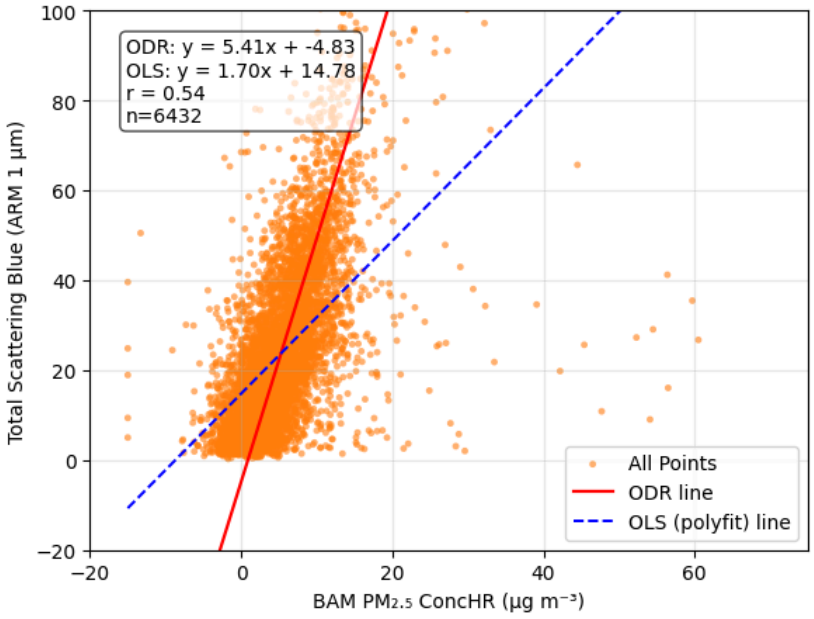

Figure 16: Comparison of ARM nephelometer (1µm) blue total scattering and BAM (2.5µm) $PM_{2.5}$ Mass Concentration measurements during the SPICE campaign (all points). Points represent concurrent hourly measurements from both instruments. The red line shows the orthogonal distance regression (ODR) fit, and the blue line shows the ordinary least squares (OLS) fit. **(A)** ARM nephelometer blue total scattering (x-axis) vs. BAM $PM_{2.5}$ mass concentration (y-axis). **(B)** BAM $PM_{2.5}$ mass concentration (x-axis) vs. ARM nephelometer blue total scattering (y-axis).

3.6.2 Fine-Mode Dataset

The ARM Nephelometer (hourly) provides two data streams corresponding to 1 μm and 10 μm size cuts. Because the BAM is equipped with a $PM_{2.5}$ cyclone, the 1 μm nephelometer stream was used to develop the calibration between total scattering and $PM_{2.5}$ mass concentration. To further refine the dataset, portions of the data were screened using the fine-mode fraction (FMF), a quantity calculated from nephelometer scattering measurements. Screening by fine-mode fraction allowed for the selection of fine-mode-dominated days when particles larger than 1 μm but less than 2.5 μm were unlikely to be present. After testing several thresholds, an FMF greater than or equal to 0.85 was selected as the most representative of fine-mode days. A more restrictive threshold was avoided to prevent excessive reduction of the dataset, which could artificially emphasize anomalous features in the regression, such as the hook-shaped behavior observed in Figure 17C.

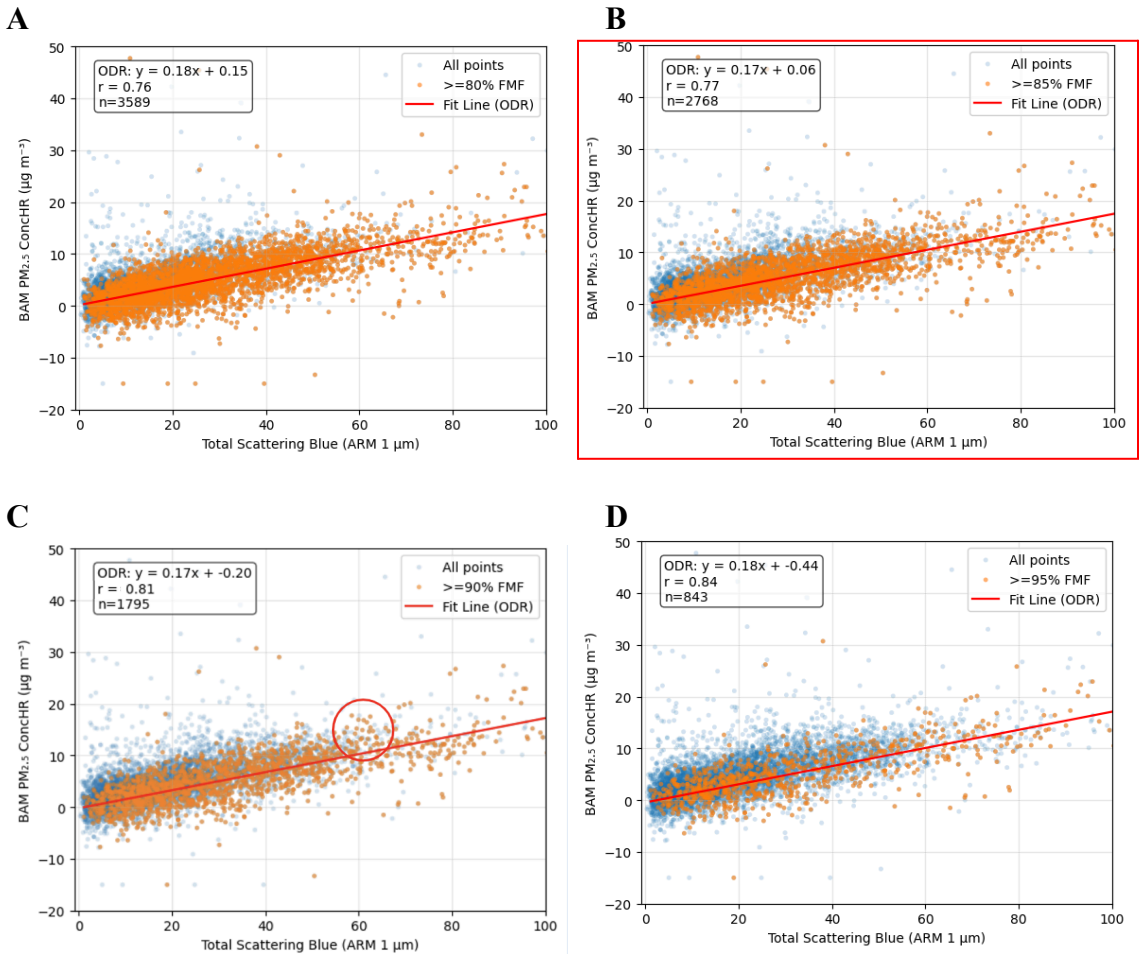

Figure 17: ARM nephelometer (1µm) blue total scattering and BAM (2.5µm) $PM_{2.5}$ Mass Concentration measurements during the SPICE campaign. Points represent concurrent hourly measurements. The red line shows the orthogonal distance regression (ODR) fit; blue dots indicate measurements excluded, and orange dots indicate measurements included due to fine-mode fraction (FMF) filtering. **(A)** Fine-Mode Fraction (FMF) ≥ 0.80, **(B)** FMF ≥ 0.85, **(C)** FMF ≥ 0.90, and **(D)** FMF ≥ 0.95

Additional analyses using only the 2025 dataset were performed to evaluate how different masking thresholds affected the uncertainty of the regression fit. Across these tests, the slope remained stable at 0.17, and the slope uncertainty remained less than $\pm$ 0.01. These results indicate that the masking criteria did not over-constrain the dataset or artificially force the regression relationship (Supplemental Figure S1).

3.6.3 Nephelometer Calibration

As discussed, hourly Beta Attenuation Monitor (BAM) observations were used as the reference aerosol mass concentration for calibrating the nephelometer total scattering and developing a nephelometer-derived $PM_{2.5}$ mass concentration. Although the initial masking procedure was applied using blue-wavelength total scattering, previous studies, such as those by Paredes-Miranda et al. (2009), and Loría-Salazer et al. (2017) use 532 and 550 nm, and 550 nm, respectively (shades of green). To evaluate whether wavelength selection affected the calibration, the same masking criterion (FMF $\geq$ 0.85) was applied to both the blue and green scattering measurements (450 and 550 nm). The resulting slopes were similar (0.17 for blue and 0.23 for green), and the correlation coefficient for the blue fit was slightly higher ($\triangle r \approx 0.01$) than for the green fit. These results suggest that both wavelengths represent $PM_{2.5}$ mass concentration well when compared with BAM observations. However, consistent with optical scattering theory, the shorter blue wavelength may be more sensitive to smaller particles, whereas the green wavelength may miss them in favor of coarser particles.

A

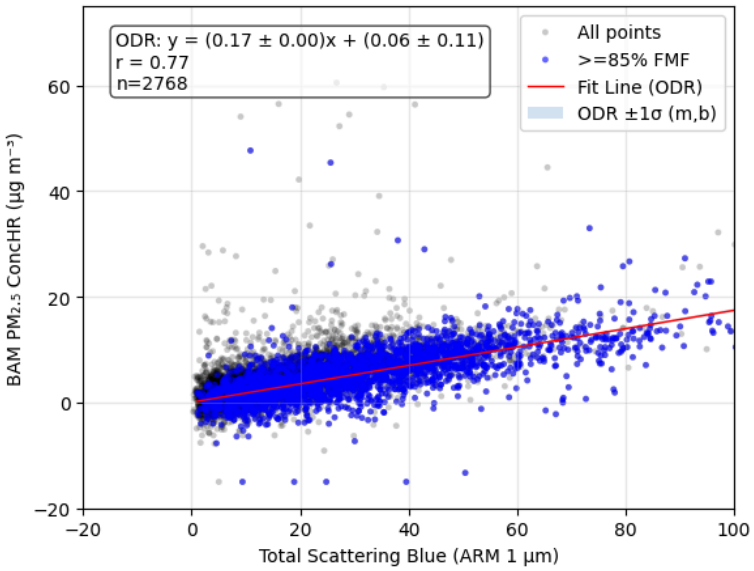

B

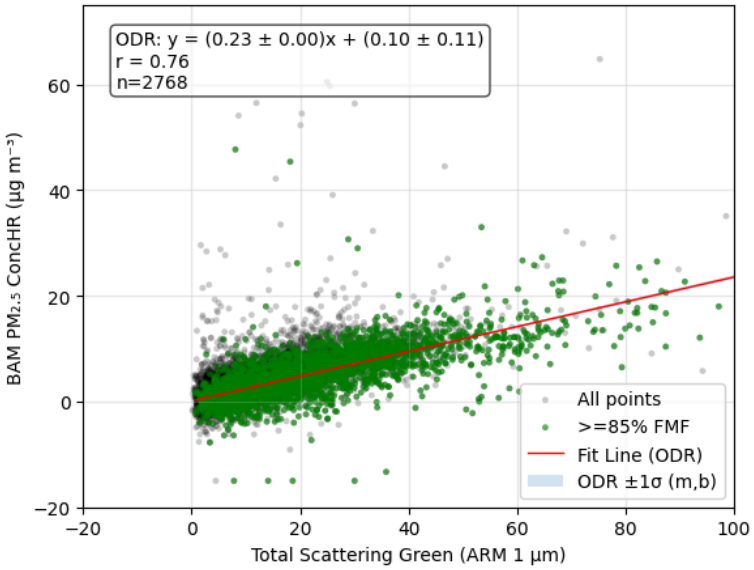

Figure 18: Orthogonal distance regression (ODR) for SPICE duration when fine-mode fraction FMF ≥ 0.85 using hourly nephelometer data. Points represent concurrent hourly measurements. The red line shows the ODR fit; grey dots indicate measurements excluded due to FMF filtering. **(A)** ARM nephelometer blue total scattering (1µm) vs. BAM $PM_{2.5}$ Mass Concentration (2.5µm), with blue dots indicating included points. **(B)** ARM nephelometer green total scattering (1µm) vs. BAM $PM_{2.5}$ Mass Concentration (2.5µm), with green dots indicating included points.

3.6.4 Blue and Green Derived "Nephelometer-Derived Mass" Comparison

Figure 19 shows the blue-wavelength total scatter nephelometer-derived $PM_{2.5}$ mass concentrations, green-wavelength nephelometer-derived $PM_{2.5}$ mass concentrations, and the BAM observed $PM_{2.5}$ mass concentrations. Subplot A shows a time series of the whole SPICE duration, while Subplots B and C zoom into May 2025. Subplot B shows all points regardless of fine-mode fraction, while Subplot C is more representative of the fine-mode days. Both the blue and green calibrations follow the BAM observations well, with minimal difference between the blue and green tracks.

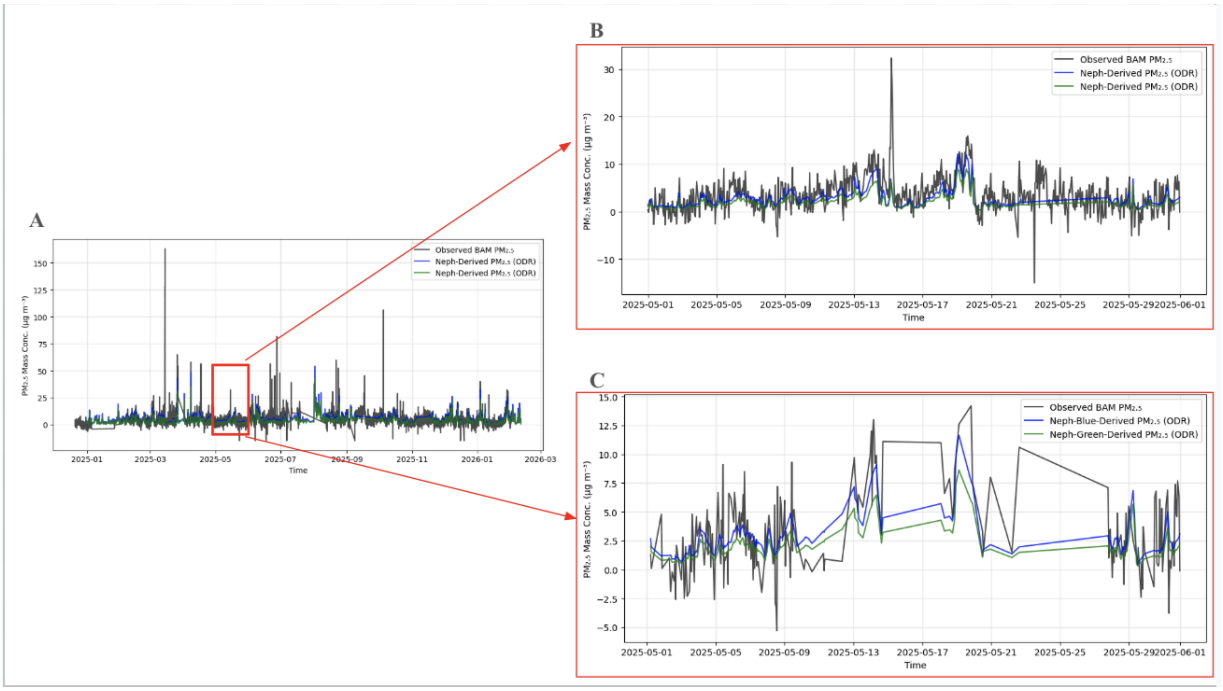

Figure 19: Time series of BAM, green nephelometer-derived, and blue nephelometer-derived $PM_{2.5}$ mass concentrations using hourly 1µm nephelometer data. **(A)** All available BAM and Neph data points for the SPICE duration (not filtered for fine-mode fraction, FMF). **(B)** All available BAM and Neph data points for May 2025 (not filtered for FMF). **(C)** Concurrent BAM and Neph data points for May 2025 when FMF ≥ 0.85.

To evaluate whether the green or blue wavelength would better represent $PM_{2.5}$ mass concentration for the remainder of the analysis, their behavior was examined during March 2025,

when a dust storm affected the state of Oklahoma. Figure 20 shows the response of each wavelength when the calibration relationship is applied to the 1 and 10 μm data streams. Under these conditions, the 10 μm data stream of both wavelengths demonstrates increased sensitivity to the coarse particles detected by the BAM.

Overall, the green and blue wavelengths exhibit comparable sensitivity to $PM_{2.5}$ mass concentration, and either wavelength could reasonably be used for subsequent analysis; however, near the end of March, an additional peak is observed that the blue nephelometer-derived mass concentration tracks more closely than the green. This peak likely corresponds to a fine-mode dominated aerosol event, during which smaller particles contributed more strongly to the observed $PM_{2.5}$ mass concentrations. The improved agreement of the blue wavelength during this period suggests that the shorter wavelength provides greater sensitivity to smaller particles, which may be less effectively captured by the longer wavelength of the green laser.

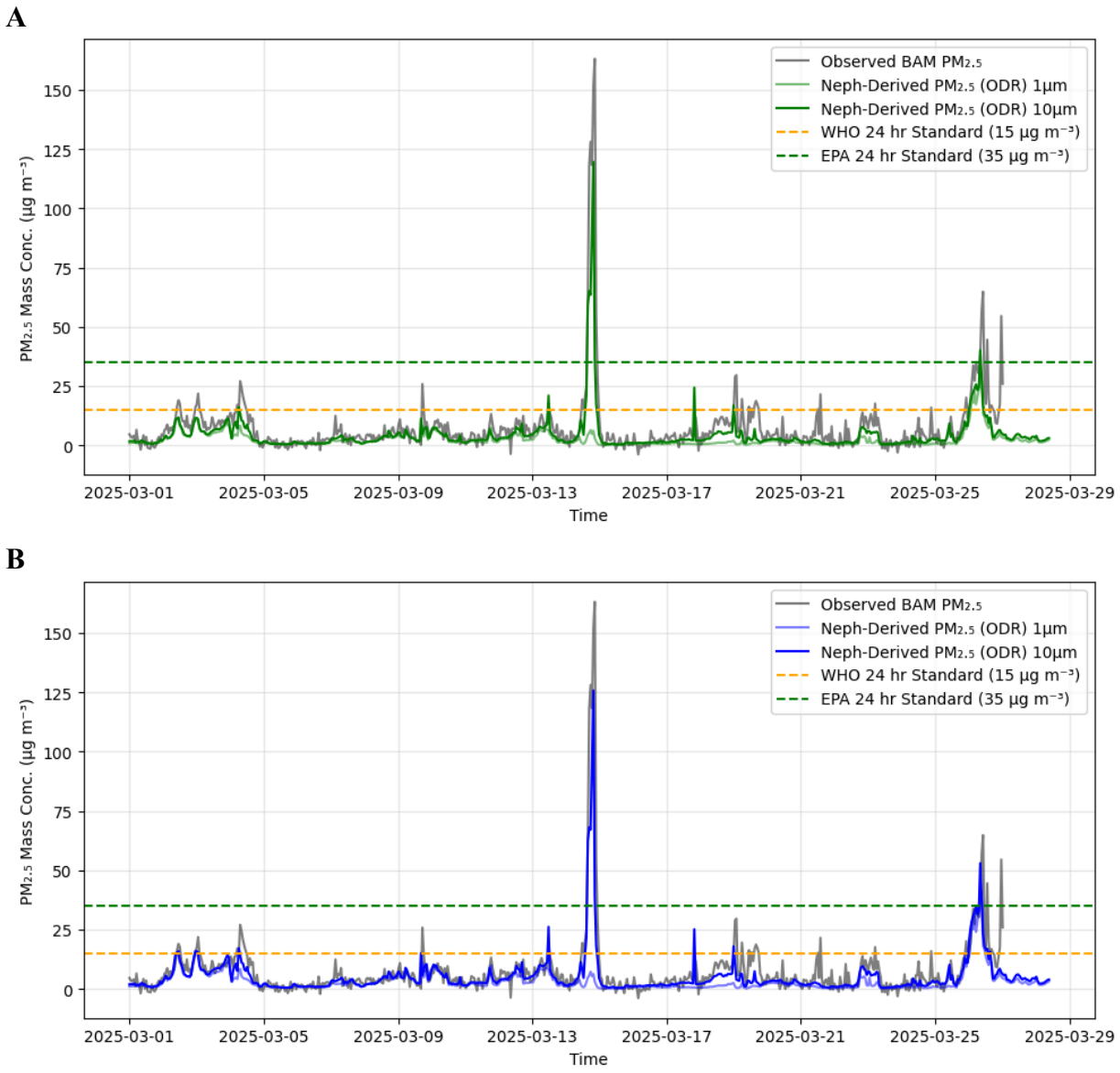

Figure 20: Time series of BAM and nephelometer-derived $PM_{2.5}$ mass concentrations using hourly 1µm and 10µm nephelometer data for March 2025. **(A)** Green nephelometer-derived $PM_{2.5}$ Mass Concentrations and **(B)** Blue nephelometer-derived $PM_{2.5}$ Mass Concentrations

For this study, the blue wavelength was selected for subsequent analysis rather than the green wavelength due to its increased sensitivity to smaller particles. The resulting calibration relationship is $y = 0.17x + 0.06$ where x represents total scattering at the blue wavelength (Mm^{-1}), and y is the estimated $PM_{2.5}$ mass concentration. Although both wavelengths showed

comparable agreement with BAM observations, the blue wavelength was selected because this study aims to support exposure assessments relevant to human health. Particles smaller than 2.5 μm can permeate the cardiovascular system more easily than 2.5 μm or greater; therefore, using the shorter wavelength (blue) increases sensitivity to smaller particle sizes.

Figure 21 presents two time series comparing BAM measurements with blue nephelometer-derived mass concentrations. Panel A includes all available data, while Panel B shows the same comparison after filtering for fine-mode-dominant days (FMF ≥ 0.85). A limitation of this calibration is that nephelometer-derived mass concentration may underestimate actual $PM_{2.5}$ mass concentration during periods dominated by coarse aerosols. The underestimation observed in Panel A is expected because the calibration relies on scattering from the 1 μm size cut. However, mismatches are also visible in Panel B, despite the FMF ≥ 0.85 filtering, most notably at the end of June. Although the disagreement appears pronounced, it is likely attributable to aerosol populations dominated by particles between 1 μm and 2.5 μm during dust and smoke events at that time. BAM measurements detect particles that are between 1 μm and 2.5 μm, while the nephelometer is limited to particles less than or equal to 1 μm. The discrepancies observed in late June, therefore, suggest that aerosol concentrations at the site during this period were dominated by particles in the intermediate size range (1-2.5 μm), which remain relevant for human health impacts.

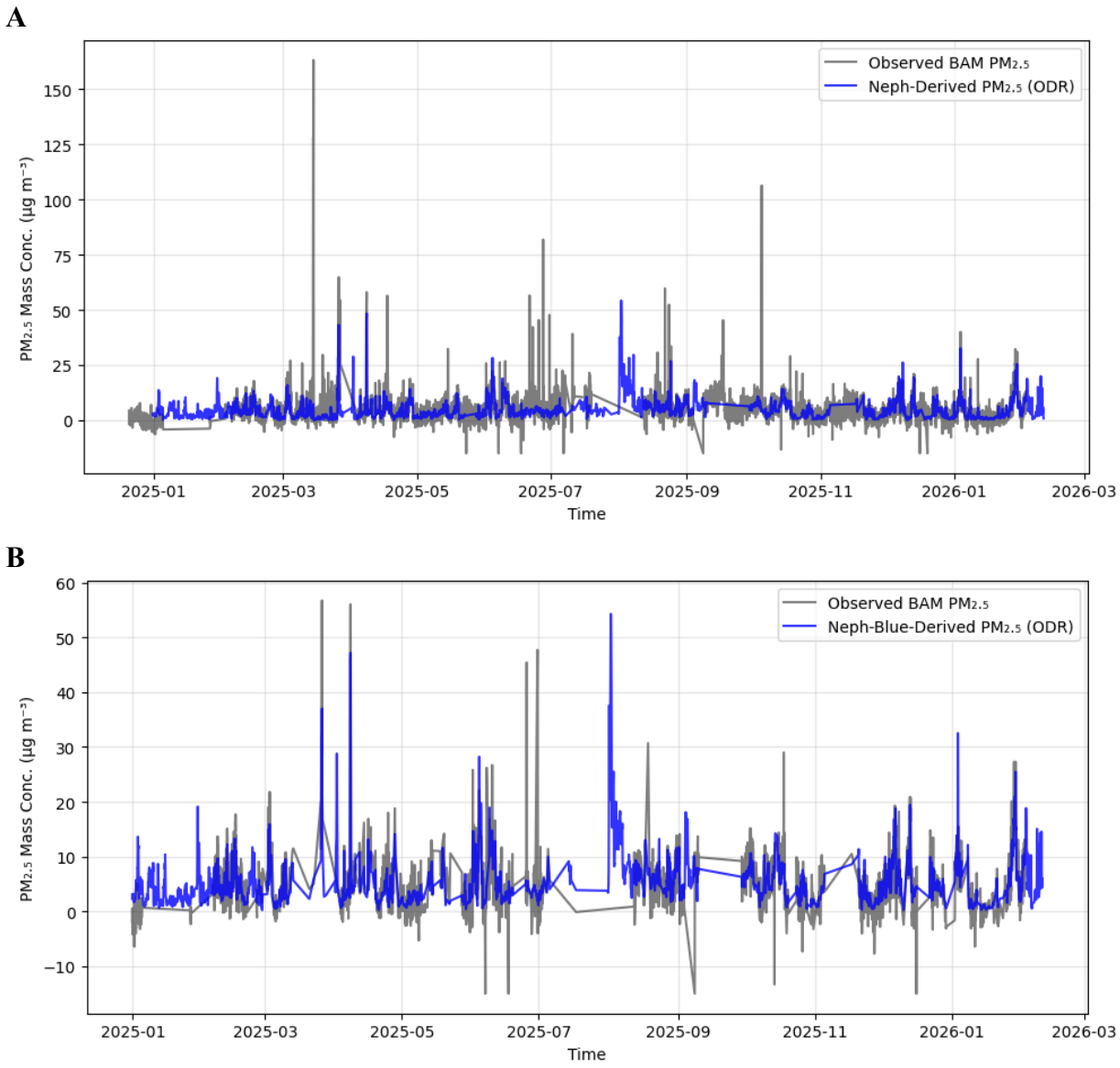

Figure 21: Time series of BAM and blue nephelometer-derived $PM_{2.5}$ mass concentrations. **(A)** All available BAM and hourly 1µm nephelometer data points for the SPICE duration (not filtered for fine-mode fraction, FMF). **(B)** Concurrent BAM and hourly 1µm nephelometer data points for the SPICE duration when FMF ≥ 0.85.

Chapter 4

Results

4.1 In-Situ Instrument Comparison

During the inception of the SPARTAN Network, Snider et al. (2015) performed a collocation study to assess how the $PM_{2.5}$ measurements of the new SPARTAN network compared to those of the established IMPROVE network, the federal reference method beta attenuation monitor (FRM-BAM), and the tapered element oscillating microbalance (TEOM). Following this approach, this study assessed the $PM_{2.5}$ mass concentration agreement among the BAM, IMPROVE, SPARTAN, and PurpleAir. As discussed above, these instruments do not share identical sampling schedules. For the SPARTAN, BAM, and IMPROVE instruments, 12 days of collocated measurements were available, while only 2 days included PurpleAir data due to its later deployment. Figure 22 shows these collocated measurements.

In Figure 22B, the maximum difference between instruments was 2 μg m^{-3}. Figure 22A shows similar agreement, except for April 4, 2025, and September 25, 2025, which were identified as outliers due to large discrepancies between SPARTAN and the other instruments. The initial step in investigating the cause of the observed outlier events was to examine the SPARTAN dataset to determine whether inconsistencies in the sampling configuration could explain the elevated values. Because the dataset had not been pre-screened according to sampling mode ($PM_{2.5}$ or PM_{10}), this was considered a potential source of bias. Inspection confirmed that April 4th corresponded to a PM_{10} filter, while September 25 corresponded to a $PM_{2.5}$ filter.

Investigating the cause of the observed April outlier event using backscatter imagery from the NOAA Scanning High Spectral Resolution Lidar (NSHSRL) at the study site, this

outlier was identified as coinciding with a dust event. Therefore, the observed discrepancies can be attributed to comparing $PM_{2.5}$ measurements to SPARTAN PM_{10} measurements. However, the same cannot be said for the September outlier. Further examination revealed that the September outlier occurred on the first filter. SPARTAN's sampling sequence is 1, 2, 3, 8, 4, 5, 6. Prior to October, filters 4, 5, and 6 were routinely extracted the day after they finished sampling. Based on this workflow, the current working hypothesis is that particulate contamination may have been inadvertently introduced during the repeated cartridge handling, resulting in an artificially elevated mass concentration for filter 1. This filter only sampled for 9 hours, less than half the intended sampling duration, additionally indicating the possibility of a user programming issue.

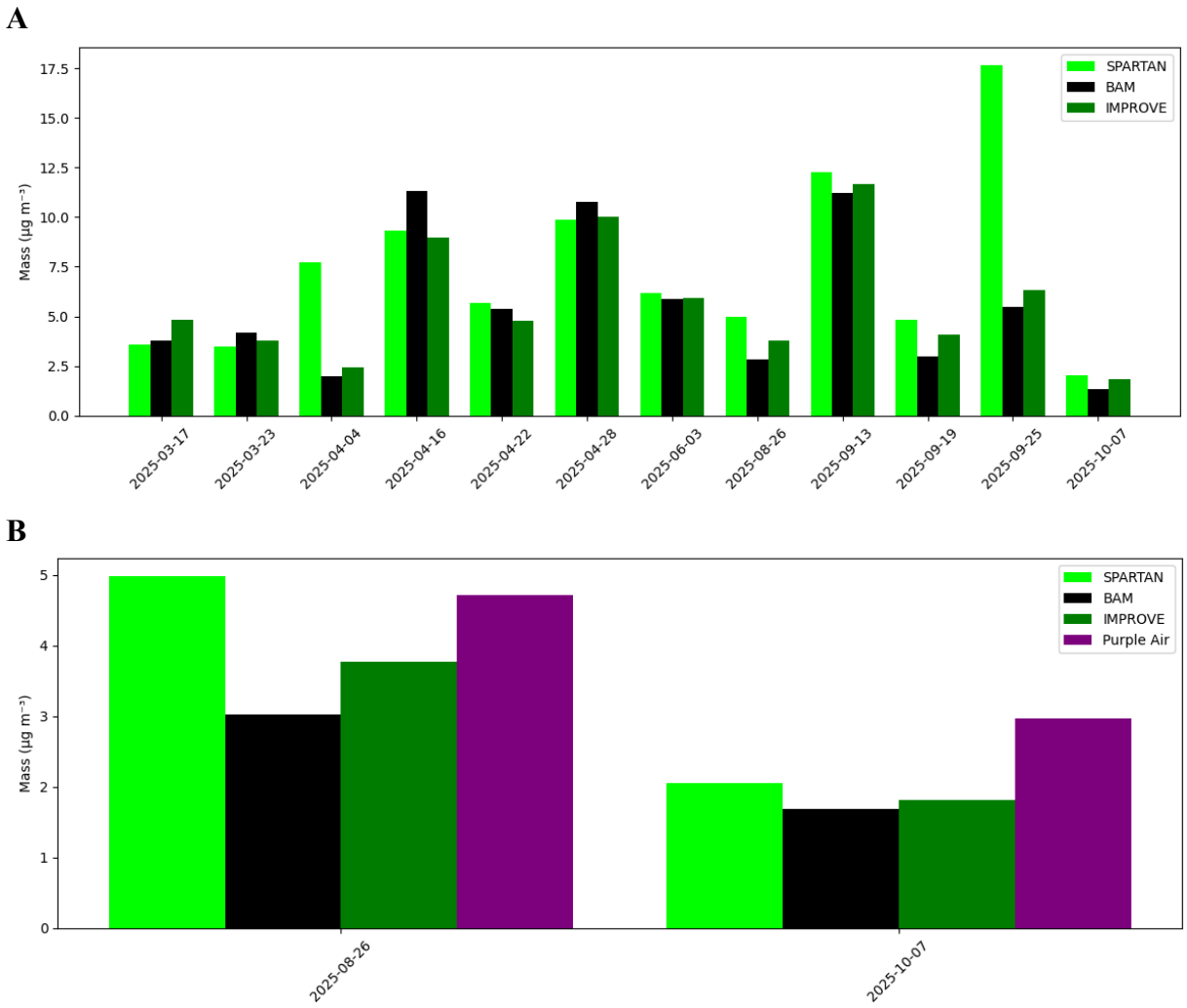

Figure 22: Concurrent daily $PM_{2.5}$ mass comparison (all concurrent observations). Daily averages were calculated from BAM and nephelometer hourly measurements. **(A)** Comparison among SPARTAN (lime green), BAM (black), and IMPROVE (green). **(B)** Comparison among SPARTAN (lime green), BAM (black), IMPROVE (green), and PurpleAir (purple).

The regression fit lines (Figure 23), produced using the ODR methodology discussed in section 3.6.1, show clearer indications of agreement between these instruments. Figure 23's subplots A and C do not include the outlier SPARTAN days, and the agreement is encouraging, with *r* values of 0.95 and 0.98, respectively. Though these analyses are limited in concurrent data points, the agreement of the sensors shown in Figure 23 gives us confidence that the findings from Snider et al. regarding inter-instrument agreement remain true 10 years later.

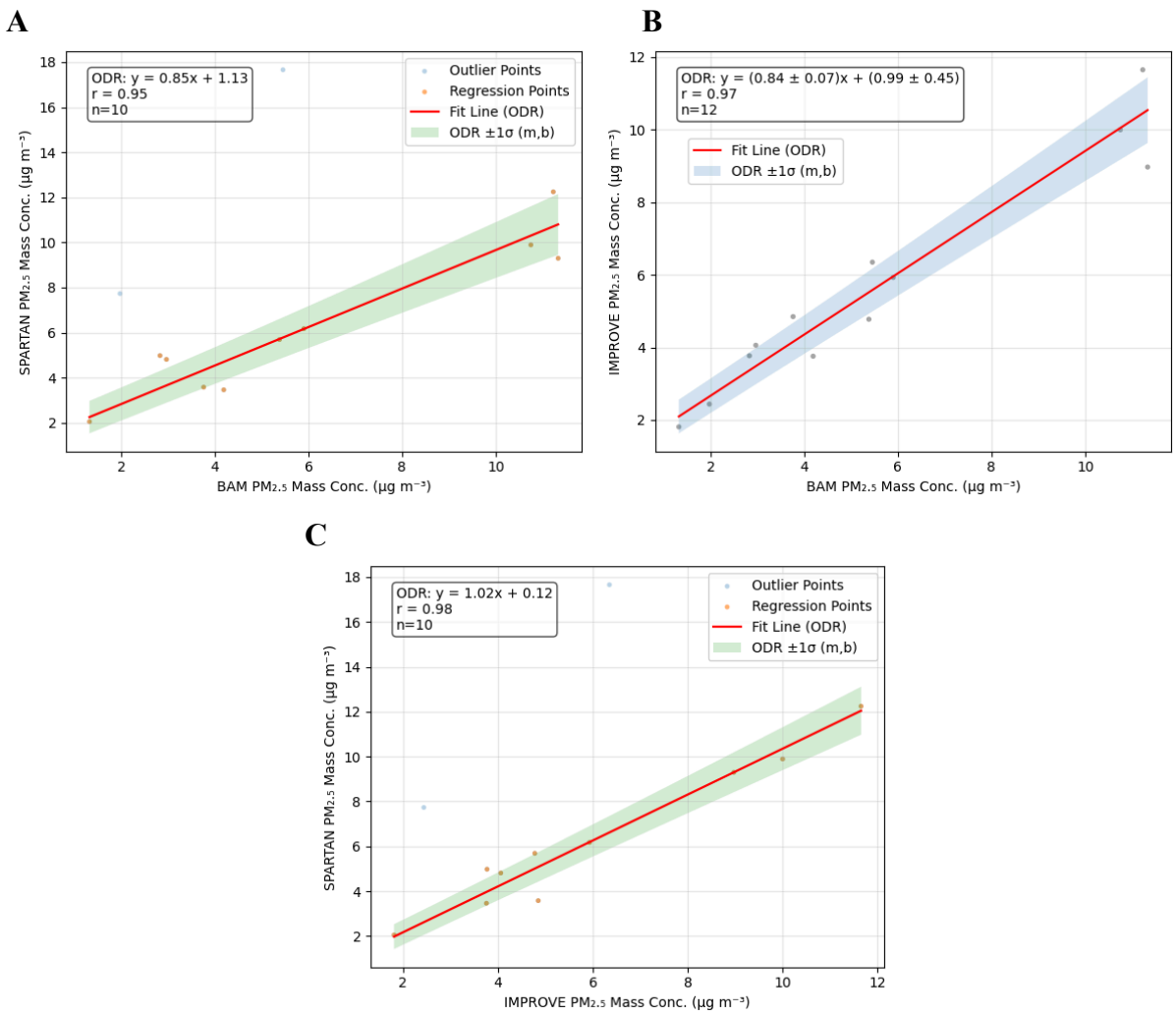

Figure 23: Orthogonal distance regression (ODR) comparisons of concurrent daily $PM_{2.5}$ mass concentrations. Daily averages were calculated from BAM and nephelometer hourly measurements. **(A)** BAM vs SPARTAN (after outlier rejection), **(B)** BAM vs IMPROVE (all points), **(C)** IMPROVE vs SPARTAN (after outlier rejection). Blue-grey points in (A) and (C) indicate observations excluded as outliers due to large discrepancies between SPARTAN and the comparison instruments, as shown in Figure 22.

4.2 Calibration Tests using Observed Data

Section 4.1 demonstrates the reliability of a skew of different instruments in the measurement of $PM_{2.5}$ mass concentrations. The goal of this study is to increase access to air quality data by developing nephelometer-derived estimates in near-real time for faster detection of exposure events, completed in section 3.6.3. Due to section 4.1's demonstrated instrument agreement, the

assessment of the agreement of the nephelometer-derived mass concentration against the individual collocated instruments is as follows.

4.2.1 Calibration (Nephelometer-Derived Mass Concentration) and IMPROVE

All of the concurrent days between IMPROVE and the nephelometer-derived mass concentrations can be found in Supplemental Figure S2. The August-October 2025 subset of these days is shown in Figure 24, where there are indications of good agreement and maximum differences valued at about 2 µg m^{-3}. The supplementary figure shows instances of differences with greater than 2 µg m^{-3}, but as a whole, agreement looks promising. This agreement is confirmed in Figure 26, where the *r* value is 0.94 for nephelometer-derived and IMPROVE measured mass concentrations.

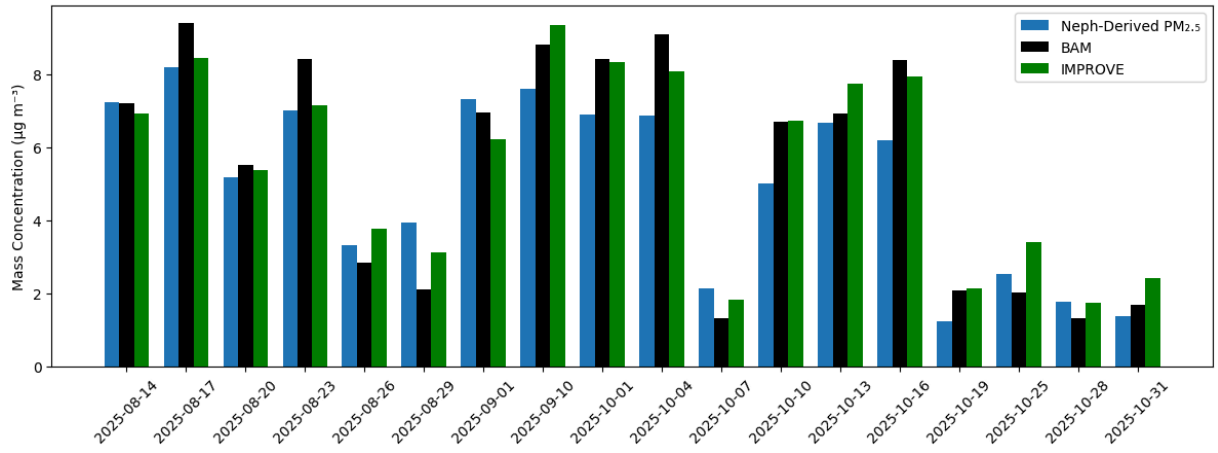

Figure 24: Concurrent daily $PM_{2.5}$ mass concentration comparison for August-October 2025. Daily averages were calculated from BAM and nephelometer hourly measurements. Bars represent 1µm nephelometer-derived mass concentration (blue), BAM (black), and IMPROVE (green). This data was not filtered according to fine-mode fraction (FMF).

Figure 25 shows the time series of observed BAM and IMPROVE $PM_{2.5}$ mass concentrations, as well as nephelometer-derived $PM_{2.5}$ mass concentrations based on both 1 µm and 10 µm nephelometer observations. At the time of initial analysis, the IMPROVE dataset included

measurements from May 2025, as shown in Figure 25. However, during subsequent analyses, these data were no longer available and are therefore absent from later figures.

This discrepancy is reflected in Figure 26. Figure 26A corresponds to the initial evaluation, which includes screening based on fine-mode fraction (FMF). In contrast, Figure 26B represents the newer analysis, in which FMF-based screening was not applied; however, the May 2025 data are missing. A clear divergence between the resulting regression relationships is observed between these two panels.

To further investigate this discrepancy, Figure 26C applies a more stringent filtering approach by excluding potential outliers. Specifically, data points were masked when the absolute difference between IMPROVE-observed and nephelometer-derived $PM_{2.5}$ mass concentrations was greater than or equal to 30 $\mu g\ m^{-3}$. Although the May data remain unavailable, this additional filtering reduces the spread between datasets and improves agreement between the fitted relationships.

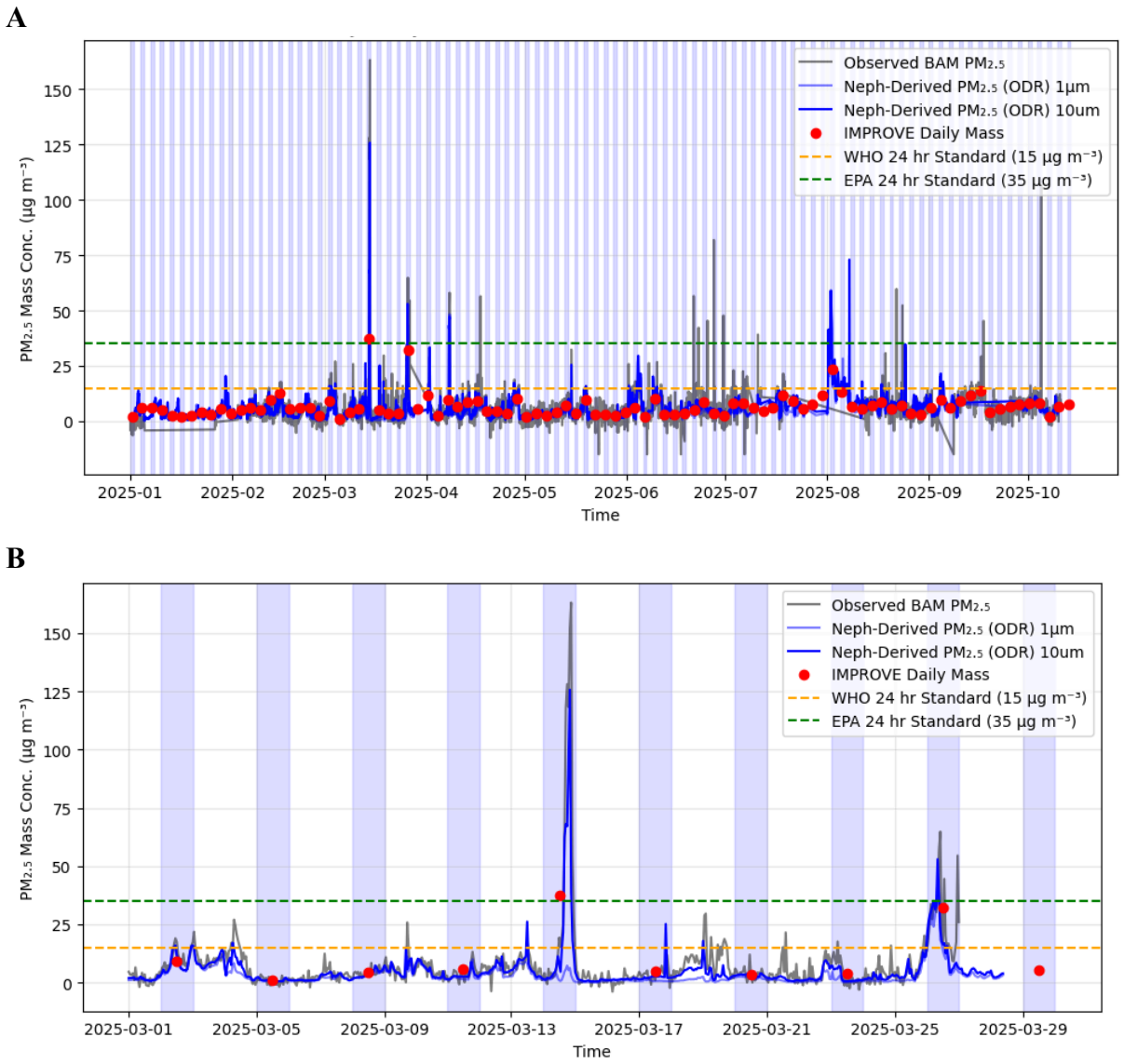

Figure 25: Time series of $PM_{2.5}$ Mass Concentrations measured by BAM, 1µm nephelometer-derived mass concentration, 10µm nephelometer-derived mass concentration, and IMPROVE. Nephelometer-derived values use hourly measurements. Blue shading indicates the IMPROVE sampling duration. This data was not filtered according to fine-mode fraction (FMF). **(A)** SPICE campaign duration. **(B)** March 2025.

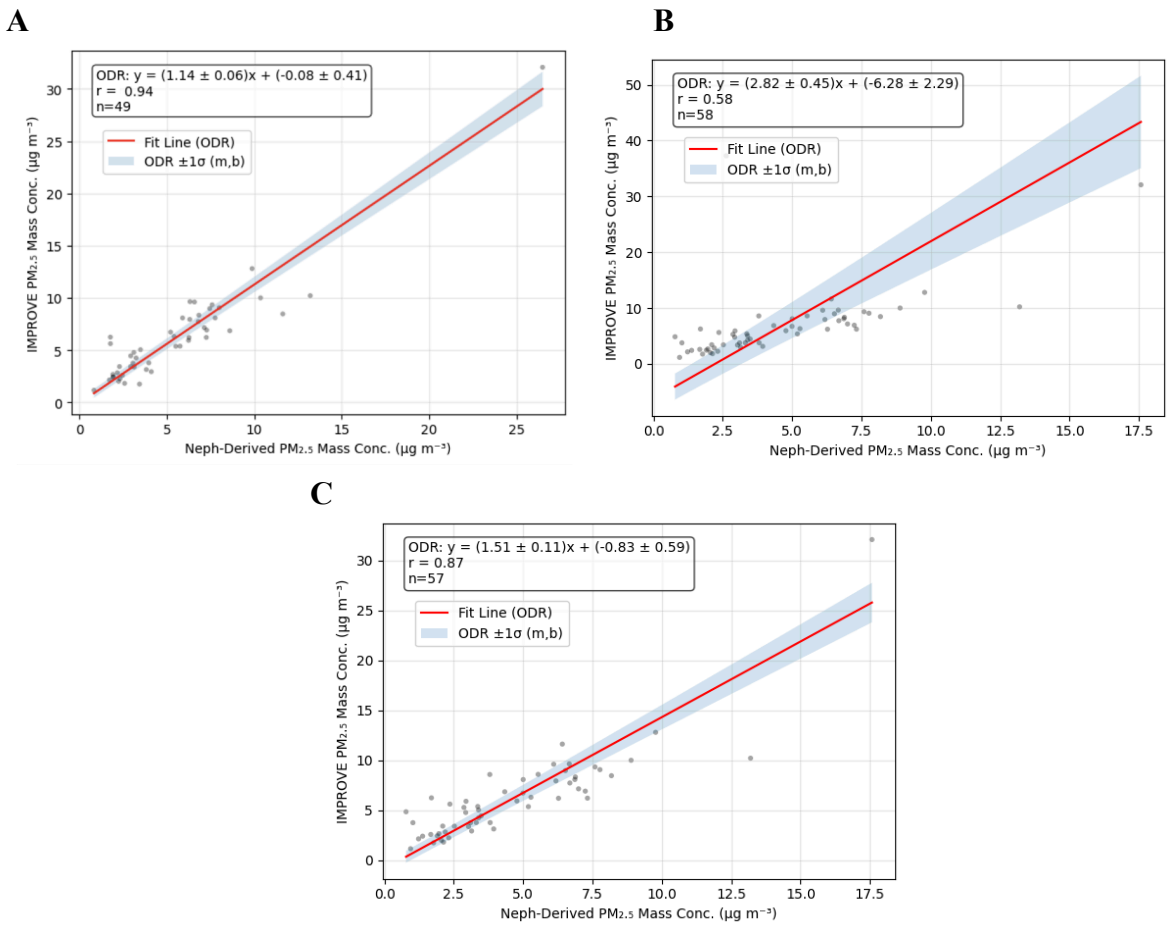

Figure 26: Orthogonal distance regression (ODR) between 1µm nephelometer-derived and IMPROVE measured $PM_{2.5}$ mass concentrations for January-October 22, 2025. Daily averages were calculated from the nephelometer hourly measurements. Points represent concurrent daily averages; the red line shows the ODR fit, and the blue shading indicates the 1σ confidence interval of the fit. **(A)** All data points when fine-mode fraction (FMF) ≥0.85. **(B)** Data not filtered for FMF, with May data unavailable. **(C)** Same as (B), with additional masking of days when the absolute difference between IMPROVE-observed and nephelometer-derived $PM_{2.5}$ is ≥ 30 µg m^{-3}.

Figure 27 compares instrument performance in identifying daily $PM_{2.5}$ exceedances relative to World Health Organization (WHO) and United States Environmental Protection Agency (EPA) guidelines. For this analysis, 24-hour average concentrations greater than or equal to 15 µg m^{-3} and 35 µg m^{-3} were used to define WHO and EPA exceedances, respectively

The nephelometer-derived $PM_{2.5}$ mass concentrations identified one exceedance day using the 1 μm size cut and two exceedance days using the 10 μm size cut relative to the WHO threshold. The 10 μm dataset captured the same exceedance identified by the 1 μm dataset, as well as one additional day not detected by the 1 μm measurements. Overall, this corresponds to one fewer WHO exceedance than detected by the BAM instrument and is equal to the number identified by IMPROVE over the same days of observation. In contrast, nephelometer-derived $PM_{2.5}$ concentrations at both size cuts failed to identify any EPA exceedance days, whereas both BAM and IMPROVE each identified one exceedance.

The collocated measurements for all months, shown in Figure S2, can help to identify when BAM and IMPROVE flagged a day, while either nephelometer-derived product (1μm or 10 μm) did not. BAM flagged the most days (three days), and these days were March 14, March 26, and July 18, 2025. These three days exemplify the limitations of the nephelometer-derived product when implemented in coarse-mode-dominant conditions.

On March 14, a large dust event swept across Oklahoma, impacting this sampling site. On this day, IMPROVE and BAM both registered mass concentrations larger than 35 $\mu m/m^3$, surpassing the EPA limit. While not in Figure S2, Figure 23 clearly shows the peak associated with the dust storm depicted in the nephelometer-derived 10 μm size cut mass concentration estimate; the same peak is not present for the 1 μm size cut of the same figure. This is the day that is present in the 10 μm WHO exceedance, but not in the 1 μm in Figure 27. The conditions of this day were caused not only by the dust storm, but also by wildfire smoke across the state.

On March 26, 2025, aerosols in the area can be attributed to smoke from prescribed burns across the state. Every instrument, IMPROVE, BAM, 1 μm size cut nephelometer, and 10 μm size cut nephelometer registered values above the WHO 24-hour limit. This event was likely

more widely recognized as an exceedance event because there was a wider size distribution of particles formed and transported due to smoke and in-motion chemical reactions that create cloud condensation nuclei scale products (0.2 μm and growing over time). This differs from March 14, when the dust event was more limited to coarser products that grew or broke apart rather than growing new particles and registering on both ends of the size spectrum.

July 18, 2025, differs from the other two events because it is only recognized as a WHO exceedance day by the BAM. The conditions of this day include brief rainfall just after midnight that morning, warm temperatures increasing from 75℉ to above 90℉ in the afternoon, accompanied by windblown dust throughout the day (Ponca City, OK, n.d.). As shown in Figure S2, on this day, BAM registers approximately 18 $\mu m/m^3$, while IMPROVE is roughly 12.5 $\mu m/m^3$; the 1 μm nephelometer-derived is only about 6 $\mu m/m^3$, and from the complete time series in Figure 25, the 10 μm nephelometer-derived is closer to the BAM/IMPROVE measurements in that it just undercuts the 15 $\mu m/m^3$ WHO limit.

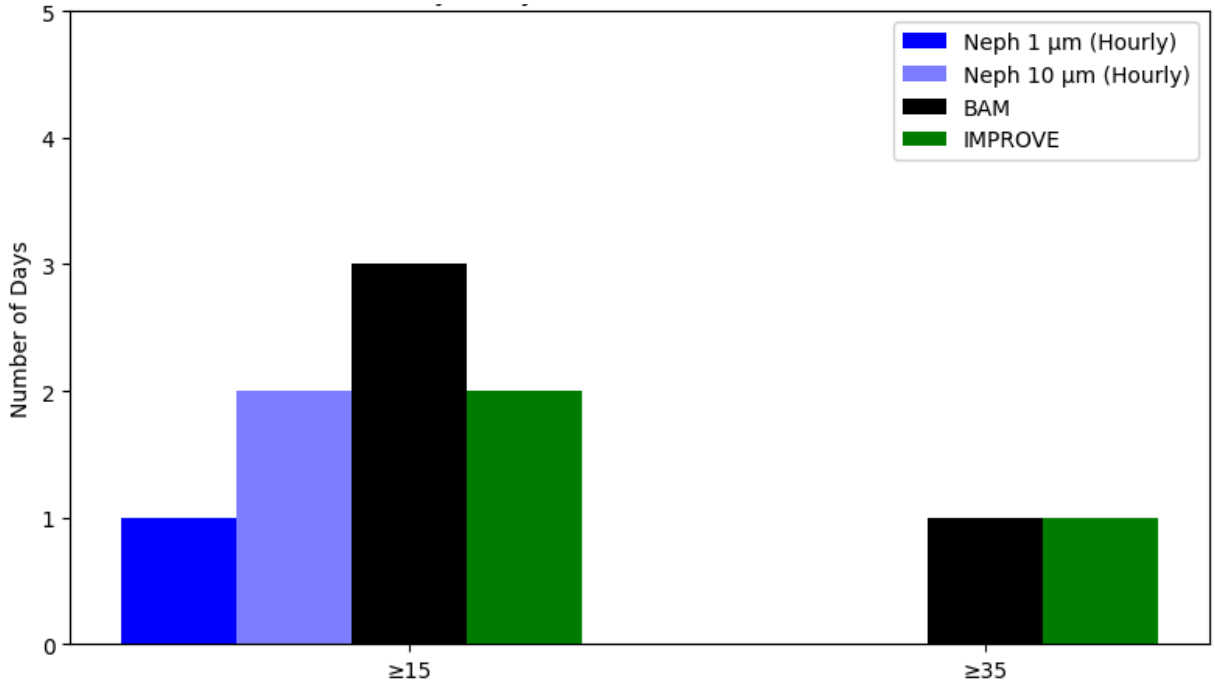

Figure 27: Daily $PM_{2.5}$ exceedances for collocated instruments from January to October 2025. Bars show the number of days that the daily average $PM_{2.5}$ mass exceeded 15 μgm^{-3} (left) or 35 μgm^{-3} (right) for 1µm and 10µm nephelometer-derived mass concentration, BAM, and IMPROVE. Daily averages were calculated from hourly nephelometer and BAM measurements. This data was not filtered according to fine-mode fraction (FMF). This data is limited to the concurrent days shown in Figure S2.

4.2.2 Calibration (Nephelometer-Derived Mass Concentration) and SPARTAN

To prevent outliers arising from artifacts of data representation, adjustments were made for SPARTAN sampling periods after October, which exceeded 24 hours. Unlike the other instruments, SPARTAN measurements are assigned to the first day of the sampling period, which can introduce temporal misalignment if aerosol loading varies across the sampling window. To account for this, the values shown in Figure 28 were calculated by averaging the hourly BAM and nephelometer measurements over the full SPARTAN sampling period for each available sample.

All of the concurrent days between SPARTAN and the nephelometer-derived mass concentrations are shown in Figure 28, where there are, once again, indications of good agreement and maximum outlier differences valuing at about 5 μg m^{-3}. The two outlier days visible here include April 4, 2025, and October 9, 2025. Following the same investigative steps as above, these outliers can be attributed to their being PM_{10} filters sampled during dusty days and then compared to $PM_{2.5}$ measurements, thus the disagreement. However, May 22 also used a PM_{10} filter, but it was not an outlier despite dusty conditions.

The agreement between the nephelometer-derived results and those of SPARTAN is confirmed in Figure 30, where the *r* value is 0.70 for nephelometer-derived and SPARTAN-measured mass concentrations (excluding the noted outliers). The different colored dots refer to the 24-hour sampling (grey) and the 144-hour sampling approaches (orange).

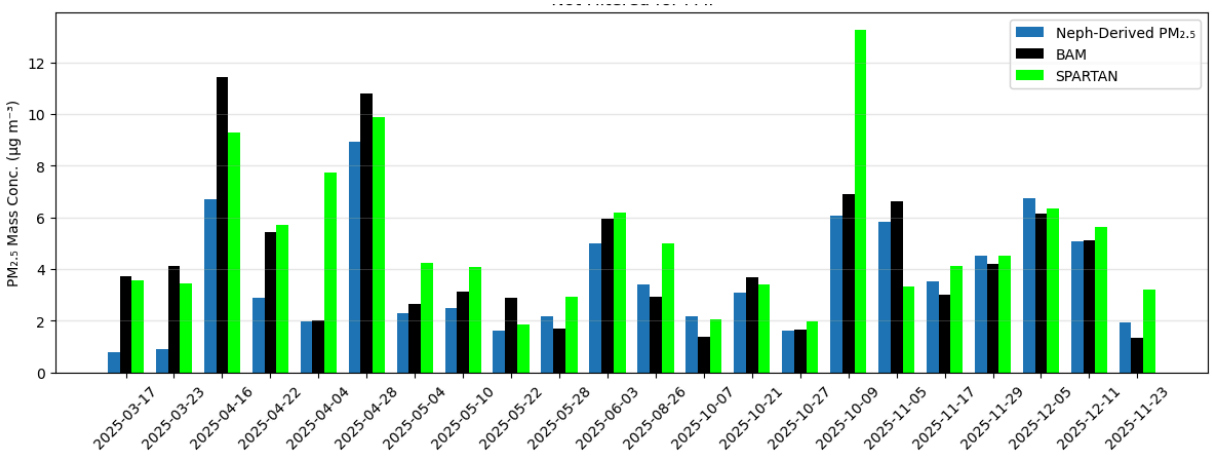

Figure 28: Concurrent daily $PM_{2.5}$ mass comparison (all concurrent observations). Daily averages were calculated from BAM and nephelometer hourly measurements by averaging over the SPARTAN sampling period for as many days as exist. Bars represent 1μm nephelometer-derived mass concentration (blue), BAM (black), and SPARTAN (lime green). This data was not filtered according to fine-mode fraction (FMF).

Figure 29 shows the time series of observed BAM and SPARTAN $PM_{2.5}$ mass concentrations, as well as nephelometer-derived $PM_{2.5}$ mass concentrations based on both 1 μm

and 10 µm nephelometer observations. None of the days with concurrent measurements exceeded either the WHO or EPA thresholds based on observations from the BAM, SPARTAN, or nephelometer-derived datasets.

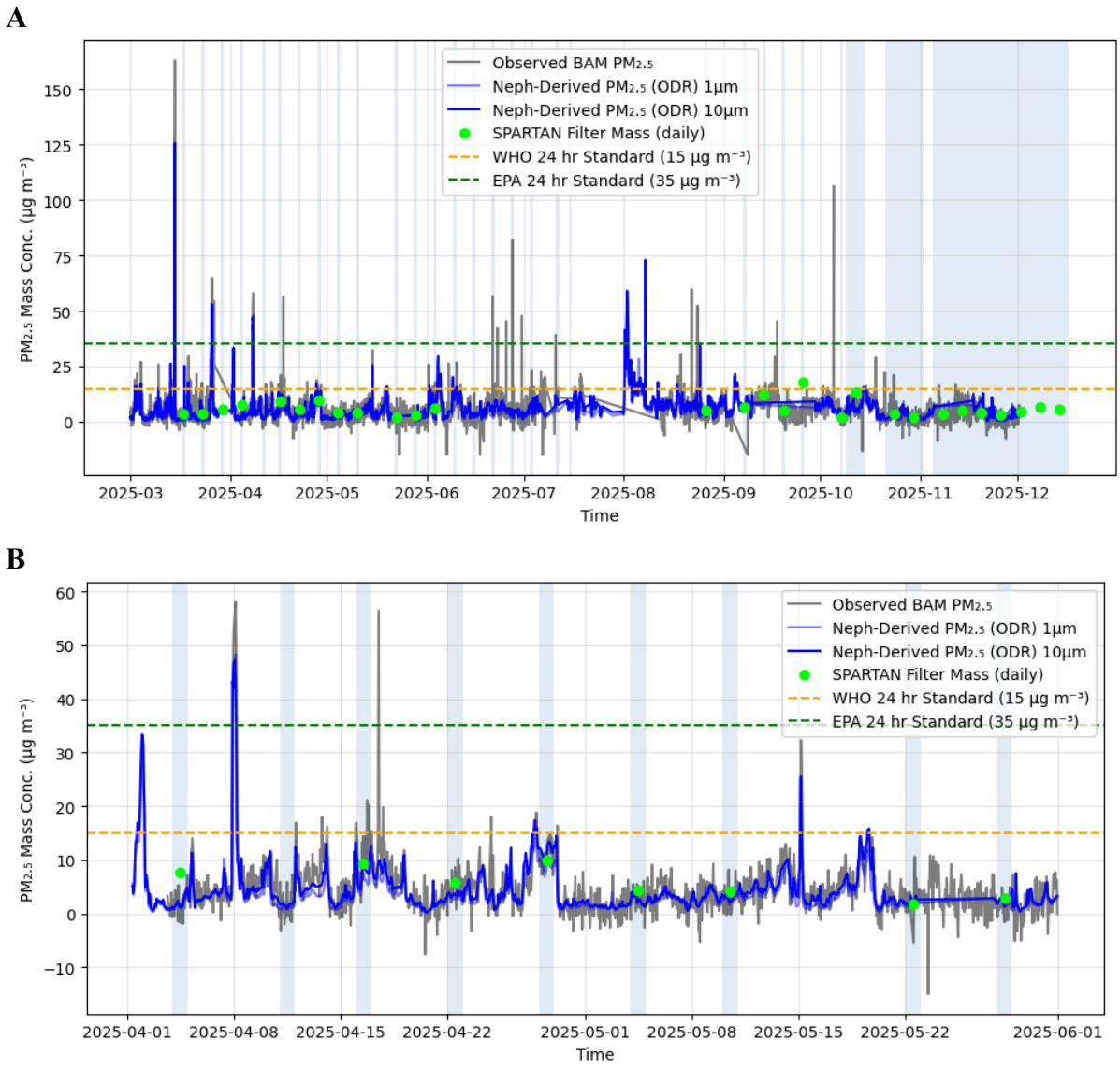

Figure 29: Time series of $PM_{2.5}$ Mass Concentrations measured by BAM, 1µm nephelometer-derived mass concentration, 10µm nephelometer-derived mass concentration, and SPARTAN. Nephelometer-derived values use hourly measurements. Blue shading indicates the SPARTAN sampling duration. This data was not filtered according to fine-mode fraction (FMF). **(A)** Available SPARTAN duration (March-November 2025). **(B)** April-May 2025.

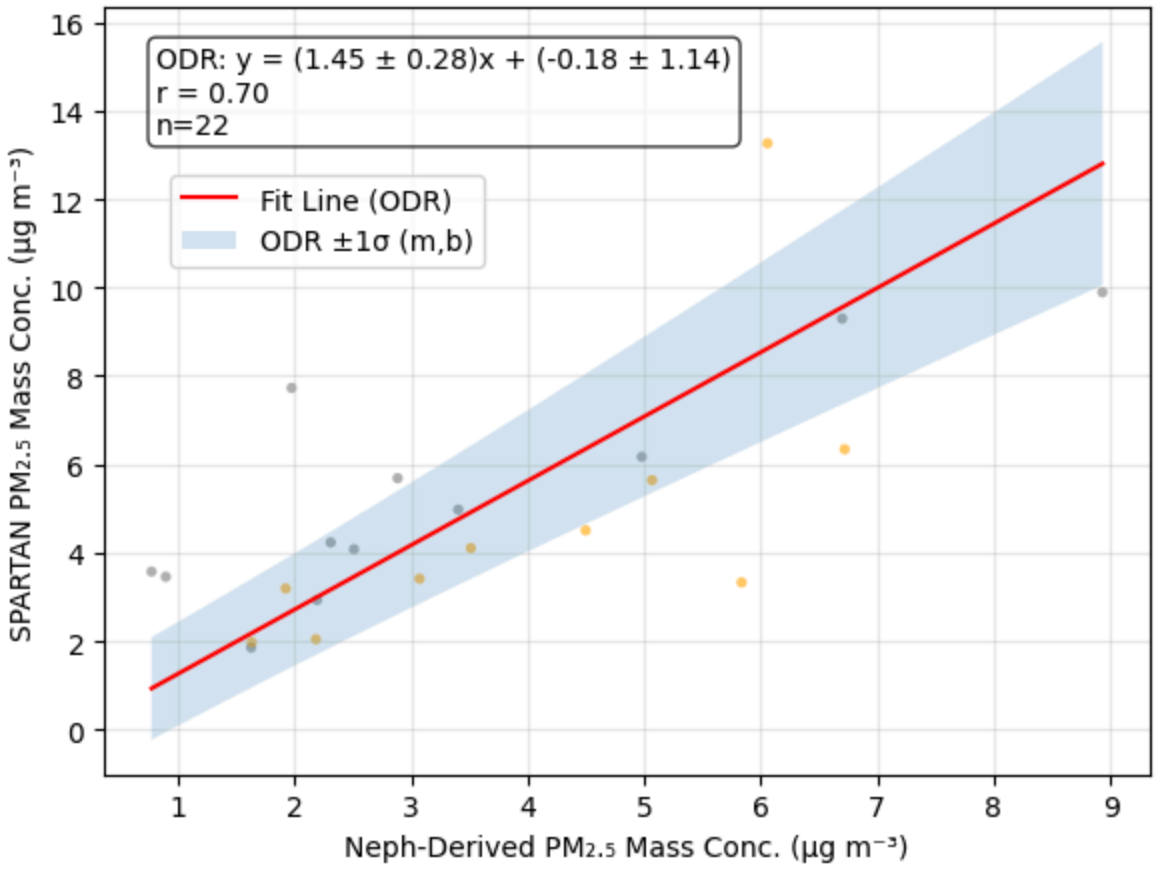

Figure 30: Orthogonal distance regression (ODR) between 1µm nephelometer-derived and SPARTAN measured $PM_{2.5}$ mass concentrations (all concurrent observations). Daily averages were calculated from the nephelometer hourly measurements. Points represent concurrent daily averages; the red line shows the ODR fit, and the blue shading indicates the 1σ confidence interval of the fit. Orange and grey dots indicate days when the SPARTAN was operating on the 144-hour and 24-hour sampling schedules, respectively. This data was not filtered according to fine-mode fraction (FMF).

Future studies should consider normalizing 24-hour measurements with respect to nephelometer-measured scattering when comparing to SPARTAN 144-hour measurements. This study does not take this into account, as the winter months were more constant in daily mass concentration, and the 144-hour sampling duration was only implemented in October. If this study had 144-hour sampling implemented during the spring and/or summer months, where the

day-to-day mass concentrations are more variable, the normalization would have helped to counter the undue effects of the extended sampling duration.

4.2.3 Calibration (Nephelometer-Derived Mass Concentration) and PurpleAir

All of the concurrent days between PurpleAir and the nephelometer-derived mass concentrations can be found in Supplemental Figure S3. The August-September 2025 subset of these days is shown in Figure 31, where indications of good agreement and few instances of notable disagreements between the nephelometer-derived and PurpleAir observed $PM_{2.5}$ mass concentrations are apparent. The supplementary figure shows similarly distributed instances of larger differences, but as a whole, agreement looks promising. This agreement is confirmed in Figure 33, where the *r* value is 0.95 for nephelometer-derived and PurpleAir-measured mass concentrations.

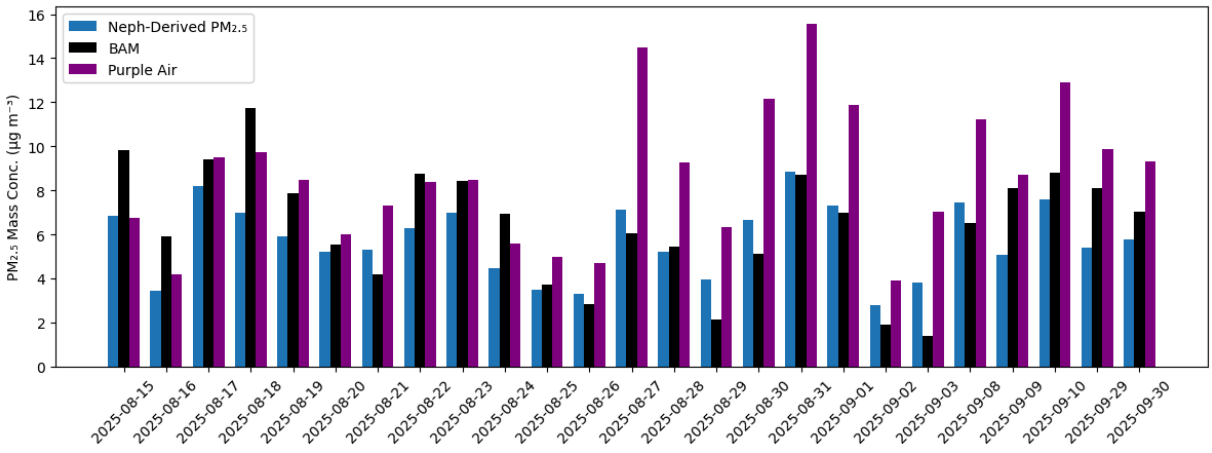

Figure 31: Concurrent daily $PM_{2.5}$ mass comparison for August-September 2025. Daily averages were calculated from BAM and nephelometer hourly measurements. Bars represent 1µm nephelometer-derived mass concentration (blue), BAM (black), and PurpleAir (purple). This data was not filtered according to fine-mode fraction (FMF).

Figure 32 shows the time series of observed BAM and PurpleAir $PM_{2.5}$ mass concentrations, as well as nephelometer-derived $PM_{2.5}$ mass concentrations based on both 1 µm and 10 µm nephelometer observations.

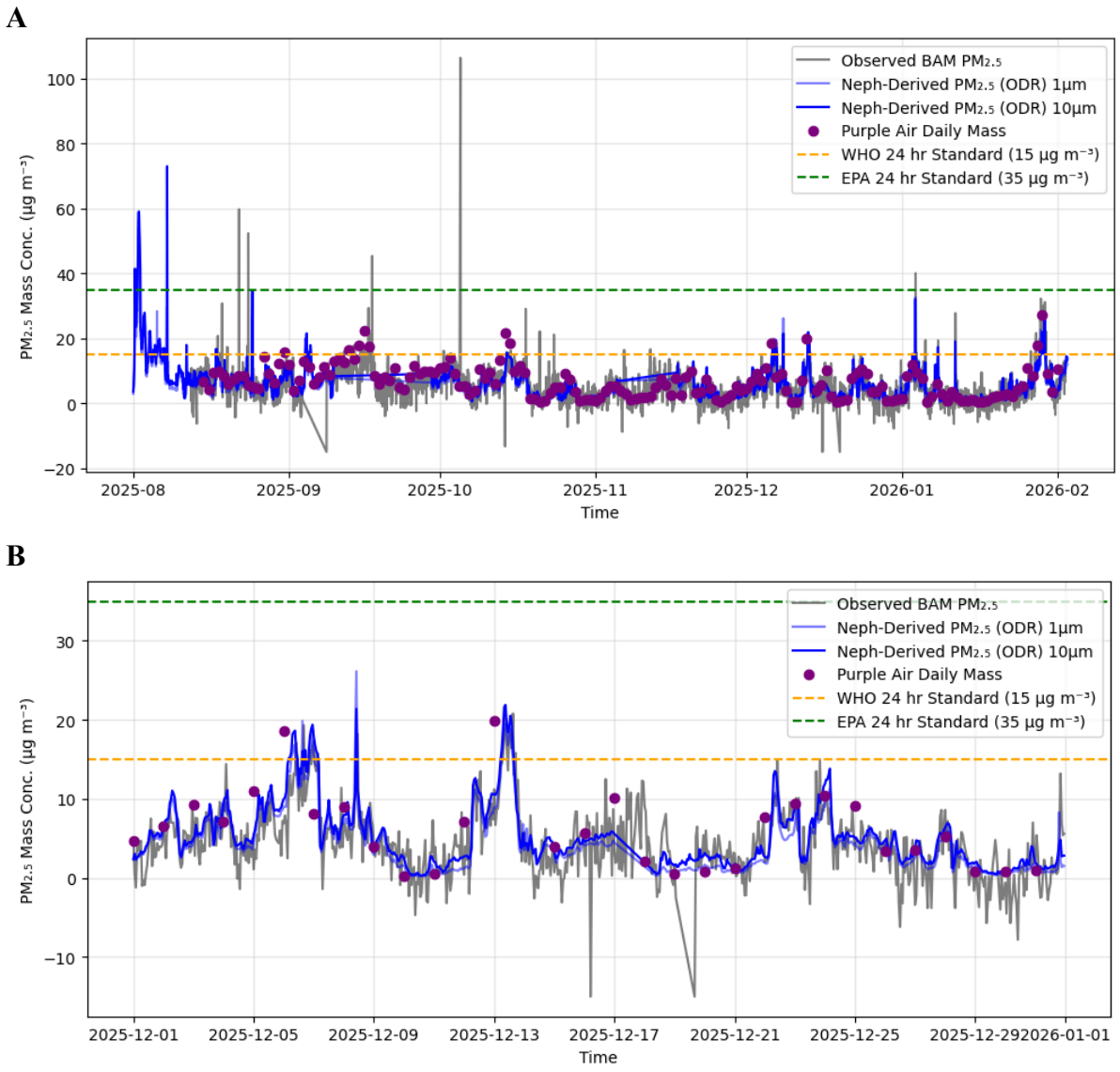

Figure 32: Time series of $PM_{2.5}$ Mass Concentrations measured by BAM, 1µm nephelometer-derived mass, 10µm nephelometer-derived mass, and PurpleAir. Nephelometer-derived values use hourly measurements. This data was not filtered according to fine-mode fraction (FMF). **(A)** Available PurpleAir duration (August 15, 2025 - February 2, 2026). **(B)** December 2025.

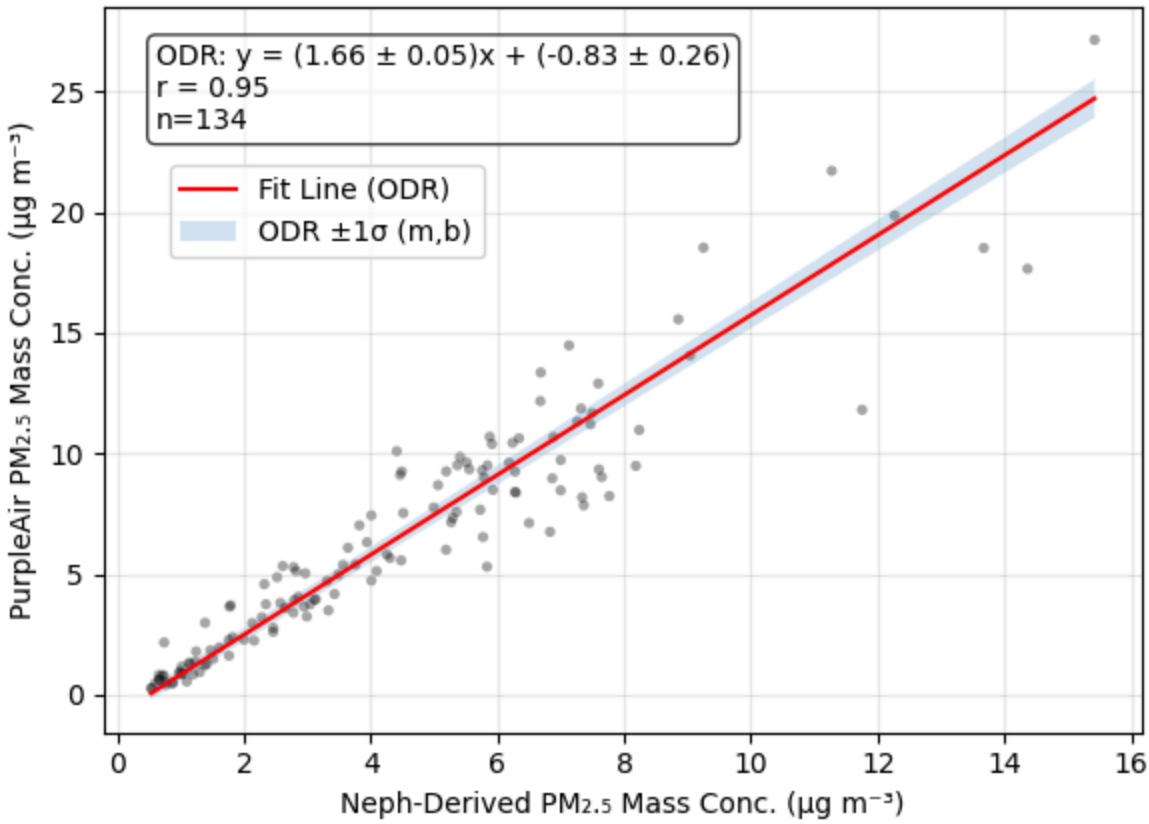

Figure 33: Orthogonal distance regression (ODR) between 1µm nephelometer-derived and PurpleAir measured $PM_{2.5}$ mass concentrations for August 15, 2025-February 2, 2025. Daily averages were calculated from the nephelometer hourly measurements. Points represent concurrent daily averages; the red line shows the ODR fit, and the blue shading indicates the 1σ confidence interval of the fit. This data was not filtered according to fine-mode fraction (FMF).

Figure 34 does the same as Figures 31 and 27, and compares instrument performance in identifying daily $PM_{2.5}$ exceedances relative to World Health Organization (WHO) and United States Environmental Protection Agency (EPA) guidelines. For this analysis, 24-hour average concentrations greater than or equal to 15 µg m^{-3} and 35 µg m^{-3} were used to define WHO and EPA exceedances, respectively

The nephelometer-derived $PM_{2.5}$ mass concentrations identified one exceedance day using the 1 µm size cut and two exceedance days using the 10 µm size cut relative to the WHO

threshold. The 10 μm dataset captured the exceedance identified by the 1 μm dataset, as well as one additional day not detected by the 1 μm measurements. Overall, this corresponds to five fewer WHO exceedances than detected by the PurpleAir instrument and is equal to the number identified by BAM over the same days of observation. None of the instruments identified EPA guideline exceedances.

The collocated measurements for all months, shown in Figure S3, can help to identify when BAM and PurpleAir flagged a day, while neither of the nephelometer-derived products did. PurpleAir registered WHO exceedances on August 31, October 14, October 15, December 6, December 13, January 28, 2026, and January 29, 2026, while BAM and nephelometer-derived (10 μm) only registered January 28 and 29 of 2026. Nephelometer-derived (1 μm) only registered a WHO exceedance on January 29, 2026. These dates follow the same patterns addressed in Figure 27, where nephelometer-derived measurements express some disagreement with other collocated instruments under coarse-mode-dominant conditions. However, this does not explain PurpleAir's classification of August 31, October 14, October 15, and December 13, 2025. Relative humidity has previously been discussed in relation to PurpleAir's higher readings, but this does not seem to be the impacting factor for this study (Couzo et al., 2024). Other contributors to these raised values could be smoke or dust events being untruly weighted due to the laser methodology employed by PurpleAir, but undue sensitivity of the PurpleAir has been discussed in other studies and its forums, and it is beyond the scope of this project to analyze these results deeply.

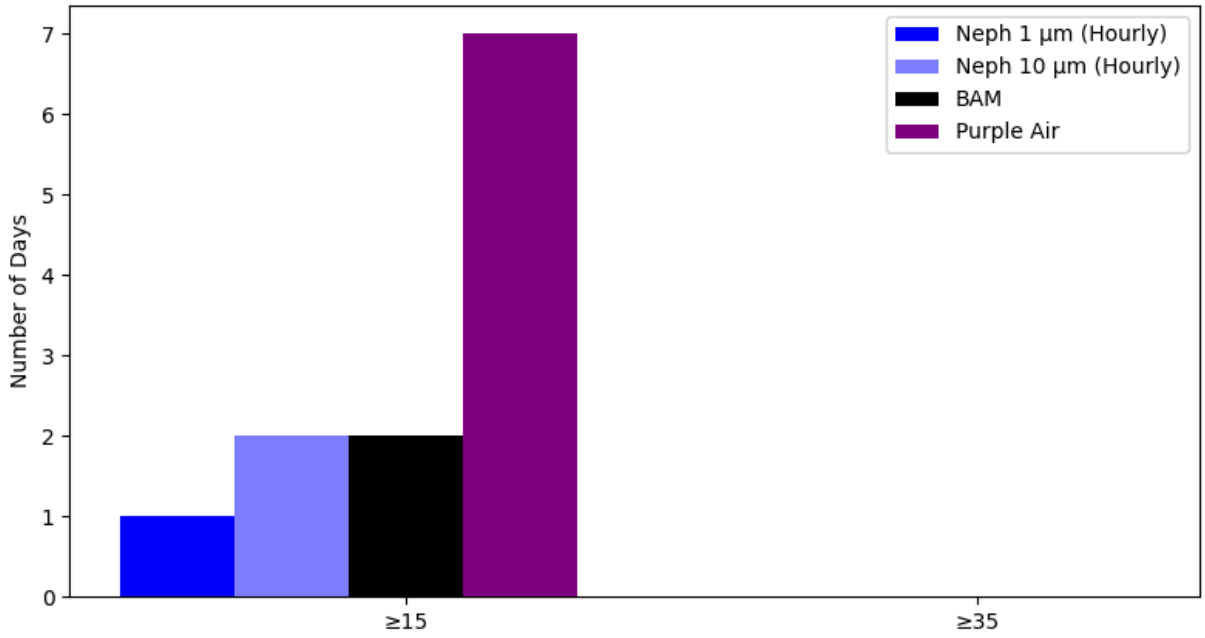

Figure 34: Daily $PM_{2.5}$ exceedances for collocated instruments from August 15, 2025, to February 2, 2025. Bars show the number of days that the daily average $PM_{2.5}$ mass exceeded 15 μgm^{-3} (left) or 35 μgm^{-3} (right) for 1µm and 10µm nephelometer-derived mass concentration, BAM, and PurpleAir. Daily averages were calculated from hourly nephelometer and BAM measurements. This data was not filtered according to fine mode fraction (FMF).

4.3 Calibration Behavior when Extended to Fine Time Scale

The nephelometer produces measurements in near-real time, whereas IMPROVE, SPARTAN, and BAM report observations at longer intervals. Therefore, the next step in this analysis was to assess the performance of the nephelometer-derived mass concentrations reported at minutely intervals compared with the hourly dataset used throughout previous sections. The advantage of this higher temporal resolution is that it may capture short-term variations in PM concentrations that would otherwise be averaged out in hourly data. In the event of accidental releases or rapidly changing meteorological conditions, the minutely dataset may provide valuable information regarding brief spikes in $PM_{2.5}$ concentrations.

Figure 35 depicts the time series of the 1µm and 10 µm nephelometer-derived mass concentrations for both hourly and minutely intervals. Figure 35A shows strong agreement between the two sampling intervals throughout the SPICE sampling duration, while Figure 35B provides a detailed view of this agreement during March 16, 2025. March 14, 2025, was the major dust event, discussed previously, that impacted the state of Oklahoma. Spikes in the minutely dataset appear in the days before and after this event in Figure 35A, and 35B shows similar short-duration peaks that are undetected (averaged out) by the hourly dataset for both the 1µm and 10µm size cuts.

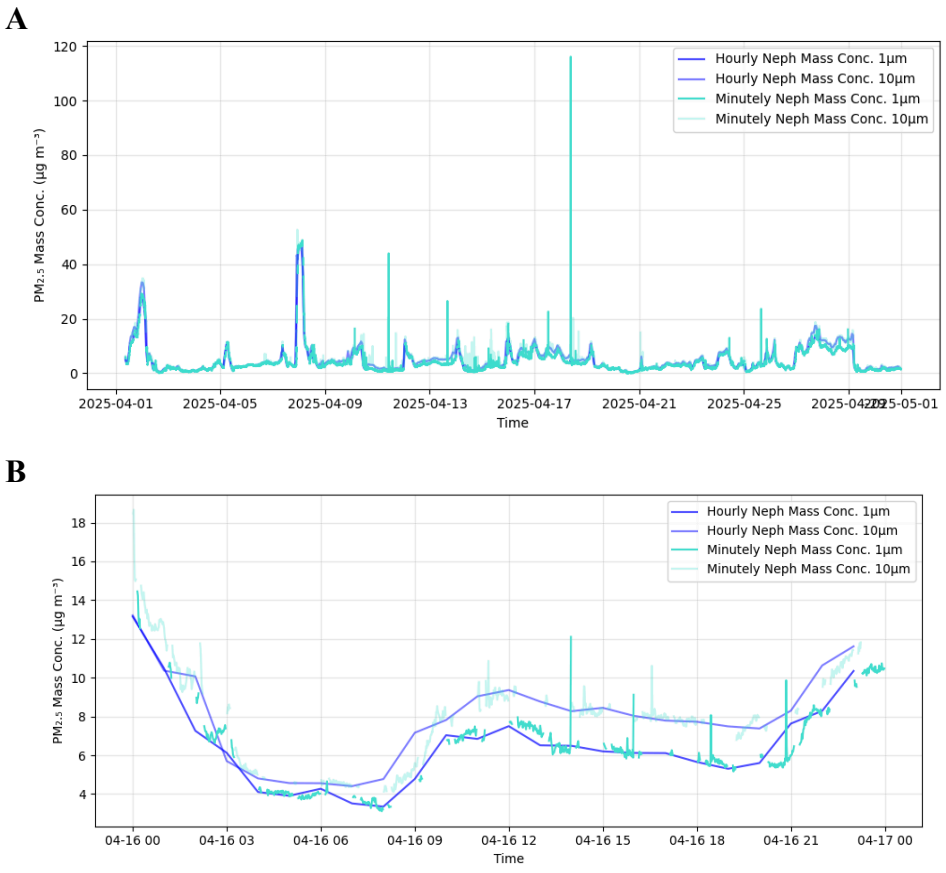

Figure 35: Time series of hourly 1µm nephelometer-derived mass concentration (royal-blue), hourly 10µm nephelometer-derived mass concentration (lavender), minutely 1µm nephelometer-derived mass concentration (cyan), and minutely 10µm nephelometer-derived mass concentration (faded cyan). This data was not filtered according to fine-mode fraction (FMF). **(A)** April 2025. **(B)** April 16, 2025.

A brief comparison was then conducted between the minutely nephelometer dataset and the measurements from the BAM (Figure 36) and PurpleAir sensors (Figure 37), which operate on more comparable time scales than IMPROVE and SPARTAN. Figure 36A shows the time series over the duration of SPICE and has a large y-axis range due to isolated minutes with very large predicted mass concentrations. The discrepancy between BAM and nephelometer-derived estimated values in late June is the same as that depicted in Figure 21 and discussed in section 3.6.4. Likewise, the disparity between BAM and nephelometer-derived measurements in Figure 36B is likely attributable to differences in particle size sensitivity. The BAM measures total $PM_{2.5}$ continuously, whereas the nephelometer alternates between size cuts. Following the March dust event, the nephelometer-derived concentrations from the 10μm channel show closer agreement with BAM observations, consistent with the presence of particles larger than 1μm during this period.

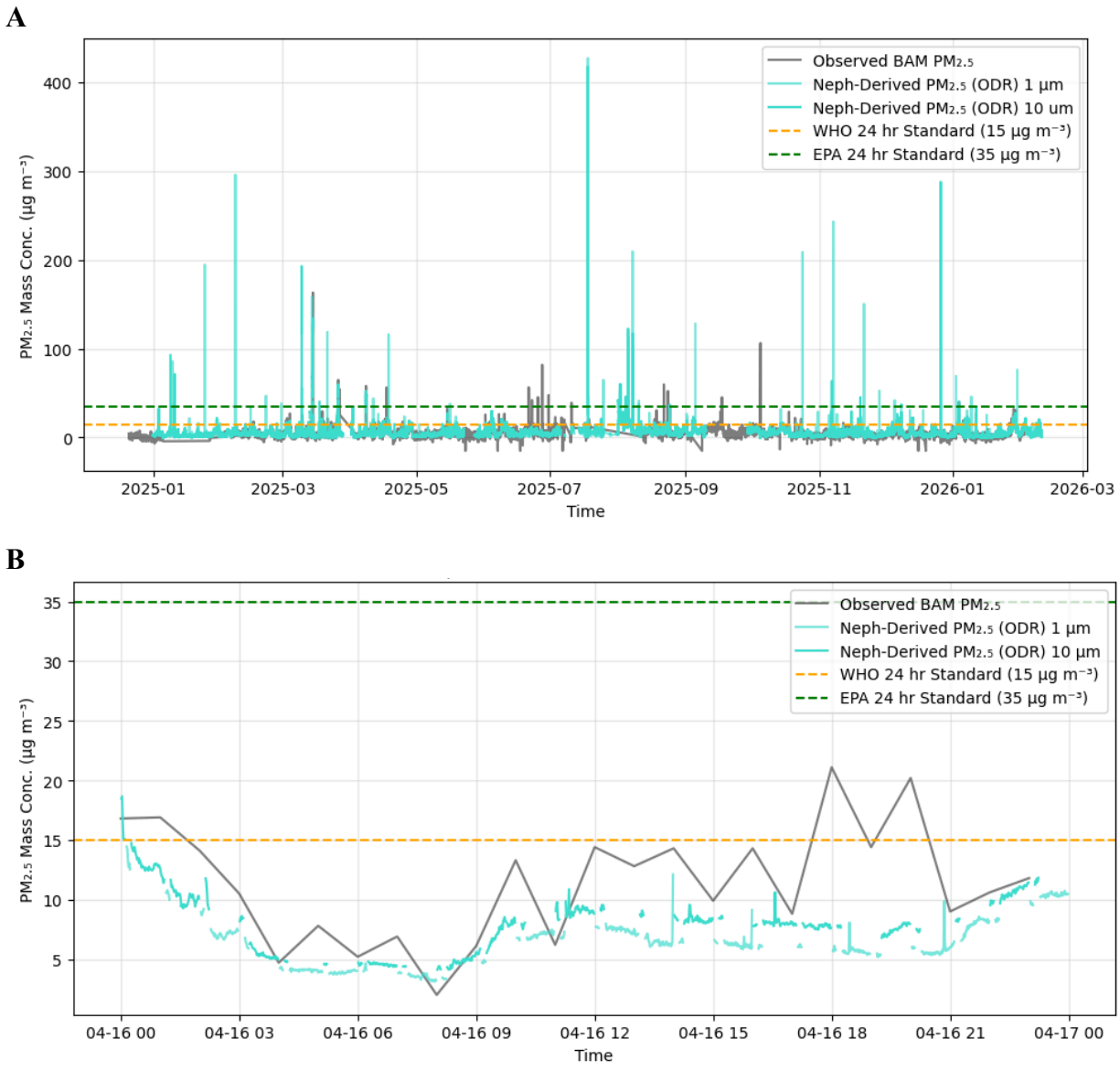

Figure 36: Time series of hourly BAM (grey), minutely 1µm nephelometer-derived mass concentration (cyan), and minutely 10µm nephelometer-derived mass concentration (faded cyan). This data was not filtered according to fine-mode fraction (FMF). **(A)** SPICE Campaign Duration. **(B)** April 16, 2025.

The most comparable temporal resolution is provided by the PurpleAir sensor, which was installed later in the SPICE campaign. Figure 37 presents the time series of the PurpleAir and nephelometer-derived mass concentrations for October 2025. Overall agreement is strong between the two instruments, with the exception of October 24, when there were wind gusts of

25-30 mph on and off throughout the day, with a maximum wind gust of 40 mph around midday, which would have transported lots of coarse-mode particles, causing the peak.

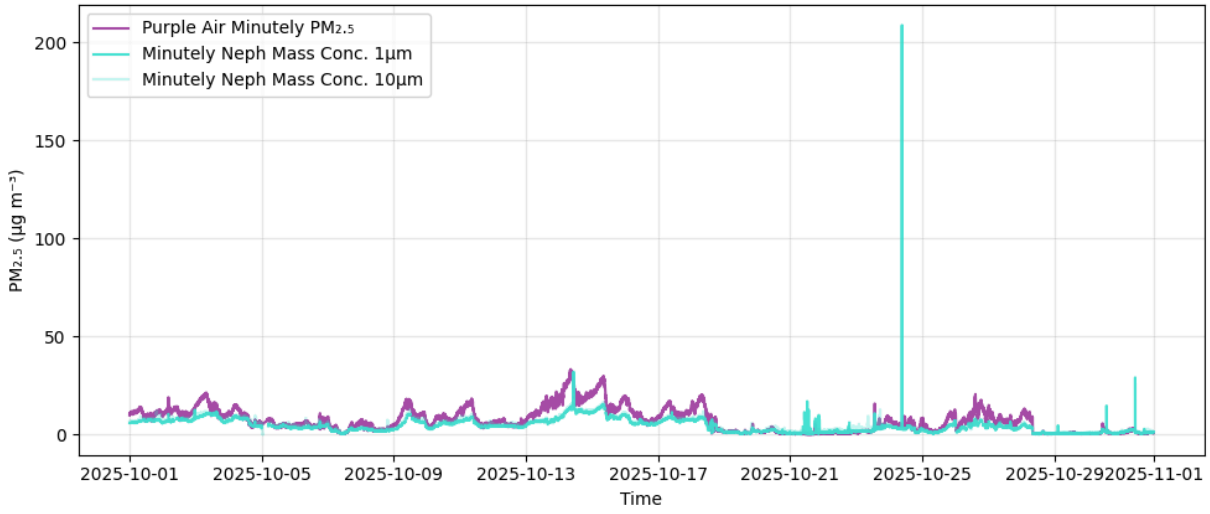

Figure 37: Time series of $PM_{2.5}$ Mass Concentrations measured by PurpleAir (purple), 1µm nephelometer-derived mass (cyan), and 10µm nephelometer-derived mass (faded cyan) for October 2025. Nephelometer-derived values and PurpleAir use minutely measurements. This data was not filtered according to fine-mode fraction (FMF).

Finally, 24-hour averages were calculated for each instrument. SPARTAN sampling periods were assigned to the first day of their respective sampling windows, as described previously. At the 1µm size cut, both the hourly and minutely nephelometer-derived hourly recorded seven WHO exceedance days, which is consistent with the exceedance count identified by the BAM observations (Figure 38). PurpleAir, IMPROVE, and SPARTAN recorded fewer WHO exceedances (five, three, and one days, respectively). The lower counts for IMPROVE and PurpleAir are expected because IMPROVE samples only every third day, missing two-thirds of possible exceedance days, and PurpleAir was installed later in the campaign. Similarly, SPARTAN followed the IMPROVE sampling protocol for every other IMPROVE sample until October, providing measurements for less than one-third of the campaign days during this period.

SPARTAN's WHO exceedance is, in fact, a coarse-mode-dominant day measured on a PM_{10} filter rather than $PM_{2.5}$, and should be considered as such. If PurpleAir had been operational for the entire SPICE campaign, it would likely have identified the most exceedance days of all the instruments.

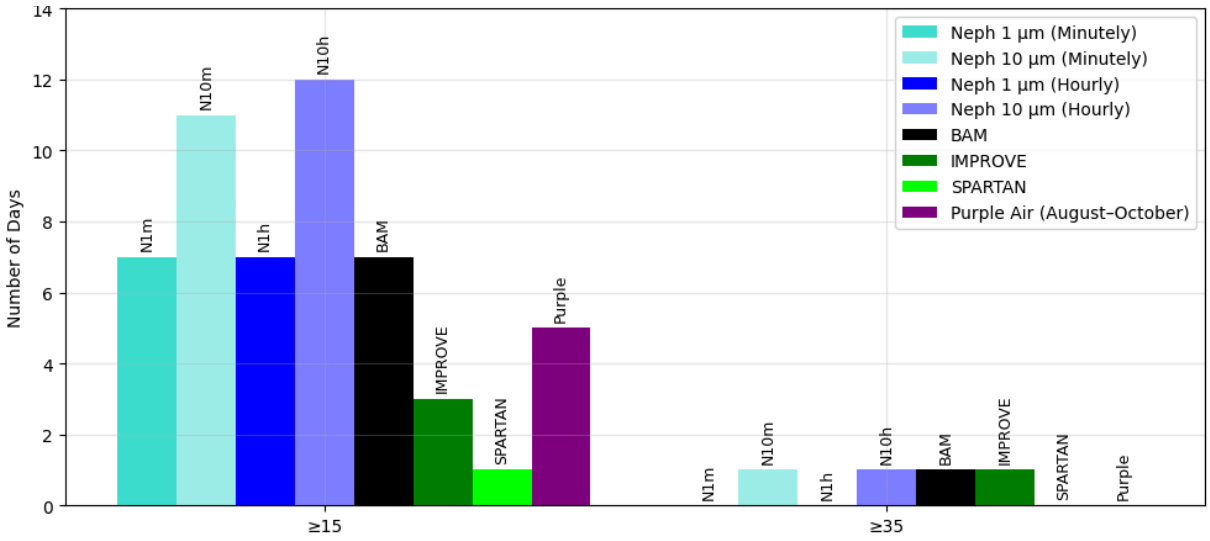

Figure 38: All available daily $PM_{2.5}$ exceedances for collocated instruments from January to October 2025. Bars show the number of days that the daily average $PM_{2.5}$ mass exceeded 15 μgm^{-3} (left) or 35 μgm^{-3} (right) for 1µm and 10µm nephelometer-derived mass concentration (hourly and minutely datasets), BAM, and PurpleAir. Daily averages were calculated from hourly nephelometer and BAM measurements except in the case of the minutely nephelometer-derived mass concentrations. SPARTAN's exceedance is due to a coarse-mode-dominant day measured with PM_{10} filter conditions. This data was not filtered according to fine-mode fraction (FMF).

4.4 Application of Calibration to SPICE Dates

In the previous section, the large y-axis range observed in Figure 36A was attributed to isolated spikes in the minutely nephelometer-derived mass concentrations. The higher temporal resolution of the minutely dataset increases sensitivity to short-duration peaks and provides a more detailed representation of daily air quality. However, exceedance exposures lasting only a single minute do not necessarily constitute a meaningful exceedance event.

To investigate this further, the minutely nephelometer-derived mass concentration dataset was compared with the hourly BAM mass concentration datasets to determine the number of measurements exceeding guideline thresholds. The minutely nephelometer-derived dataset recorded **more than 12,500 minutes that were above the WHO guidelines** and **1,650 above the EPA limit**, while the BAM recorded **230 hours and 31 hours**, respectively.

To better characterize exceedance events rather than isolated spikes, the minutely dataset was further analyzed by identifying consecutive exceedance periods. This filtering allowed exceedance events to be categorized based on durations of **10+, 30+, 40+, 50+, and 55+ consecutive minutes**.

Figure 38 previously illustrated the number of exceedance **days** identified using 24-hour averages. When examining shorter-duration events in the minutely dataset against these daily exceedances, the number of exceedances (daily or event) increases substantially for events lasting **10+, 30+, 40+, and 50+ minutes** in duration, but decreases for events persisting **55 minutes or longer**.

These results demonstrate that nephelometer-derived mass concentrations provide high temporal resolution measurements that can capture short-duration exceedance events that may be obscured in hourly or daily averages. At the same time, the dataset can be aggregated across multiple temporal scales (e.g., daily, monthly, and seasonal) to support analyses relevant to human health exposure studies. The exceedance event durations identified in this analysis are summarized in Table 5.

Table 5: Counts of WHO and EPA PM2.5 Exceedance Events: Hourly BAM vs. Consecutive-Duration Nephelometer Criteria

	Neph n	**10+ Min.**	**30+ Min.**	**40+ Min.**	**50+ Min.**	**55+ Min.**	**BAM n**
WHO Exceedance Events	12,587	284	228	209	62	5	230
EPA Exceedance Events	1,650	30	24	23	6	0	31

4.5 Application of Calibration to Interpolated Speciation

At the beginning of this work, the growing importance of monitoring aerosol composition (speciation) in addition to mass concentration was discussed. Aerosols of different chemical compositions interact differently with biological systems at the cellular level, and many toxic compounds can induce oxidative stress and other forms of damage within the cardiopulmonary system. For this reason, the analysis was extended beyond total mass concentration in order to develop a more complete representation of air quality at the site.

The IMPROVE network reports both $PM_{2.5}$ mass concentration and chemical speciation derived from multiple filter analyses. However, due to the IMPROVE sampling schedule, measurements are only collected every third day, leaving two days between each sampling event without speciated observations. To estimate speciated mass concentrations during these unsampled periods, an interpolation approach was applied.

First, all occurrences of two consecutive days without IMPROVE measurements that were bounded by valid measurement days were identified. For each of these cases, the mass fraction of each reported chemical component relative to the total IMPROVE mass concentration was calculated for both the preceding and following measurement days. Mass fractions were then

linearly interpolated for the two intervening days for each major contributory component, including **nitrate, organic carbon, sulfate, soil, total carbon, ammonium nitrate, and ammonium sulfate**. The interpolated mass fractions were subsequently multiplied by the nephelometer-derived mass concentration to estimate speciated mass concentrations for each available day during the period January 2025 through May 1, 2025.

Figure 39A shows the mass concentrations of the speciated components measured directly by the IMPROVE station on its standard sampling schedule. Figure 39B presents the reconstructed time series over the same period using the 24-hour average nephelometer-derived mass concentration, calculated from both the $PM_{2.5}$ and PM_{10} size cuts to obtain a single daily mass concentration estimate for each component. The hourly and minutely reconstructions, which treat the $PM_{2.5}$ and PM_{10} size cuts independently, are shown in Figures 39C and 39D, respectively.

During the March 14 dust event, Figure 39B underestimates the soil mass contribution relative to the IMPROVE observations. This discrepancy results from averaging $PM_{2.5}$ and PM_{10} mass concentrations together when the nephelometer alternates between size cuts during sampling. In this case, the PM_{10} fraction dominated the total mass concentration, and averaging the two size cuts reduced the reconstructed soil contribution. This behavior was anticipated and discussed previously. When the PM_{10} size cuts are examined independently (Figures 39C and 39D), the nephelometer-derived mass concentration more accurately captures the elevated mass concentrations associated with the dust event, despite the calibration being developed primarily under fine-mode-dominant conditions.

Overall, the reconstructed $PM_{2.5}$ speciated mass concentrations show good agreement with the IMPROVE measurements presented in Figure 39A. Additional speciated components,

including several trace metals, were processed using the same method; however, these species contributed less than 10% of the total mass and were omitted from the figures for clarity.

A

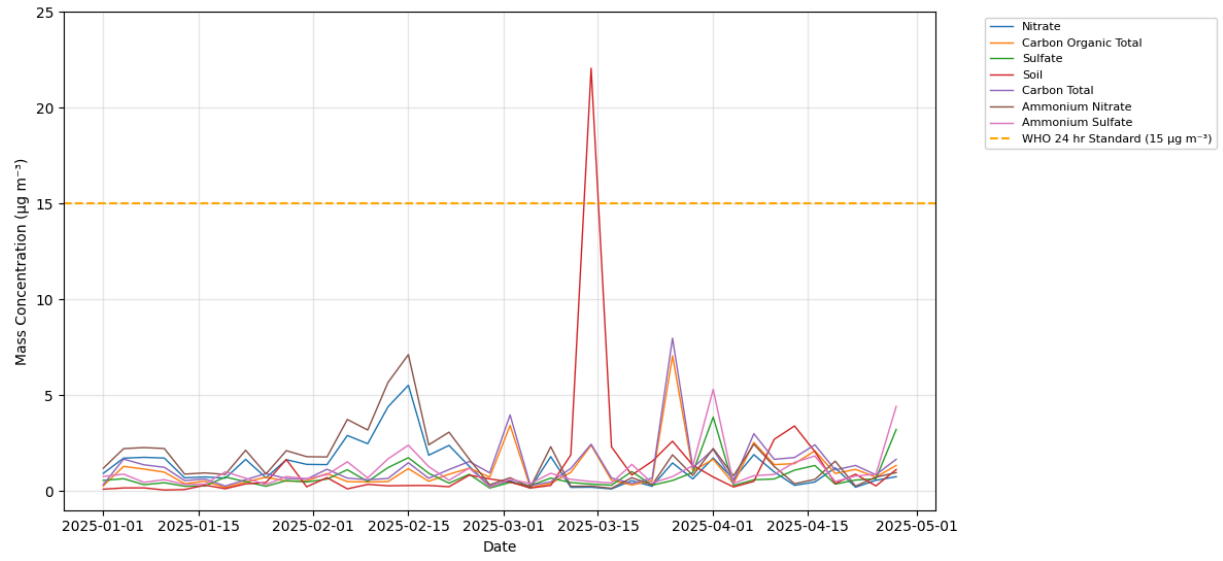

B

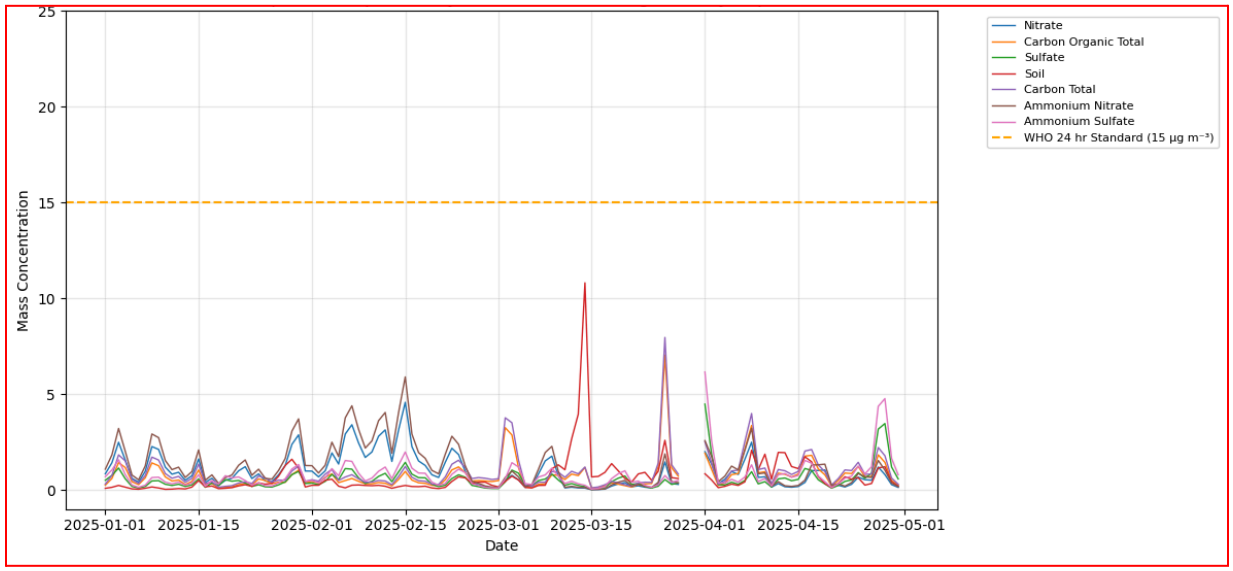

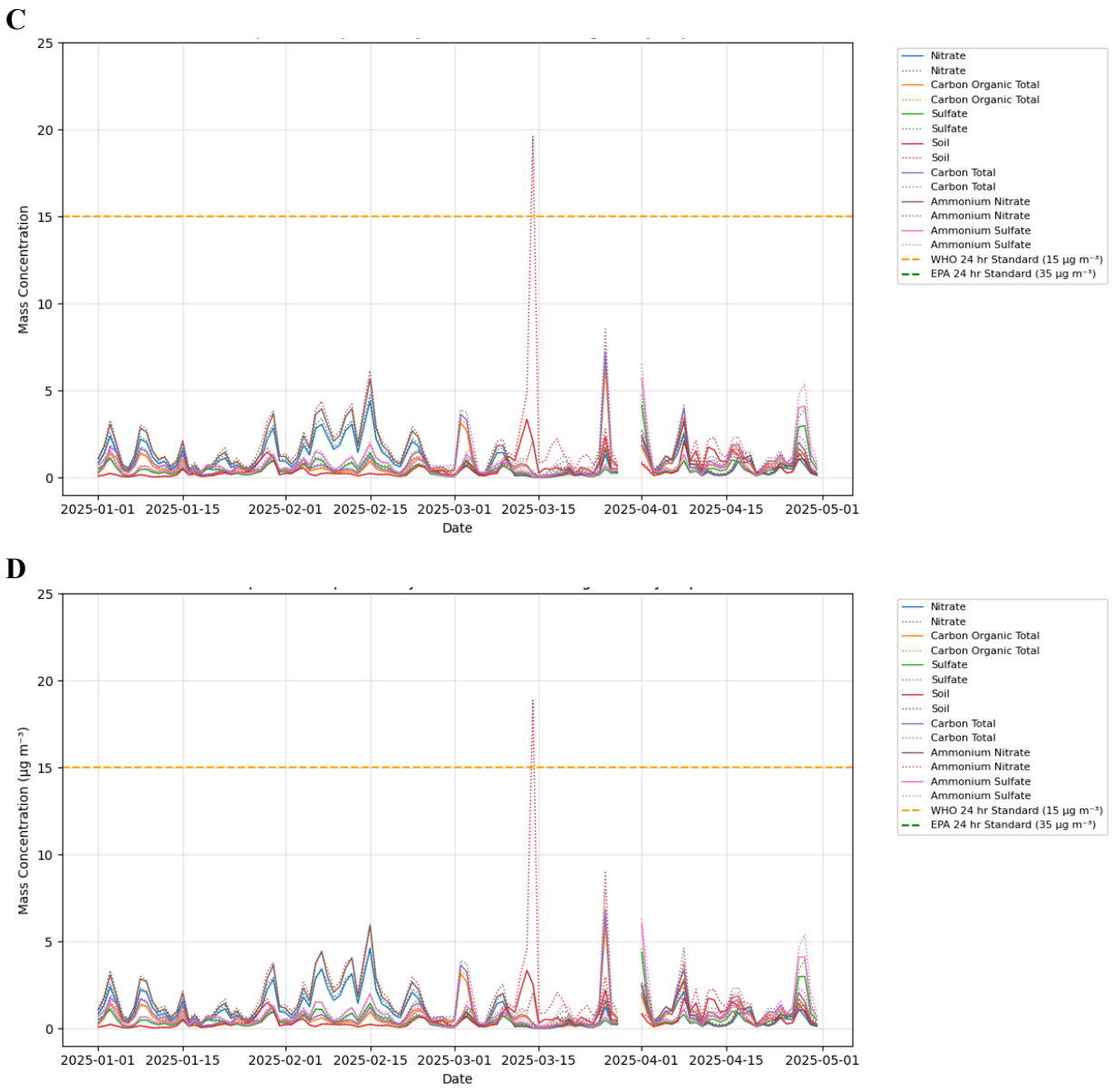

Figure 39: Time series of speciated $PM_{2.5}$ mass concentration depicting only compounds that have a mean mass fraction ≥ 10% of the total mass for the duration of IMPROVE speciated data availability (January - May 1, 2025). This data was not filtered according to fine-mode fraction (FMF). **(A)** IMPROVE Network $PM_{2.5}$ Dataset (sampled every third day). **(B)** Average estimated mass concentration using both PM10 and PM2.5 mode data from the minutely dataset. **(C)** Estimated speciated mass concentration using the hourly nephelometer dataset and IMPROVE mass fractions to interpolate missing days. **(D)** Estimated speciated mass concentration using the minutely nephelometer dataset and IMPROVE mass fractions to interpolate missing days. In plots (C) and (D), dotted lines show values associated with PM_{10} observations, while solid lines are $PM_{2.5}$. Plots (B), (C), and (D) use mass fraction to interpolate the mass of and identity of contributing compounds when there are ≤ 2 days between IMPROVE measurements.

Chapter 5

Discussion

Chapters 3 and 4 presented the development and testing of a method for deriving $PM_{2.5}$ mass concentration from nephelometer total scattering measurements using the blue wavelength. An inherent limitation discussed throughout this work is the underestimation of $PM_{2.5}$, particularly under coarse-mode-dominant conditions. This occurs because the nephelometer does not have an explicit $PM_{2.5}$ size cut, and the derived relationship was established by comparing 1μm size cut nephelometer data with BAM measurements using a 2.5μm size cut, calibrated only under fine-mode-dominant days. This limitation is reflected throughout the analysis and remains relevant in the results presented in this chapter. The following discussion evaluates the impact of this source of error and concludes by considering the broader implications and potential applications of this work.

5.1 Speciation Application Partial Seasonality

While developing a predictive relationship between nephelometer total scattering and speciated $PM_{2.5}$ mass concentration was beyond the scope of this study, the interpolation methods described in Chapter 4 were used to address gaps in the observational record. The performance of these interpolated estimates was evaluated against IMPROVE-derived partial seasonal averages for January-February (JF) and March-April (MA) of 2025 (Figure 40). As expected, the relative component contributions remained constant because they were derived directly from the IMPROVE observations; however, differences emerged in the seasonal results.

For the January-February period, the standard deviation between the IMPROVE measurements and the interpolated estimates increased slightly from approximately 2.3 to 2.5

µg/m^3, while the mean daily mass concentration was underestimated by 1.2 µg/m^3. In contrast, for the March-April period, the standard deviation decreased more substantially, from approximately 6.0 to 3.7 µg/m^3, and the mean daily mass concentration was underestimated by 3.3 µg/m^3.

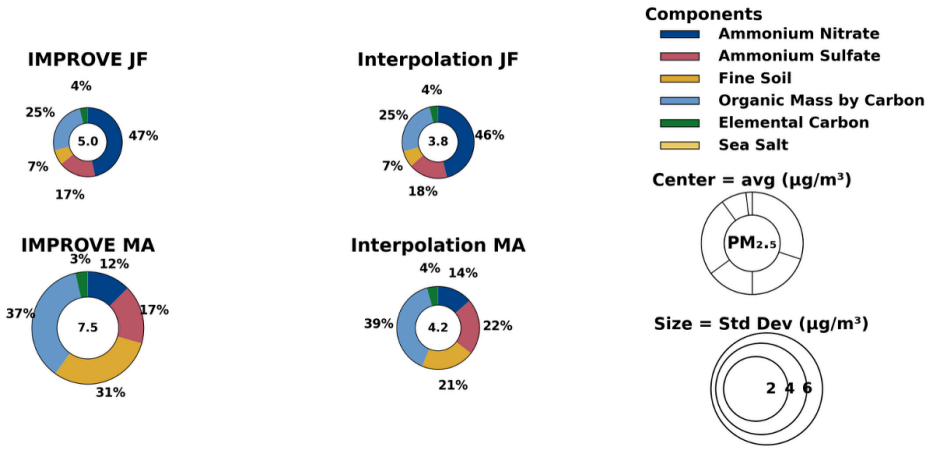

Figure 40: SOGP1's seasonal aerosol composition (January-April 2025)with partial seasonally averaged daily $PM_{2.5}$ mass concentrations (µg/m^3). The left column represents IMPROVE observed data, while the right column of pie charts represents the data from the interpolated estimation.

The differences in standard deviation can be explained by both historical trends and the interpolation methodology used in this study. According to the five-year averages shown in Figure 41, January and February are typically low-aerosol months, with total daily averages of approximately 4.5 and 6.9 µg/m^{3,} respectively, and relatively small variability at the monthly scale. In 2025, January exhibited a standard deviation consistent with these historical expectations, while February showed an even lower variability for both the IMPROVE observations and the interpolated estimates compared with the five-year average (Figure 42A).

In contrast, although March and April have similar five-year average variability (Figure 41), the 2025 data reveal that March experienced an unusually high spread in values (Figure 42).

This elevated variability was likely driven by the dust storm event on March 14, which substantially increased aerosol concentrations during that period. As a result, the IMPROVE observations reflect a larger standard deviation, while the interpolation methodology moderated this effect, resulting in a lower variability in the interpolated estimates.

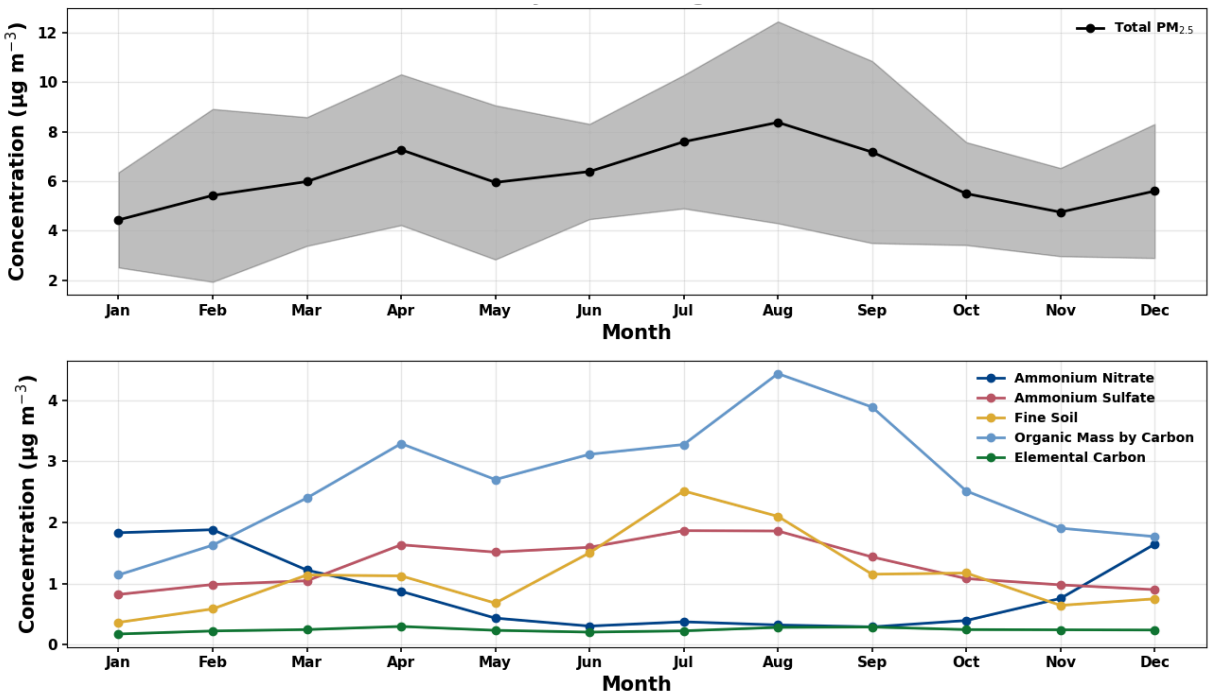

Figure 41: Five-year (2020-January 1, 2025) monthly average $PM_{2.5}$ mass concentration for SOGP1 (top) and five-year monthly speciated average $PM_{2.5}$ mass concentration for SOGP1 (bottom).

Another factor that may contribute to the lower variability observed in the interpolated estimates is the known underestimation tendency of the nephelometer-derived relationship, particularly under coarse-mode conditions. As discussed previously, this relationship can underestimate $PM_{2.5}$ mass concentration when larger particles contribute substantially to total aerosol mass. Figure 42 (top) shows that the daily average total $PM_{2.5}$ mass concentration varied by no more than approximately ± 6 µg/m^3, with the maximum occurring in March. Among the

speciated components, Fine Soil exhibited the largest variation, yet still changed by only about 3 $\mu g/m^3$ during March.

Taken together, these results suggest that the interpolated speciation estimates remain reliable for monthly and seasonal averages, even though individual daily values may underestimate $PM_{2.5}$ mass concentration under coarse-mode-dominated periods. Figure 43 further demonstrates that although the 2025 daily averages are somewhat lower than the five-year average, the SPICE sampling year (2025) does not represent an outlier relative to the longer-term record.

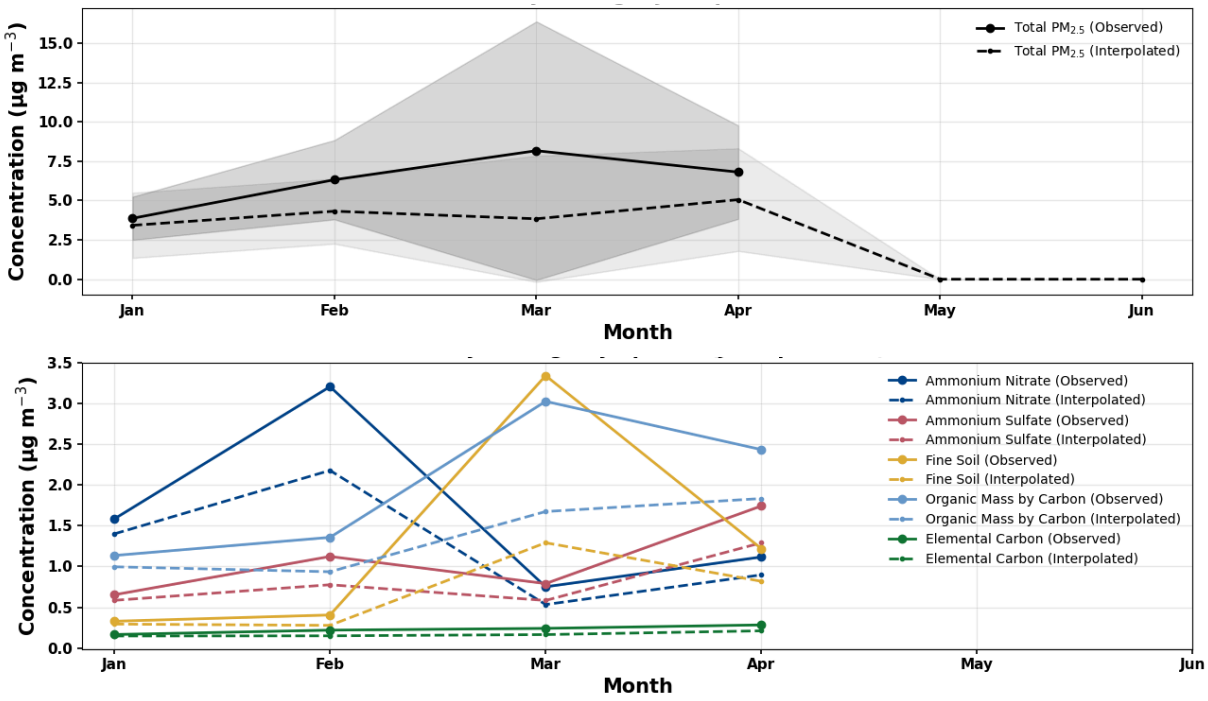

Figure 42: January - April 2025 Monthly average $PM_{2.5}$ mass concentration for SOGP1 (top) and January - April 2025 Monthly average speciated $PM_{2.5}$ mass concentration for SOGP1 (bottom).

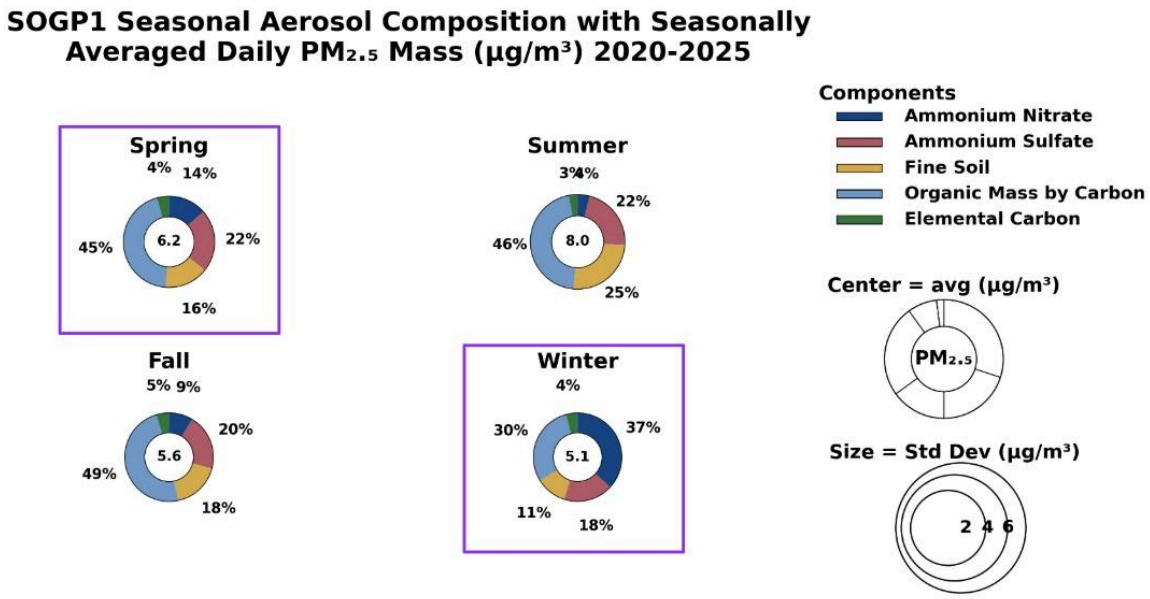

Figure 43: Five-year average (2020-January 1, 2025) of SOGP1's Seasonal Aerosol Composition with Seasonally Averaged Daily $PM_{2.5}$ Mass Concentrations (µg/m^3). Spring (MAM) and Winter (DJF) are boxed for easier comparison with Figure 40.

5.2 Implications at the ARM SGP Site

The ARM SGP site IMPROVE measurements, as discussed above, are comparable to the interpolated mass concentration measurements. This implies that the ARM SGP site collects enough information for seasonal and monthly average analyses; however, this may not be the case in all locations. The ARM SGP site is a relatively clean site, though the short-term exceedance plots discussed in Chapter 4 demonstrate that IMPROVE missed numerous exposure events that would be necessary to identify in acute health studies. Implementation of the nephelometer-derived $PM_{2.5}$ estimates and speciated estimates can help inform the agricultural and indigenous communities nearby.

5.3 Broad Implications

At this time, monitoring of acute $PM_{2.5}$ exposure events due to ambient outdoor aerosols is limited. The fastest public sector operations tend to produce data hourly, which can still miss short-term exceedances. The nephelometer-derived mass concentration developed in this work is a step forward in making high temporal resolution estimates of $PM_{2.5}$ mass concentration, and potentially $PM_{2.5}$ speciated, more widely available.

Because nephelometers measure a fundamental physical property of aerosols (light scattering), the derived relationship with mass concentration may be broadly applicable and may not require full recalibration at every monitoring site. Incorporating fine-mode considerations, along with the use of both the 1 μm and 10 μm size cuts, improves the robustness of the relationship, provided that the limitations associated with the absence of a direct 2.5 μm to 2.5 μm comparison between the BAM and the nephelometer measurements are acknowledged.

This relationship provides a useful starting point for the retrospective analysis of aerosol exposure events using nephelometer data. However, it is important to recognize that these nephelometer-derived mass estimates may underestimate $PM_{2.5}$ under coarse-mode dominated conditions, when larger particles contribute more significantly to mass but are underrepresented in the 1μm size cut measurements.

Despite this limitation, nephelometer-derived mass concentrations can provide reliable monthly and seasonal averages of $PM_{2.5}$ mass concentrations that are useful for evaluating long-term exposure and health-relevant trends. These estimates are particularly valuable for assessing total $PM_{2.5}$ mass concentration, whereas aerosol composition cannot be generalized in the same way.

In contrast to total mass concentration, aerosol speciation depends strongly on local sources, atmospheric chemistry, and seasonal transport trends. As a result, speciated composition relationships require calibration using site-specific filter-based measurements. Establishing accurate speciation estimates, therefore, requires the presence of a reference monitoring site capable of providing chemical composition data, which is not as widely applicable as the total $PM_{2.5}$ mass concentration estimates developed in this work.

The primary novelty of the nephelometer-derived mass concentration is that it provides reliable monthly, seasonal, and annual averages while simultaneously preserving the high temporal resolution necessary to identify short-duration exposure events. These events are often averaged out or missed entirely by monitoring systems with limited sampling frequency, such as the IMPROVE network. Consequently, nephelometer-derived $PM_{2.5}$ mass concentrations provide a valuable tool for estimating particulate mass concentration and evaluating exposure trends in locations where full chemical speciation measurements are unavailable.

Future work can further refine the nephelometer-derived mass concentration relationship by incorporating seasonal variability and more fully integrating BAM observations under conditions where the fine-mode fraction (FMF) is less than 0.85. Such work may enable the development of a multiplicative correction factor to account for particles between 1μm and 2.5μm, which are currently underrepresented in the 1μm nephelometer measurements and only partially captured in the 1μm size cut data.

A particularly valuable next step would be the development of predictive relationships for aerosol speciation rather than retrospective gap filling. Results could be compared to both IMPROVE and SPARTAN speciated measurements to assess performance. Achieving this would require incorporating additional environmental variables such as wind speed, wind direction,

seasonal aerosol behavior, atmospheric transport mechanisms, and atmospheric chemistry. Nevertheless, such predictive capability could significantly improve air-quality alert systems. As discussed above, most instruments capable of measuring aerosol mass concentration operate at lower temporal resolution than is ideal for acute exposure warnings, and speciated measurements require even longer processing times. Predictive speciated estimates derived from nephelometers combined with basic meteorological observations could therefore substantially enhance the timeliness and specificity of air-quality alerts.

Chapter 6

Conclusion

The SPICE Campaign in Billings, Oklahoma, observed one year of aerosol activity in a rural, agricultural setting. Due to the high density of instruments and extensive historical dataset at the ARM SGP site, this site was the ideal location for an instrumentation study such as this. Using total scattering at 1 μm from the nephelometer and $PM_{2.5}$ mass concentration from the BAM, this study investigates the possibility of creating proxy measurements from nephelometers to improve the availability of aerosol monitoring. The nephelometer is advantageous primarily for its high temporal resolution, but it is also deployable in ARM's mobile facility and can provide measurements in remote, rural, or other communities that don't normally have relevant aerosol mass concentration information. Access to these enhanced datasets has the potential to improve public health by enabling more accurate exposure assessments and supporting real-time alert systems to mitigate risks during periods of elevated $PM_{2.5}$ concentrations.

Despite our best efforts, the nature of each of these instruments and this study does not allow us to have a majority of co-sampled days for all of these instruments. We worked with our data availability according to the sampling schedule, and future studies can adjust these strategies accordingly.

To conclude, each of the three primary science questions outlined in Section 2.4 will be addressed and answered.

SQ (1) asked how well co-incident mass concentration measurements from existing monitoring systems aligned. Figures 22 and 23 answered this question by demonstrating the agreement between each of the instruments through correlation coefficients (r) values all above 0.94 after eliminating outliers attributed to non-conducive conditions as discussed.

SQ (2) uses the reassurance from SQ (1) to investigate the extent to which the nephelometer-derived mass concentration (1 μm) is representative of the observed mass concentrations from the existing instruments (BAM, IMPROVE, PurpleAir, SPARTAN). Figures 26, 30, and 33, as well as Table 5, serve to answer this inquiry by depicting how the short-term agreement between the nephelometer-derived mass concentration and the selection of instruments was satisfactory; however, the long-term agreement is much more inspiring, as discussed in Chapter 5. This is not to say that the short-term comparisons are disagreeable; rather, the differences open the door to more detailed exposure studies, also discussed in Chapter 5.

SQ (3) targeted an understanding of the conditions under which the nephelometer-derived dataset would recognize air quality risk days that were not previously identified by existing instruments. The minutely nephelometer-derived air quality risk days registered in Figure 38 and Table 5 overtook the IMPROVE and SPARTAN measurements due to the nephelometer's temporal availability. IMPROVE and SPARTAN, in this study, are likely to miss poor air quality events caused by short-term meteorological drivers such as temperature inversions that do not persist for longer than three days, wildfires, prescribed fires, and high wind events.

Overall, the results of this study support the plausibility of using nephelometer measurements to derive total $PM_{2.5}$ mass concentration in regions where other $PM_{2.5}$ measurements are lacking or nonexistent. This work demonstrates the applicability of this calibration not only to provide reliable mass concentration data but also to detect potential exposure events more quickly and in more detail than its counterparts and provide speciated estimates to complete pre-existing observation profiles. A longer collocation period with complete speciated data would only improve these calibrations. As they stand, the high temporal

frequency of nephelometer-derived $PM_{2.5}$ datasets have applications in public health, environmental monitoring, and industry

Bibliography

2012_aqi_factsheet, 2016. Accessed 12 March 2026, https://www.epa.gov/sites/default/files/2016-04/documents/2012_aqi_factsheet.pdf.

2025-AQRC-Calendar_WEB, 2025. UC Davis.

Anderson, T. L., and Coauthors, 1996: Performance Characteristics of a High-Sensitivity, Three-Wavelength, Total Scatter/Backscatter Nephelometer.

B01003: Total—Estimate in 2021 - Census Bureau Map,. Accessed 1 April 2026a, https://data.census.gov/map?tid=ACSDT1Y2021.B01003&layer=VT_2021_040_00_PP_D1&loc=43.3512,-113.0431,z2.6797.

Beagley, J.,: Clean Air NDC Scorecard 2023 - The Global Climate and Health Alliance. Accessed 12 March 2026, https://climateandhealthalliance.org/clean-air-ndc-scorecard-2023/.

Berryman, K., 2025: How to calculate Raw PM2.5 ALT cf=3.4 from SD card files - Data. *PurpleAir Community*. Accessed 12 March 2026, https://community.purpleair.com/t/how-to-calculate-raw-pm2-5-alt-cf-3-4-from-sd-card-files/22388.

Bishop, S., 2025: Ambient air quality standards & regulations around the world. Accessed 12 March 2026, https://www.clarity.io/blog/the-new-who-air-quality-guidelines-and-how-they-compare-with-air-pollution-regulations-around-the-world.

Bissonnette, P. P., C. Weagle, E. Stone, and E. L. Roy, 2020: Determination of Fine Particulate Matter Mass Concentration on PTFE® Filters.

Burns, A. M., G. Chandler, K. J. Dunham, and A. G. Carlton, 2023: Data Gap: Air Quality Networks Miss Air Pollution from Concentrated Animal Feeding Operations. *Environ. Sci. Technol.*, **57**, 20718–20725, https://doi.org/10.1021/acs.est.3c06947.

CDC, 2023: Protect Yourself From Histoplasmosis. *Centers for Disease Control and Prevention*. Accessed 1 May 2024, https://www.cdc.gov/fungal/features/histoplasmosis.html.

Chow, J. C., J. G. Watson, L.-W. A. Chen, W. P. Arnott, H. Moosmüller, and K. Fung, 2004: Equivalence of Elemental Carbon by Thermal/Optical Reflectance and Transmittance with Different Temperature Protocols. *Environ. Sci. Technol.*, **38**, 4414–4422, https://doi.org/10.1021/es034936u.

Couzo, E., A. Valencia, and P. Gittis, 2024: Evaluation and Correction of PurpleAir Temperature and Relative Humidity Measurements. *Atmosphere*, **15**, 415, https://doi.org/10.3390/atmos15040415.

Current Air Quality & Forecasts,. *Oklahoma Department of Environmental Quality*. Accessed 1 May 2024b, https://oklahoma.gov/deq/divisions/air-quality/ambient-monitoring/current-air-quality-forecasts.html.

Determination of Anions and Cations Extracted from Nylon® Filters by Ion Chromatography (IC),. Research Triangle Institute.

Dillner, A. M., 2016: Recent Changes to the IMPROVE and CSN Organic Carbon Artifact Adjustment Method.

El Haddad, I., and Coauthors, 2023: Opinion: how are advances in aerosol science informing our understanding of the health impacts of outdoor particulate pollution? *EGUsphere*, 1–38, https://doi.org/10.5194/egusphere-2023-1472.

Felder, B., 2024: Fertilizer from human waste faces scrutiny but remains a profitable industry. *Investigate Midwest*. Accessed 12 March 2026, https://investigatemidwest.org/2024/08/07/fertilizer-from-human-waste-faces-scrutiny-but-remains-a-profitable-industry/.

Filter Conditioning and Weighing Facilities and Procedures for PM2.5 Reference and Class I Equivalent Methods,. EPA.

GML Web Team, 1996: Mauna Loa Observatory - NOAA Global Monitoring Laboratory. Accessed 12 March 2026, https://gml.noaa.gov/obop/mlo/programs/coop/nasa/aeronet/aeronet.html.

——,: Aerosol Network - NOAA Global Monitoring Laboratory. Accessed 12 March 2026e, https://gml.noaa.gov/aero/science/index.html.

Green, G., 2025: Senator Green's bill prohibiting biosolids as fertilizer passes Senate | Oklahoma Senate. Accessed 12 March 2026, https://oksenate.gov/press-releases/senator-greens-bill-prohibiting-biosolids-fertilizer-passes-senate.

Hazardous Substance Fact Sheet, 2008. New Jersey Department of Health, accessed 12 March 2026, https://www.nj.gov/health/eoh/rtkweb/documents/fs/0152.pdf.

Histoplasma Capsulatum | Texas A&M University Kingsville,. Accessed 1 May 2024f, https://www.tamuk.edu/finance/risk/animal-safety/histoplasma-capsulatum.html.

IMPROVE Program – Improve,. Accessed 12 March 2026g, https://vista.cira.colostate.edu/Improve/improve-program/.

Income Map for Oklahoma Counties | HDPulse Data Portal,. *HDPulse: An Ecosystem of Health Disparities and Minority Health Resources*. Accessed 30 April 2024h, https://hdpulse.nimhd.nih.gov/data-portal/social/map?socialtopic=030&socialtopic_options=social_6&demo=01001&demo_options=income_3&race=00&race_options=raceall_1&sex=0&sex_options=sexboth_1&age=001&age_options=ageall_1&statefips=40&statefips_options=area_states.

Inhalable Particulate Matter and Health (PM2.5 and PM10) | California Air Resources Board,. Accessed 12 March 2026i, https://ww2.arb.ca.gov/resources/inhalable-particulate-matter-and-health.

Institute for Health Metrics and Evaluation,: GBD Compare. Accessed 1 May 2024, https://vizhub.healthdata.org/gbd-compare/.

Katz, D. J., E. Browne, and S. Maltarich, 2025a: First-ever airborne toxin detected in Western Hemisphere. Accessed 12 March 2026, https://cires.colorado.edu.

——, B. Dobson, M. Alton, H. Stark, D. R. Worsnop, M. R. Canagaratna, and E. C. Browne, 2025b: Real-Time Measurements of Gas-Phase Medium-Chain Chlorinated Paraffins Reveal Daily Changes in Gas-Particle Partitioning Controlled by Ambient Temperature. *ACS Environ. Au*, **5**, 415–426, https://doi.org/10.1021/acsenvironau.5c00038.

Kaw Nation, and Fox Nation,: 37 FEDERALLY RECOGNIZED TRIBES.

Kline, L., 2020: Performing HIPS Analysis.

——, 2022a: UCD IMPROVE Standard Operating Procedure #301. **2.5**.

——, 2022b: UCD IMPROVE Standard Operating Procedure #276.

Loría-Salazar, S. M., A. Panorska, W. P. Arnott, J. C. Barnard, J. M. Boehmler, and H. A. Holmes, 2017: Toward understanding atmospheric physics impacting the relationship between columnar aerosol optical depth and near-surface *PM*2.5 mass concentrations in Nevada and California, U.S.A., during 2013. *Atmospheric Environment*, **171**, 289–300, https://doi.org/10.1016/j.atmosenv.2017.10.023.

Martin Jean & Jackson,: 2019 & 2020 Oklahoma Fatal Car Accident Statistics. *Martin Jean & Jackson*. Accessed 30 April 2024, https://www.mjjlawfirm.com/blog/2021/may/2019-2020-oklahoma-fatal-car-accident-statistics/.

McNeill, J., and X. Liu, 2022: Determination of Trace Metals Deposited on PTFE Filters by X-Ray Fluorescence Analysis.

Met One Instruments Inc., 2019: *BAM-1022-9805-Operation-Manual-Rev-C*. Met One Instruments Inc.

Native American Population by State 2024,. Accessed 1 May 2024j, https://worldpopulationreview.com/state-rankings/native-american-population.

New York State Department of Health, 2024: Particle Pollution and Health. Accessed 1 May 2024, https://www.health.ny.gov/environmental/indoors/air/pmq_a.htm.

Nguyen, T. T. N., H. V. Pham, K. Lasko, M. T. Bui, D. Laffly, A. Jourdan, and H. Q. Bui, 2019: Spatiotemporal analysis of ground and satellite-based aerosol for air quality assessment in the Southeast Asia region. *Environmental Pollution*, **255**, 113106, https://doi.org/10.1016/j.envpol.2019.113106.

Oklahoma Profile, 2023a. Accessed 1 May 2024, https://www.eia.gov/state/print.php?sid=OK.

Oklahoma State Legislature,: Bill Information. Accessed 12 March 2026k, https://www.oklegislature.gov/BillInfo.aspx?Bill=SB3&Session=2500.

Paredes-Miranda, G., W. P. Arnott, J. L. Jimenez, A. C. Aiken, J. S. Gaffney, and N. A. Marley, 2009: Primary and secondary contributions to aerosol light scattering and absorption in Mexico City during the MILAGRO 2006 campaign. *Atmospheric Chemistry and Physics*, **9**, 3721–3730, https://doi.org/10.5194/acp-9-3721-2009.

Ponca City, OK Weather History | Weather Underground,. Accessed 1 April 2026l, https://www.wunderground.com/history/daily/us/ok/ponca-city/KPNC/date/2025-7-18.

PurpleAir, 2023b: What Do PurpleAir Sensors Measure and How Do They Work? - Sensors. *PurpleAir Community*. Accessed 12 March 2026, https://community.purpleair.com/t/what-do-purpleair-sensors-measure-and-how-do-they-work/3499.

Rukikaire, K., 2021: One in three countries in the world lack any legally mandated standards for outdoor air quality. Accessed 12 March 2026, https://www.unep.org/news-and-stories/press-release/one-three-countries-world-lack-any-legally-mandated-standards.

Salazar, S. M. L., and Coauthors, 2025: Smoke, Dust, and Resilience: Unraveling the March 2025 Oklahoma Compound Hazards. AGU25, AGU.

Sensor Owner's Guide - Sensors, 2024a. *PurpleAir Community*. Accessed 12 March 2026, https://community.purpleair.com/t/sensor-owners-guide/8170.

SGP-Central-Facility-Instrument-Locations.png (785×935),.

Smirnov, A., B. N. Holben, T. F. Eck, I. Slutsker, B. Chatenet, and R. T. Pinker, 2002: Diurnal variability of aerosol optical depth observed at AERONET (Aerosol Robotic Network) sites. *Geophysical Research Letters*, **29**, https://doi.org/10.1029/2002GL016305.

Smith, D., F. Solano, L. Woodruff, W. Cannon, and K. Ellefsen,: USGS Scientific Investigations Report 2017-5118: Geochemical and Mineralogical Maps, with Interpretation, for Soils of the Conterminous United States. Accessed 12 March 2026, https://pubs.usgs.gov/sir/2017/5118/sir20175118_element.php?el=82.

Snider, G., and Coauthors, 2015: SPARTAN: a global network to evaluate and enhance satellite-based estimates of ground-level particulate matter for global health

applications. *Atmospheric Measurement Techniques*, **8**, 505–521, https://doi.org/10.5194/amt-8-505-2015.

SPARTAN, 2018: *SS5_setup*. SPARTAN.

Tar Creek Superfund Site,. *Oklahoma Department of Environmental Quality*. Accessed 1 May 2024n, https://oklahoma.gov/deq/divisions/land-protection/cleanup-redevelopment/superfund/tar-creek-superfund-site.html.

Tulchinsky, T. H., and E. A. Varavikova, 2014: Chapter 3 - Measuring, Monitoring, and Evaluating the Health of a Population. *The New Public Health (Third Edition)*, T.H. Tulchinsky and E.A. Varavikova, Eds, Academic Press, 91–147, https://doi.org/10.1016/B978-0-12-415766-8.00003-3.

Uin, J., 2024: Nephelometer Instrument Handbook.

US EPA, O., 1992: EPA - Environmental Justice: Reducing Risk For All Communities Volume 1. Accessed 1 May 2024, https://www.epa.gov/environmentaljustice/epa-environmental-justice-reducing-risk-all-communities-volume-1.

US EPA, O., 2015: Evolution of the Clean Air Act. Accessed 12 March 2026, https://www.epa.gov/clean-air-act-overview/evolution-clean-air-act.

——, 2016: Particulate Matter (PM) Basics. Accessed 1 May 2024, https://www.epa.gov/pm-pollution/particulate-matter-pm-basics.

——, 2017: Chemical Speciation Network (CSN). Accessed 12 March 2026, https://www.epa.gov/amtic/chemical-speciation-network-csn.

US EPA, R. 07, 2024: Celebrating 10 Years of Tribe's Cleanup Partnership at Tar Creek Superfund Site. Accessed 12 March 2026, https://www.epa.gov/mo/celebrating-10-years-tribes-cleanup-partnership-tar-creek-superfund-site.

Vilcassim, R., and G. D. Thurston, 2023: Gaps and future directions in research on health effects of air pollution. *eBioMedicine*, **93**, 104668, https://doi.org/10.1016/j.ebiom.2023.104668.

Wallace, L., 2022: Intercomparison of PurpleAir Sensor Performance over Three Years Indoors and Outdoors at a Home: Bias, Precision, and Limit of Detection Using an Improved Algorithm for Calculating PM2.5. Accessed 12 March 2026, https://www.mdpi.com/1424-8220/22/7/2755.

Weagle, C., 2019: *Determining Equivalent Black Carbon from PTFE Filters with a Smoke Stain Reflectometer*. SPARTAN.

——, E. Stone, and E. Le Roy, 2019: *Determination of Anions and Cations Extracted from PTFE® Filters by Ion Chromatography*. SPARTAN.

WHO, 2023: Household air pollution. Accessed 1 May 2024, https://www.who.int/news-room/fact-sheets/detail/household-air-pollution-and-health.

——, 2024b: *ghe2021_daly_methods*.

——,: Indicator Metadata Registry Details. Accessed 12 March 2026, https://www.who.int/data/gho/indicator-metadata-registry/imr-details/4654.

WHO global air quality guidelines, 2021. World Health Organization.

WHO Media Team,: WHO unveils updated global database of air quality standards. Accessed 12 March 2026o, https://www.who.int/news/item/26-02-2025-who-unveils-updated-global-database-of-air-quality-standards.

Xin, J., and Coauthors, 2015: The Campaign on Atmospheric Aerosol Research Network of China: CARE-China, https://doi.org/10.1175/BAMS-D-14-00039.1.

Yoksoulian, L., 2022: Rural air pollution may be as hazardous as urban, study finds. Accessed 1 May 2024, https://news.illinois.edu/view/6367/13739985.

Yong, Z., and Z. Haoxin, 2016: Digital universal particle concentration sensor.

Youth in Agriculture - Organic Dust | Occupational Safety and Health Administration,. Accessed 1 May 2024p, https://www.osha.gov/etools/youth-agriculture/organic-dust.

Zhang, H., 2017: Using Biosolids as a Plant Nutrient Source - Oklahoma State University. Accessed 12 March 2026,

https://extension.okstate.edu/fact-sheets/using-biosolids-as-a-plant-nutrient-source.html
.

——, 2018: Background Metal Concentrations in Oklahoma Soils - Oklahoma State University. Accessed 12 March 2026, https://extension.okstate.edu/fact-sheets/background-metal-concentrations-in-oklahoma-soils.html.

Supplementary Material:

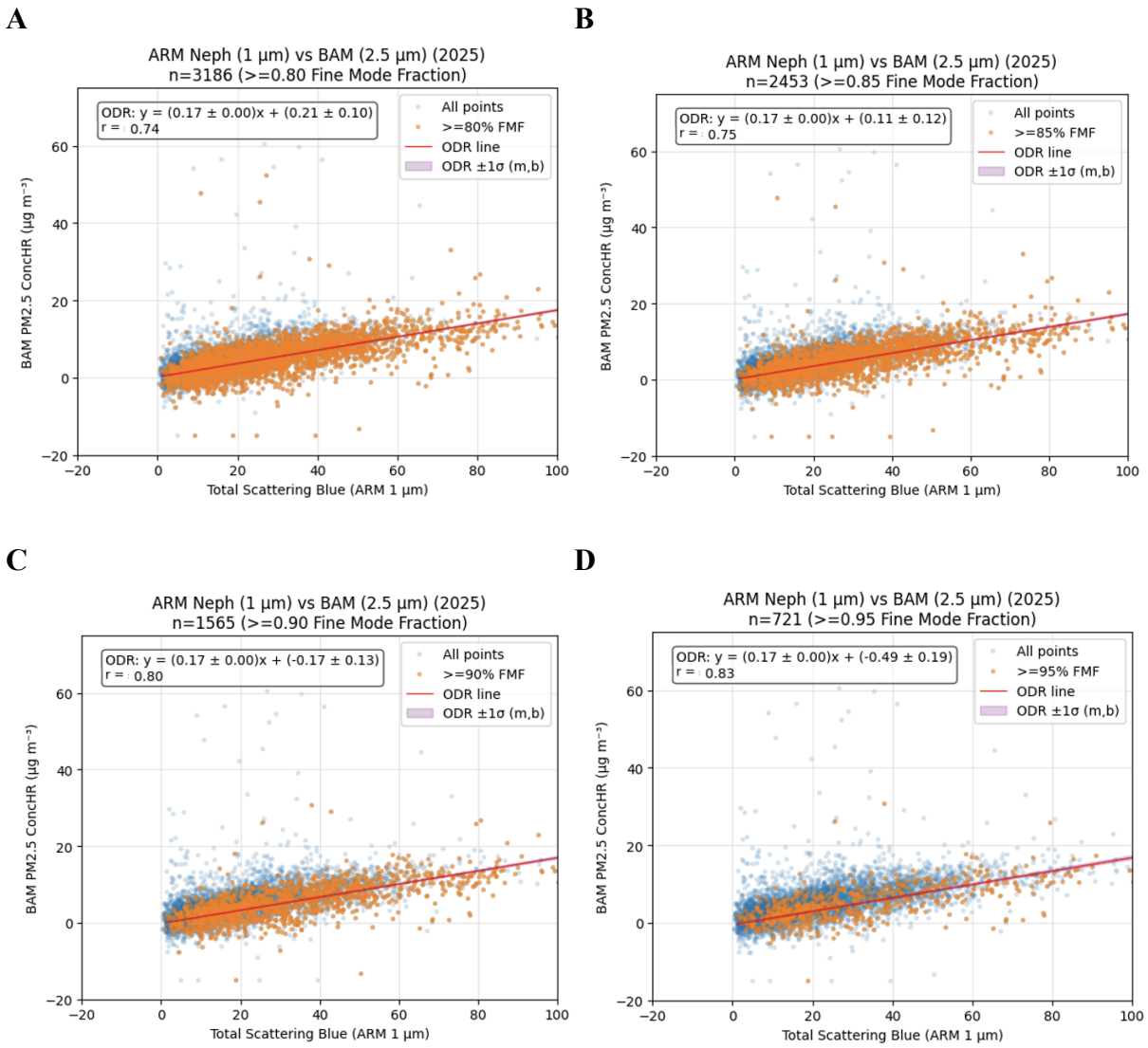

Figure S1: ARM nephelometer (1µm) blue total scattering and BAM (2.5µm) $PM_{2.5}$ Mass Concentration measurements during a portion of 2025 with uncertainty. Points represent concurrent hourly measurements. The red line shows the orthogonal distance regression (ODR) fit; blue dots indicate measurements excluded, and orange dots indicate measurements included due to fine-mode fraction (FMF) filtering. **(A)** Fine-Mode Fraction (FMF) ≥ 0.80, **(B)** FMF ≥ 0.85, **(C)** FMF ≥ 0.90, and **(D)** FMF ≥ 0.95

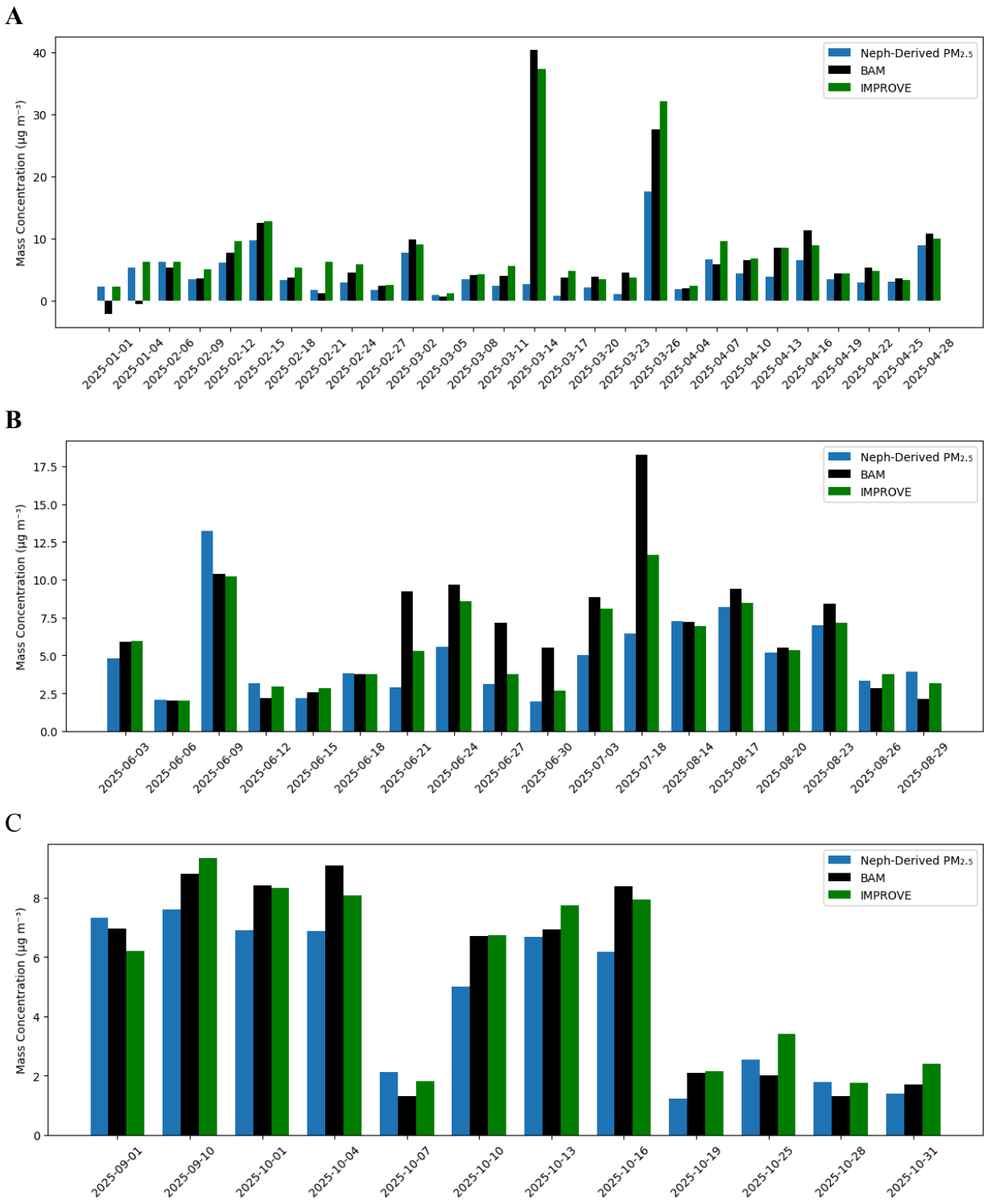

Figure S2: Concurrent daily $PM_{2.5}$ mass concentration comparison for August-October 2025. Daily averages were calculated from BAM and nephelometer hourly measurements. Bars represent 1µm nephelometer-derived mass concentration (blue), BAM (black), and IMPROVE (green). This data was not filtered according to fine-mode fraction (FMF). **(A)** January-April 2025. **(B)** May-August 2025. May data is unavailable. **(C)** September-October 2025.

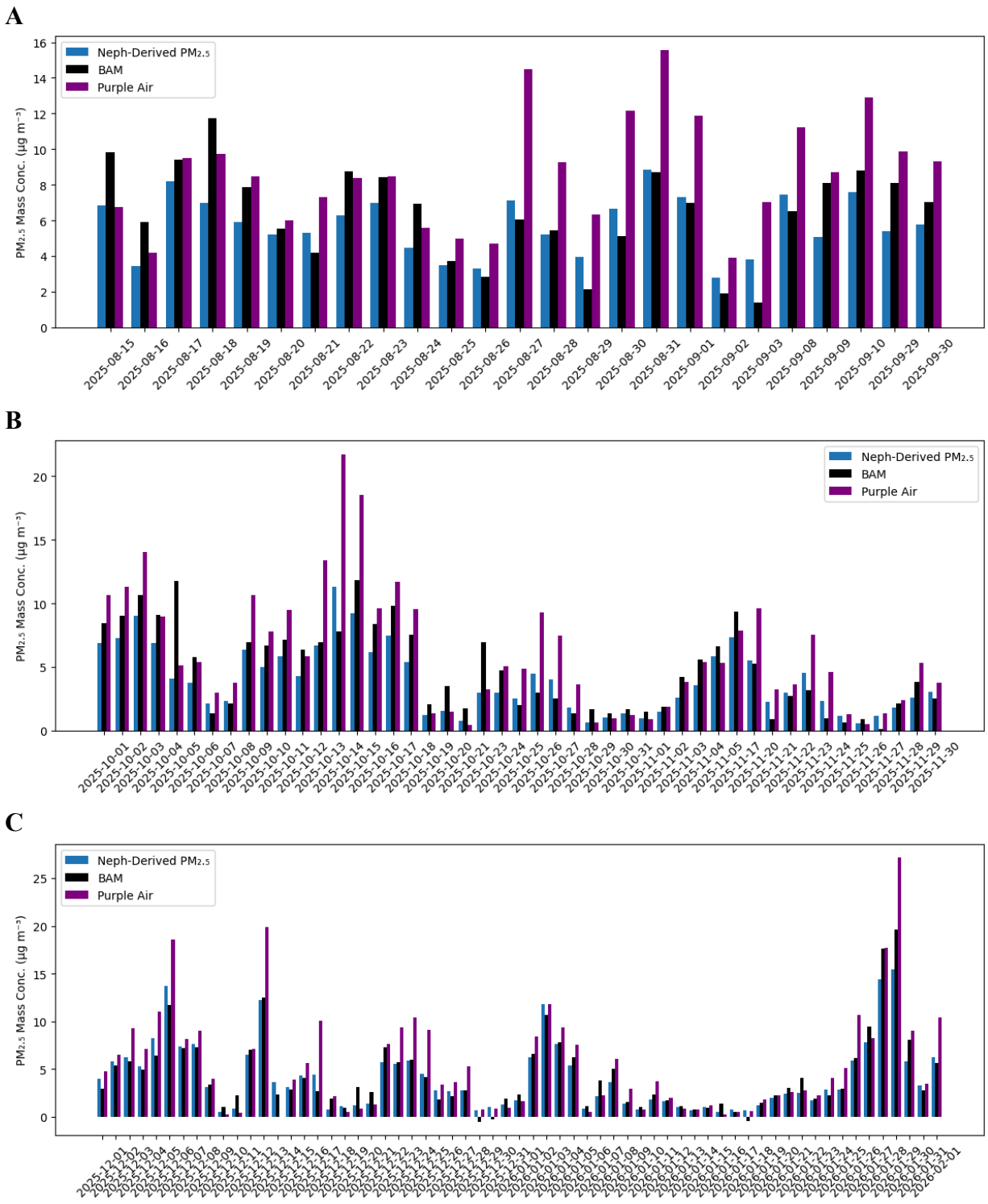

Figure S3: Concurrent daily $PM_{2.5}$ mass comparison for August-September 2025. Daily averages were calculated from BAM and nephelometer hourly measurements. Bars represent 1µm nephelometer-derived mass concentration (blue), BAM (black), and PurpleAir (purple). This data was not filtered according to fine-mode fraction (FMF). **(A)** August-September 2025. **(B)** October-November 2025. **(C)** December 2025 - February 2026.

A

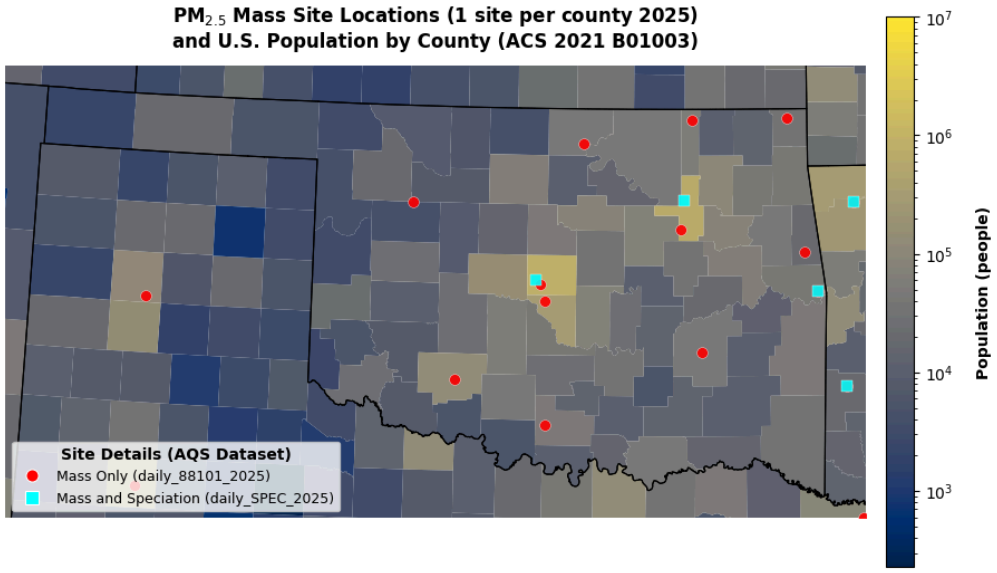

B

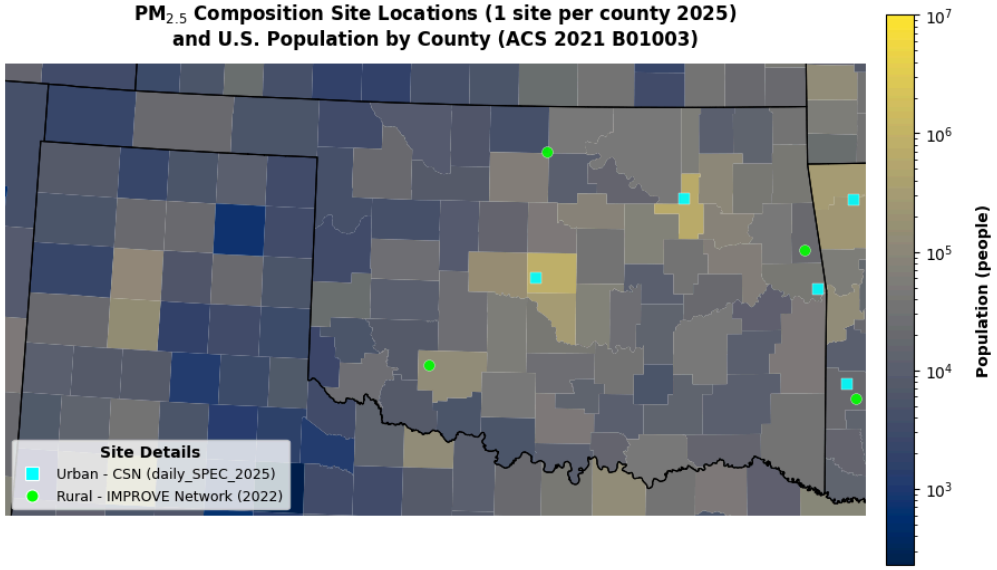

Figure S4: PM2.5 measuring site locations in Oklahoma with one site per county and U.S. population by County ("B0103: Total–Estimate", 2021). (A) PM2.5 mass concentration measuring sites, including Teledyne T640 real-time PM Monitor, Thermo Scientific Model 2025 Sequential Air Sampler, and Met One Environmental Federal Reference Method Sampler (E-FRM). (B) PM2.5 speciated mass concentration measuring sites, including the CSN and IMPROVE network.